



**CHARACTERISTICS AND CATALYTIC ACTIVITY OF
ACTIVATED CARBON SUPPORTED HYDROTALCITE FOR
FERMENTATIVE HYDROGEN PRODUCTION**

BY

MS. SOUTHISA SYBOUNYA

**A THISIS SUBMITTED IN PARTIAL FULFILLMENT OF THE
REQUIREMENTS FOR THE DEGREE OF MASTER OF SCIENCE
(ENGINEERING AND TECHNOLOGY)
SIRINDHORN INTERNATIONAL INSTITUTE OF TECHNOLOGY
THAMMASAT UNIVERSITY
ACADEMIC YEAR 2020
COPYRIGHT OF THAMMASAT UNIVERSITY**

**CHARACTERISTICS AND CATALYTIC ACTIVITY OF
ACTIVATED CARBON SUPPORTED HYDROTALCITE FOR
FERMENTATIVE HYDROGEN PRODUCTION**

**BY
MS. SOUTHISA SYBOUNYA**

**A THISIS SUBMITTED IN PARTIAL FULFILLMENT OF THE
REQUIREMENTS FOR THE DEGREE OF MASTER OF SCIENCE
(ENGINEERING AND TECHNOLOGY)**

**SIRINDHORN INTERNATIONAL INSTITUTE OF
TECHNOLOGY**

THAMMASAT UNIVERSITY

ACADEMIC YEAR 2020

COPYRIGHT OF THAMMASAT UNIVERSIT

THAMMASAT UNIVERSITY
SIRINDHORN INTERNATIONAL INSTITUTE OF TECHNOLOGY

THESIS

BY

MS. SOUTHISA SYBOUNYA

ENTITLED

CHARACTERISTICS AND CATALYTIC ACTIVITY OF ACTIVATED CARBON
SUPPORTED HYDROTALCITE FOR FERMENTATIVE HYDROGEN
PRODUCTION

was approved as partial fulfillment of the requirements for
the degree of Master of Science (Engineering and Technology)

on November 17, 2020

Chairperson



(Professor Chongrak Polprasert, Ph.D.)

Member and Advisor



(Associate Professor Rachnarin Nitorisavut, Ph.D.)

Member



(Associate Professor Pongsak Noophan, Ph.D.)

Director



(Professor Pruetha Nanakorn, D.Eng.)

eThesis Title	CHARACTERISTICS AND CATALYTIC ACTIVITY OF ACTIVATED CARBON SUPPORTED HYDROTALCITE FOR FERMENTATIVE HYDROGEN PRODUCTION
Author	Ms. Southisa Sybounya
Degree	Master of Science (Engineering and Technology)
Faculty/University	Sirindhorn International Institute of Technology/ Thammasat University
Thesis Advisor	Associate Professor Rachnarin Nitorisravut, Ph.D.
Academic Years	2020

ABSTRACT

Commercial activated carbon (CAC) was modified by a chemical activation agent, H_3PO_4 with the temperature ranging from 400 to 900°C (400°C, 500°C, 600°C, 700°C, 800°C and 900°C) for 1 h under N_2 atmosphere. The modified commercial activated carbon (mCAC) samples were characterized for surface area, morphology, structure and functional groups to understand the roles of the modified activated carbon in fermentation. All samples (CAC and mCAC) were employed at a concentration of 8.33 g/L. The possible enhancement of hydrogen production via dark fermentation was investigated using sucrose as the substrate. The best catalytic performance was observed at an activation temperature of 600°C (mCAC600) with hydrogen production of 2.62 mol H_2 /mol sucrose. This was 17% higher than the control. The temperatures continuous to increase, great weight loss was produced at very high temperature practically 700 to 900°C by volatilization of phosphorous compound functional groups. Similar with the low temperature (400-500°C) caused change the characteristics of activated carbon as such a loss of weight, surface area and porosity reduction. In addition, the increment of hydrogen production was associated with the properties of activated carbon such as surface area, pore structure, and adsorption ability especially

pore size. The mCAC600 has the biggest pore size (2.31 nm) compared to all treatments, which could improve microbial colonization and thereby, enhance the hydrogen production.

The mCACs (400 to 700°C) were then used as a supporting material for Zn-Ni-HT. The Zn-Ni-HT/mCAC600 was obtained by the incipient impregnation method. The maximum hydrogen production yield was found at 2.95 mol H₂/mol sucrose, which was 30% higher than the control. The possible reason is that mCAC600 has the biggest in pore size. When Zn-Ni-HT loaded on mCAC600, it could help HT spread in the pore. Therefore, Zn-Ni-HT/mCAC600 showed a good performance as compared to all materials. Moreover, both acetic and butyric acids were observed as by-product. The highest concentration of acetic acid was observed for Zn-Ni-HT/mCAC600, which also provided the highest hydrogen production yield. Zn-Ni-HT/mCAC600 had highest percent adsorption of VFAs particularly butyric acid, which was 63.78%. While the percent adsorption of VFAs for mCAC600 was found for butyric acid only 25.93%. Zn-Ni-HT/mCAC600 is 40% higher than mCAC600. Base on the Langmuir and Freundlich isotherm models, it shows that the volatile fatty acids were covered only by a monolayer on the surface of the materials. There is no stacking adsorbed molecules. Therefore, volatile fatty acids were adsorbed on the pore of the supported materials. It should be noted that Zn-Ni-HT/mCAC600 could be used once as gradual decline in performance was found for recyclability tests.

The Zn-Ni-HT/mCAC600 acted as an alkaline reagent to encounter fatty acid, thereby preventing a pH drop during the fermentation process. Moreover, the supported activated carbon can also adsorb unfavorable VFAs in the system. The release of metal ions from the structure of Zn-Ni-HT/mCAC600 was lower than that of Zn-Ni-HT/CAC, especially for Mg²⁺ and Al³⁺. The released ions also helped to enhance the hydrogen production yield, particularly for Ni²⁺. It is, therefore, concluded the Zn-Ni-HT/mCAC600 composite created hybrid functions to promote fermentative hydrogen production.

Keywords: biohydrogen production, modified activated carbon, catalyst, dark fermentation, metals leaching, volatile fatty acid

ACKNOWLEDGEMENTS

I would like to express my special thanks to my advisor, Assoc. Prof. Dr. Rachnarin Nitisoravut for his contribution, valuable guidance, kindness, support and helping me through my research and my postgraduate studies. Special thanks are extended to Prof. Dr. Chongrak Polpasert and Assoc. Prof. Dr. Pongsak Noopahan were served as the thesis committee members, for their suggestion, insightful comments to help me improve my research.

I am grateful to EFS scholarship and SIIT Faculty's Quota scholarship under Assoc. Prof. Dr. Rachnarin Nitisoravut for supporting fund for my research work.

I also thanks to my senior, Ms. Pornthip Wimonsong, for suggestion and her guidance to my experiments in laboratory.

I would like to thank my family who always support, help, understanding and motivate me when I have problem with my life and my studies.

Finally, I am truly thankful to my friends for their help in laboratory works, throughout my study SIIT.

Ms. Southisa Sybounya

TABLE OF CONTENTS

	Page
ABSTRACT	(1)
ACKNOWLEDGEMENTS	(3)
LIST OF TABLES	(7)
LIST OF FIGURES	(8)
LIST OF SYMBOLS/ABBREVIATIONS	(9)
CHAPTER 1 INTRODUCTION	1
1.1 Statement of problem	1
1.2 Aim of study	4
1.3 Scope of work	4
CHAPTER 2 REVIEW OF LITERATURE	5
2.1 Dark fermentation	5
2.2 Factors affecting dark fermentation	6
2.2.1 pH	6
2.2.2 Volatile fatty acids	7
2.2.3 Temperature	8
2.3 Materials used for enhancement of biohydrogen production	8
2.3.1 Metals nanoparticles	10
2.3.2 Nickel and Nickel oxide	14
2.3.3 Iron and iron oxide	16

	(5)
2.3.4 Hydrotalcites	21
2.3.5 Activated carbon	22
2.3.6 Nanocomposite of catalyst	23
CHAPTER 3 MATERIALS AND METHODS	26
3.1 Materials	26
3.1.1 Inoculum	26
3.1.2 Substrate	26
3.1.3 Commercial activated carbon	26
3.1.4 Hydrotalcites	26
3.1.5 Activated carbon supported HT	27
3.1.6 Volatile fatty acid solution	28
3.2 Methodology	28
3.2.1 Experimental procedures	28
3.2.1.1 Fermentative hydrogen production	28
3.2.2 Catalytic activity of activated carbon supported HT	29
3.2.2.1 Volatile fatty acid adsorption	29
3.2.2.2 Catalysts recyclability	29
3.2.3 Analytical methods	29
3.2.3.1 Commercial activated carbon supported HT characterization	29
3.2.3.2 Determination of gas compositions	30
3.2.3.3 Determination of metals	30
3.2.3.4 Determination of VFAs	30
3.2.3.5 Kinetic modeling	30
3.2.3.6 Langmuir adsorption isotherm	31
3.2.3.7 Freundlich adsorption isotherm	31

	(6)
CHAPTER 4 RESULTS AND DISSCUSTION	33
4.1 Modified activated carbon characterizations	33
4.1.1 Functional groups	33
4.1.2 Surface area and pore volume	38
4.1.3 Structure of hydrotalcite	40
4.1.4 Morphology and porosity	40
4.2 Effect of modified commercial activated carbon on biohydrogen production	42
4.3 Effect of modified commercial activated carbon supported HT on biohydrogen production	46
4.4 Metabolize distribution	51
4.5 Metals leaching of supporting materials	53
4.6 Volatile fatty acids adsorption	54
4.7 Recyclability of Zn-Ni-HT/mCAC600	59
CHAPTER 5 CONCLUSIONS AND RECOMMENDATION	60
REFERENCES	62
APPENDICES	71
APPENDIX A	72
APPENDIX B	75
APPENDIX C	76
APPENDIX D	77
BIOGRAPHY	78

LIST OF TABLES

Tables	Page
2.1 Metals nanoparticles used in batch biohydrogen production	12
2.2 Application of metal ions in dark fermentation	13
2.3 The use of Ni and NiO nanoparticles in batch biohydrogen production	15
2.4 The use of Fe, Fe ₂ O ₃ , Fe ₃ O ₄ and FeSO ₄ nanoparticles in batch biohydrogen production	19
2.5 The use of combination catalyst in batch biohydrogen production	24
2.6 The possible roles of catalysts in biohydrogen production	25
3.1 The ratio of HT	27
3.2 Hydrotalcites preparation and loading methods	27
4.1 The possible functional groups present on CAC and mCAC	35
4.2 The functional groups present in modified CAC supported HT	37
4.3 Surface area and pore distribution of mCAC and modified CAC supported HT	39
4.4 Samples descriptive statistics using the t-test for H ₂ yield, compared to the control	45
4.5 Parameters estimation by Gompertz model and Hydrogen production yield for CAC and mCAC	46
4.6 Samples descriptive statistics using t-test for H ₂ yield of Zn-Ni-HT/mCAC600 compared to mCAC600 and Zn-Ni-HT/CAC	49
4.7 Parameters estimation by the Gompertz model and Hydrogen production yield of mCAC supported HT	50
4.8 Langmuir parameters and percent adsorption of VFAs on materials	55
4.9 Freundlich adsorption isotherm for VFAs adsorption onto materials	57

LIST OF FIGURES

Figures	Page
2.1 H ₂ production mechanism via dark fermentation	6
2.2 The mechanism of nanoparticle in biohydrogen production	9
2.3 Nanoparticles in fermentative hydrogen production	10
2.4 Structure of Hydrotalcite	22
3.1 Overall of experimentation analyses	32
4.1 FTIR spectra for CAC and modified CAC	34
4.2 FTIR spectra of modified CAC supported HT	36
4.3 XRD pattern of Zn-Ni-HT/CAC and Zn-Ni-HT/mCAC600	40
4.4 FESEM image of mCAC: (a) CAC, (b) mCAC400, (c) mCAC500, (d) mCAC600 and (e) mCAC700	41
4.5 FESEM images of Zn-Ni-HT/CAC: (a) × 3000, (b) × 15,000 and Zn-Ni-HT/mCAC600: (c) × 3000, (d) × 15,000	42
4.6 Hydrogen production of modified CAC in dark fermentation	43
4.7 Cumulative hydrogen production yield of the modified CAC	44
4.8 Percent increments of H ₂ production of modified CAC as related to control	44
4.9 Hydrogen production of modified CAC supported HT during fermentation	47
4.10 Cumulative hydrogen production of modified CAC supported HT	47
4.11 Percent increments of H ₂ production of modified CAC supported HT as related to control	48
4.12 Metabolites concentration	52
4.13 Final pH of different samples	52
4.14 Metals leaching during fermentative hydrogen production	54
4.15 Langmuir adsorption of VFAs on mCAC600	55
4.16 Langmuir adsorption of VFAs onto Zn-Ni-HT/mCAC600	56
4.17 Freundlich adsorption of VFAs on mCAC600	58
4.18 Freundlich adsorption of VFAs on Zn-Ni-HT/mCAC600	58
4.19 Hydrogen production yield of mCAC600 and Zn-Ni-HT/mCAC600 for repeat use three cycles for biohydrogen production	59

LIST OF SYMBOLS/ABBREVIATIONS

Symbols/Abbreviations	Description
SIIT	Sirindhorn International Institute of Technology
TU	Thammasat University
Au/Zn-Mg-Al	Zinc hydrotalcite supported Au
BET	Brunauer-Emmett Teller
CAC	Commercial activated carbon
COD	Chemical oxygen demand
FHL	Formate hydrogenlyase
Fd _{red}	Ferredoxin reductase
Fd _{ox}	Ferredoxin oxidase
HT	Hydrotalcite
H ₃ PO ₄	Phosphoric acid
HydA	Fd-dependent hydrogenase
HTLCs	Hydrotalcite-like compounds
KOH	Potassium hydroxide
K ₂ CO ₃	Potassium carbonate
LDHs	Layered double hydroxides
mCAC	Modified commercial activated carbon
NPs	Nanoparticles
NAD(P)H	Nitrite reductase
NADH	Nicotinamideadenine dinucleotide
NAD ⁺	Nicotinamideadenine dinucleotide ion
Ni-Mg-Al HT	Nickel hydrotalcite
PFL	Pyruvate formate-lyase
PFL	Pyruvate ferredoxin oxidoreductases-
VFAs	Volatile fatty acids
VS	Volatile solid

ZnCl₂

Zinc chloride

Zn-Ni-HT

Zinc nickel hydrotalcite



CHAPTER 1

INTRODUCTION

1.1 Statement of problem

Increasing demand for fossil fuels is one of the main causes of climate change and global warming. Fuel deposits are rapidly decreasing, and there is a limited energy supply for the next 150-200 years (Joshi, Pandey, Rana, & Rawat, 2017; Mullai, Yogeswari, & Sridevi, 2013; Patel, Lee, & Kalia, 2017). It is important to find alternative energy resources that are environmentally friendly, low cost, and renewable (Patel et al., 2017). Biofuels are one of the possible renewable energy sources and are expected to play an important function in the energy supply in the future (Mishra, Medhi, Maheshwari, Srivastava, & Thakur, 2018). Hydrogen is known as a clean energy source, with a high energy capacity and a high energy yield of 122 kJ/g, which is 2.75 times greater than hydrocarbon fuels (Sekoai & Daramola, 2015). Biological hydrogen production is an environmentally-friendly way of hydrogen production from renewable sources. While non-biological processes rely on non-renewable materials and fossil feedstocks which release gaseous emissions, particularly CO and CO₂ (Batista, 2014; Elbeshbishy, Dhar, Nakhla, & Lee, 2017; Srivastava et al., 2019). There are four different biological processes that can produce biohydrogen gas. Among these processes, dark fermentation is the most widely reported in the literature (Kim, Nhat, Chun, & Kim, 2008; Yokoyama, Waki, Ogino, Ohmori, & Tanaka, 2007; Zhang, Liu, & Shen, 2005). The advantages of dark fermentation are high yield, low cost, and simple operation on a small scale (Kumar, Mathimani, Rene, & Pugazhendhi, 2019). However, a drawback is a low hydrogen production rate. In the fermentative process, volatile fatty acids (VFAs) such as acetic, butyric, propionic and lactic acids occur as intermediates and by-products (Khanal, Chen, Li, & Sung, 2004). The VFAs cause a pH drop in the system and inhibit bacterial growth, which is the main cause of an unexpectedly low hydrogen production yield (Bundhoo & Mohee, 2016; Kapdan & Kargi, 2006; Mudhoo, Forster Carneiro, & Sánchez, 2011).

Nanoparticles are widely used in biosystems. Many researchers have attempted to use nanotechnology for enhancing biohydrogen production rate and yield. Nanoparticles react rapidly with electron donors leading to a kinetic improvement (Engliman, Abdul, Wu, & Jamaliah, 2017). They also act as biocatalysts to improve the performance and enhance the activities of microorganisms (Pugazhendhi et al., 2019). Numerous nanoparticles have been applied to promote biohydrogen production including gold (Zhang & Shen, 2007), silver (Zhao et al., 2013), copper (Mohanraj, Anbalagan, Rajaguru, & Pugalenti, 2016), Ni and NiO (Gadhe, Sonawane, & Varma, 2015a; Mishra et al., 2019), Fe₂O₃ (Han, Cui, Wei, Yang, & Shen, 2011), Fe₃O₄ (Seelert, Ghosh, & Yargeau, 2015), hydrotalcite (HT) (Wimonsong, Nitorisavut, & Llorca, 2014) and activated carbon (Zhang, Kang, Liang, & Abdullah, 2017). Activated carbon is known to be a versatile and effective adsorbent. It is mainly used for removing metals from wastewater and unwanted compounds from gas, vapors, and liquids in the chemical industries, and removing pollutants in soil. Activated carbon possesses a highly porous structure, large surface area and high adsorption capacity (Karnib, Kabbani, Holail, & Olama, 2014; Kim, Jeong, Park, & Kim, 2019; Yi, Wu, Fan, & Hu, 2019). Thus, it was used as a supporting material for metal nanoparticles (Akbarak, Özçifçi, & Tabak, 2019) such as Ni loaded on activated carbon (Bai, Chen, Li, & Li, 2007) and zerovalent iron on activated carbon (Zhang, Zhang, & Li, 2015).

In general, there are two main processes for preparing activated carbon: physical and chemical activations. In chemical activation, KOH, ZnCl₂, H₃PO₄, and K₂CO₃ are commonly used as chemical activation agents to activate the precursor materials (Ahmed et al., 2019). H₃PO₄ is a more preferable chemical agent for replacing ZnCl₂ because of environmental and economic concerns, lower temperature and easy recovery (Girgis, Attia, & Fathy, 2007). The advantages of using commercial activated carbon are time savings and no requirements for burning bio-char. Numerous studies were interested in the modification of commercial activated carbon by using H₃PO₄ as a chemical agent for improving the efficiency of adsorption capacity, especially for organic compounds (Anisuzzaman, Joseph, Taufiq-Yap, Krishnaiah, & Tay, 2015; Carvajal Bernal, Gómez, Giraldo, & Moreno Pirajá, 2015; Eustáquio, Lopes, Rocha, Cardoso, & Pergher, 2015). In dark fermentation, activated carbon was added into a

system with an optimum concentration of cocultures, 200 g/L (C. Zhang et al., 2017). Efficient hydrogen production was achieved at a yield of 1.203 mol H₂/mol glucose. Wimonsong and Nitorisravut (2014) found that the optimum loading of activated carbon was 33.3 g/L. This enhanced the hydrogen production yield to 2.60 mol H₂/mol sucrose, which was a 73% increment as compared to the control. The possible roles of activated carbon are to adsorb VFAs and to provide a high surface area where the microorganisms can grow easily on surfaces, as well as to sustain the cell viability and enhance the density (Jamali, Md Jahim, & Wan Isahak, 2016). HTs and HT-like compounds (HTLCs) or layered double hydroxides (LDHs), which are also known as anionic clays, have been used in many applications such as adsorption, catalysis, biomedicine, separation, ion exchange, acidic-basic buffering, and environmental treatment (Costantino, Nocchetti, Gorrasi, & Tammara, 2011; Sikander, Sufian, & Salam, 2017).

There were also a few studies that used HTs to improve the hydrogen production via dark fermentation (Le & Nitorisravut, 2015; Wimonsong, Llorca, & Nitorisravut, 2013; Wimonsong et al., 2014). The effects of HT concentrations ranging from 0 mg/L to 833 mg/L were studied. The optimum concentration for biohydrogen production was 167 mg/L using anaerobic sludge as the inoculum and sucrose as the substrate. The maximum hydrogen production was up to 2.30 mol H₂/mol sucrose (Wimonsong et al., 2013). Similarly, Ni-Mg-Al HT was used in batch experiments using sucrose as the substrate and anaerobic sludge as the inoculum. The optimum concentration was 250 mg/L, and the maximum hydrogen production yield was 3.37 mol H₂/mol (Le & Nitorisravut, 2015). In the study of Wimonsong et al. (2014), HT combined with Au nanoparticle could enhance the hydrogen production yield up to 2.74 mol H₂/mol sucrose with the optimum concentration of 167 mg/L. The structure of HT consists of elements, which microorganisms can use as micronutrients once released. The biohydrogen production was enhanced due to the presence of basic centers in HTs and bacteria immobilized in the interlaminar structure of HTs, which enabled electron transfer. This provided a better chance of contact with the substrate (Le & Nitorisravut, 2015; Wimonsong et al., 2013; Wimonsong et al., 2014). This study improves the biohydrogen production rate and yield by using a composite material of modified commercial activated carbon as the support for Zn-Ni-HT.

1.2 Aim of study

- To modify the commercial activated carbon by H_3PO_4 as a chemical activation agent.
- To characterize the physical-chemical properties of modified commercial activated carbon and commercial activated carbon supported hydrotalcite.
- To investigate effect of activated carbon supported hydrotalcite as catalyst for biohydrogen production.
- To investigate effect of metabolize distribution in fermentative hydrogen production.
- To evaluate recycle ability of activated carbon supported HT.
- To determine metals leaching during fermentative hydrogen production process
- To determine the adsorption capacity of the material.
- A relationship between physical-chemical properties of the catalysts and their performance for hydrogen generation was investigated

1.3 Scope of work

- Biohydrogen enhancement was studied by using modified commercial activated carbon and commercial activated carbon supported hydrotalcite.
- Zn and Ni hydrotalcite (Zn-Ni-HT) was used as combine with modified commercial activated carbon.
- Hydrogen fermentation process was carried out in batch tests by using sucrose as the substrate and mixed culture as the inoculum
- Dark fermentation was operated under temperature of $37^\circ C$ and pH of 5.5

CHAPTER 2

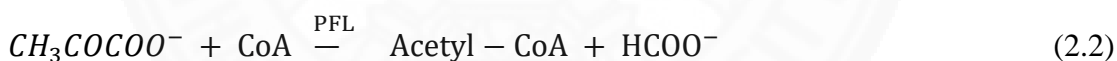
REVIEW OF LITERATURE

2.1 Dark fermentation

In dark fermentation process, anaerobic fermentative bacteria can produce hydrogen under mesophilic and thermophilic temperature with pure or mixed cultures. There are many species of hydrogen-producing bacteria such as facultative anaerobe (*Bacillus*, *Citrobacter*, *Escherichia coli*, *Enterobacter*) and obligate anaerobe (*Clostridium*, *Desulfovibrio*, *Ethanoligenens*) (Lee, Vermaas, & Rittmann, 2010). **Figure 2.1** shows the mechanism of H₂ production by dark fermentation. The primary, glycolysis pathway can convert glucose into pyruvate CH₃COCOO⁻ and H⁺ by Nicotinamide adenine dinucleotide (NADH) action (Bundhoo & Mohee, 2016) as shown in Equation 2.1:



The first step occurs mainly by *Enterobacteriaceae* and *Escherichia coli* by using pyruvate formate hydrogenlyase (FHL) enzyme and pyruvate formate-lyase enzyme (PFL). PFL can split pyruvate into formate and acetyl-CoA. After that, formate (HCOO⁻) is separated to carbon dioxide and hydrogen by formate hydrogen lyase.



The next step occurs by *Clostridium* as bacterium with relates to Fd-dependent hydrogenase (HydA) and pyruvate ferredoxin oxidoreductase (PFOR). Pyruvate ferredoxin oxidoreductase catalyze the oxidative decarboxylation of pyruvate to form carbon dioxide and acetyl-CoA. Fd decreases simultaneously. Then, the electrons in Fd_{red} are transferred to protons to form hydrogen by Fd-dependent hydrogenase (HydA).



The final step occurs by bacteria (thermophilic), which can grow at high temperature and *Clostridium* including NAD(P)H. Fd_{red} is reduced by NAD(P)H and the electrons are transferred to protons to form H_2 by HydA.

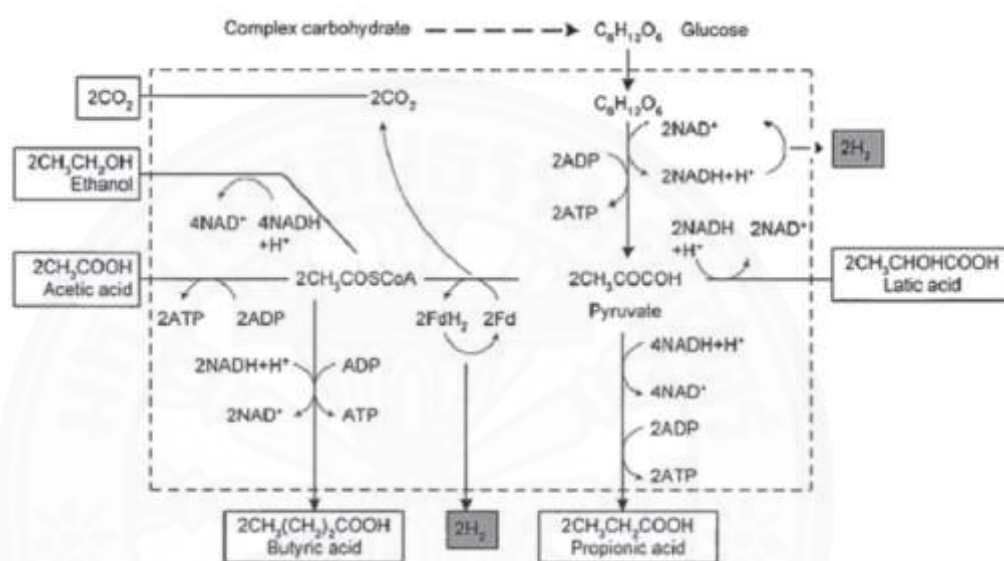
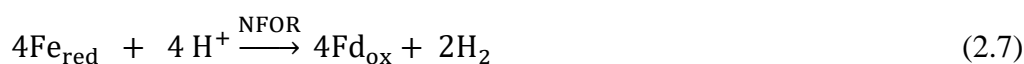
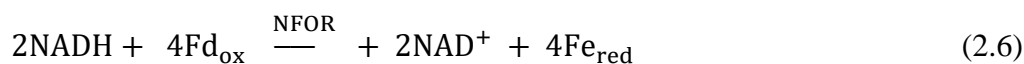


Figure 2.1 H_2 production mechanism via dark fermentation (Kumar et al., 2019)

2.2 Factors affecting dark fermentation

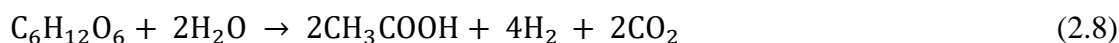
2.2.1 pH

pH is one of the important factors in biohydrogen production that affect the activities of hydrogenase or hydrogen-producing bacteria activity as well as the metabolism pathway. If the pH in the system is either low or high, the efficiency of the system decreases. The range of pH is also important in fermentation as an increasing pH can increase the ability of hydrogenase bacteria (Wang & Wan, 2009). When the pH is low, the hydrogen production is very less, while volatile fatty acids as by-product is produced. In contrast, when the pH is higher, it can also inhibit the activities of bacteria (Wimonsong & Nitorisavut, 2014). In addition, Hydrogen production is maximized at operating pH values from 5 to 6.5 (Baldi et al., 2019).

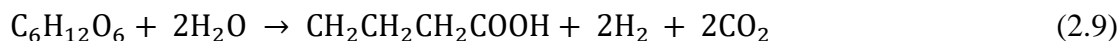
It has been demonstrated that initial pH affect the hydrogen product. The effect of initial pH in a range of 4.0 to 8.0 showed that the maximum hydrogen production was observed at initial pH of 5.5, while the hydrogen production was inhibited when the pH was either too low or too high from the optimum level. This is mainly due to enzymatic inhibition (Engliman et al., 2017). Similarly, in another study (Han et al., 2011), with the initial pH values between pH 4.0 to 10.0, the result showed that the maximum hydrogen production was obtained at initial pH 6.0 , while no hydrogen was produced when pH was lower or higher than pH 6.0. It indicated that the hydrogen producing bacteria in the system was inhibited. Besides, when pH is too low, the volatile fatty acid is produced that causes decrease in the hydrogen production (Han et al., 2011). The pH is important in biohydrogen production. If the pH is not in the optimum, it can inhibit the hydrogen production.

2.2.2 Volatile fatty acids

Volatile fatty acids (VFAs) such as acetic, butyric, propionic, and lactic acids are the end-products of biohydrogen production process. During a fermentation process, the VFAs can decrease hydrogen production and causes drop in pH in the system. Butyric acid and acetic acid are two main products that are produced during fermentation. The VFAs can negatively affect or inhibit the hydrogen-producing bacteria depending on their concentrations (Wimonsong & Nitorisavut, 2014). The lower concentration of VFAs may have no effect on hydrogen production, while higher concentration of VFAs can inhibit hydrogen production. Generally, the product of VFAs is butyric acid and acetic acid. When acetic acid is the by-product, the theoretical maximum of 4 moles H₂ per mole of glucose or eight moles of hydrogen per mole of sucrose is represented as Equation 2.8:

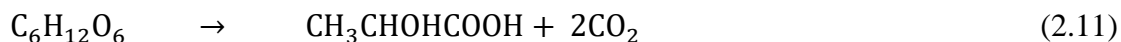
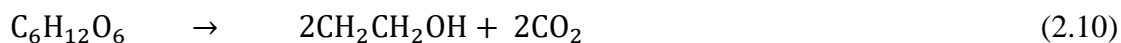


When the butyric acid is by-product, the theoretical maximum of 2 moles hydrogen per mole of glucose is represented as:

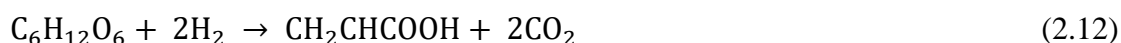


In metabolic pathway, when ethanol or lactic acid is the final product, no

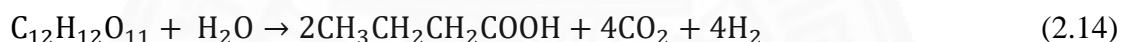
hydrogen is produced as represented in equations:



Another fermentation pathway is the production of propionate by *Clostridium articum* which is a hydrogen consuming pathway (Ghimire et al., 2015) as represented in equation 2.12:



Moreover, the use of sucrose as a substrate, when acetic and butyric are produced as by-products gives the maximum 8 moles and 4 moles of hydrogen per mol of sucrose, respectively. In addition, no hydrogen is produced when lactic and butyric are produced as by-products.



Nevertheless, the significant accumulation of these soluble metabolites can inhibit the metabolic activity of hydrogenase or hydrogen-producing bacteria. Thus, the production of these volatile fatty acids may indirectly reflect to hydrogen activity in dark fermentation (Elbeshbishy et al., 2017).

2.2.3 Temperature

Temperature is one of the most important factors that can significantly affect either hydrogen production yield or microbial metabolism in mixed culture. Temperature can influence the substrate biodegradation rate, the activity of hydrogen producing enzymes and metabolism of hydrogen producers. Operation temperature of fermentation normally depends on choice of microorganism used such as mesophilic (25-40°C), thermophilic (40-60°C) and hyperthermophilic (65-80°C). Among these conditions, mesophilic has been widely used in fermentative hydrogen production (Elbeshbishy et al., 2017; Guo, Trably, Latrille, Carrère, & Steyer, 2010)

2.3 Materials used for enhancement of biohydrogen production

To enhance fermentative hydrogen production, there are many strategies available such as pretreatment, hybrid system, metabolic engineering and removal of dissolved gas. However, those materials have advantage and disadvantage.

Nanoparticles (NPs) enhance the hydrogen yield by directly targeting the hydrogenase enzyme, which increases the electron transfer efficiency (Lin et al., 2016).

Nevertheless, there are two metabolic pathways to produce hydrogen by glucose fermentation specifically, the formate and the reduced nicotinamide adenine dinucleotide (NADH)-dependent hydrogen production pathway. In the formate hydrogen pathway, formate is decomposed by the enzyme formate hydrogen lyase. In the NADH dependent hydrogen producing pathway, with the assistance of the hydrogenase enzyme, re-oxidation of NAD occurs (Kumar et al., 2019) (**Figure 2.2**).

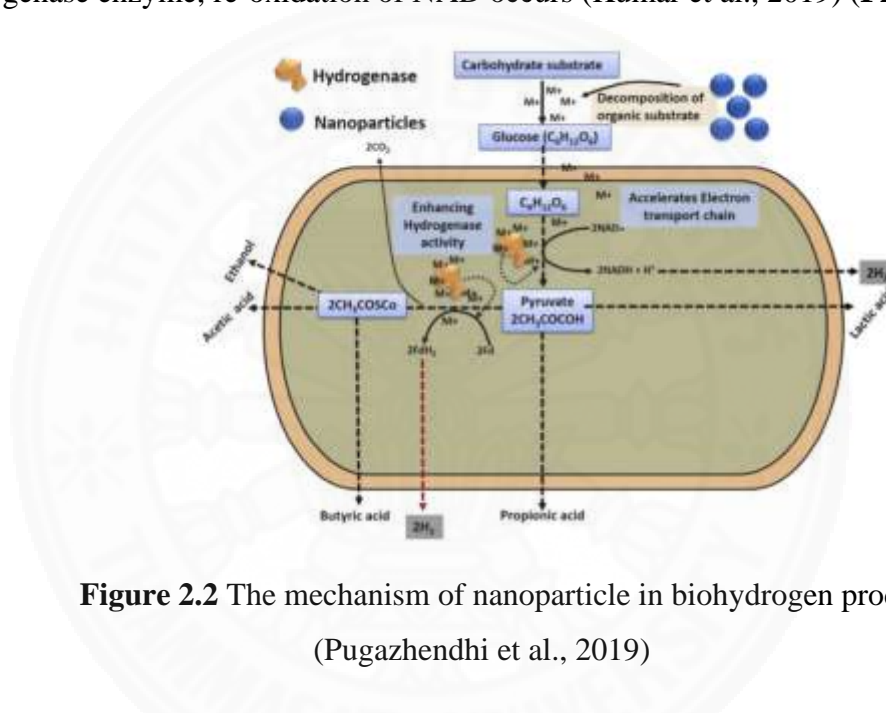


Figure 2.2 The mechanism of nanoparticle in biohydrogen production (Pugazhendhi et al., 2019)

There are many types of materials that are used on biohydrogen production especially nanoparticles such as metals nanoparticles (Au, Ag, Cu, Ni, Fe and Pd), NiO, activated carbon, hydrotalcite and nanocomposite materials (**Figure 2.3**). Enhancing biohydrogen process by catalysts is important to improve the yield because they have different functions. Therefore, many researchers have successfully used the nanoparticles in biohydrogen production.

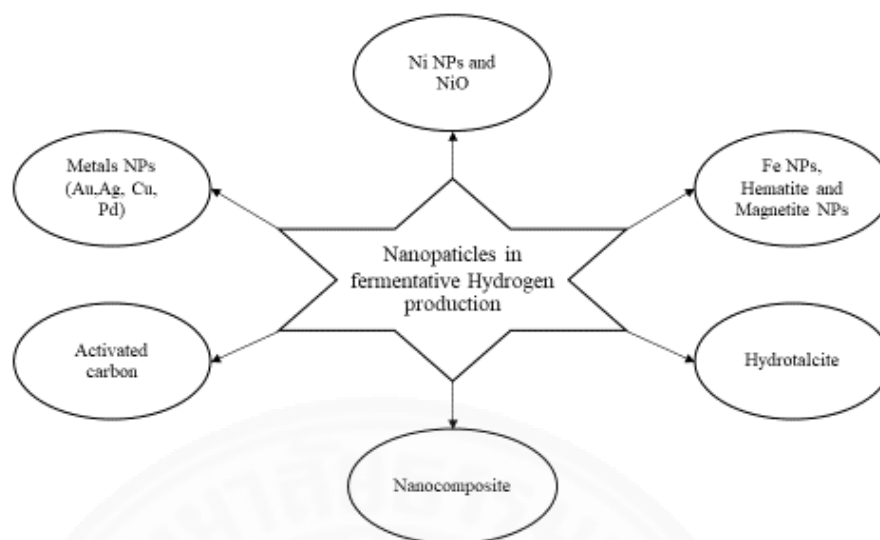


Figure 2.3 Nanoparticles in fermentative hydrogen production

2.3.1 Metals nanoparticles

There are many metals catalysts and nanoparticles that were applied in biohydrogen fermentation including Au, Ag, nickel, iron and other metals. Nanomaterials is important to improve the yield because they have different functions. Therefore, many researchers have successfully used nanomaterials in biohydrogen production (**Table 2.1**). Metals nanoparticle of various types has been demonstrated using in biological process for their application. Gold nanoparticles was applied in dark fermentation using anaerobic sludge as the inoculum and sucrose as the substrate. The concentration of 5nM Au nanoparticles showed the maximum of hydrogen yield of 4.48 mol H₂/mol sucrose. The role of Au nanoparticles could enhance catalytic properties in biological application and chemical process by enhancing enzyme activity on immobilization. These nanoparticles can stimulate hydrogen production by their quantum size effect and surface effect. The surface area and small-size particle of gold nanoparticle enables the strong ability to adsorb electron. The transfer of electrons between nanoparticles and enzyme molecules depends on the concentration of quantum size. For example, hydrogenase catalyzes hydrogen conversion to proton and vice versa. The reaction either reduces power from hydrogen oxidation or act as “electron sink” as given by the following reaction: $H_2 \rightleftharpoons 2H^+ + 2e^-$ (Zhang & Shen, 2007).

Despite its antimicrobial activity, silver nanoparticles (AgNPs) was used in many fields as a catalyst due to their distinct characteristics (Villalan et al., 2017; Zhao et al., 2013). The applications include food, electronic and medical industries as well as support for the immobilization of protein. In dark fermentation, Zhao et al. (2013) found that Ag nanoparticles with concentration of 20nM enhance in the hydrogen production yield to 2.48 mol H₂/mol glucose using mixed culture as the inoculum and glucose as the substrate. The presence of Ag nanoparticles significantly affected the production of metabolic pathway. The hydrogen production yield was higher as compared to the control along with an increase in the amount of acetic and butyric acids while ethanol and propionic acid decreased. The high concentration of silver nanoparticles stimulated higher production rate of cell biomass and decreased the lag phase in hydrogen production process (Zhao et al., 2013). Beckers, Hiligsmann, Lambert, Heinrichs, and Thonart (2013) studied the use of Ag NPs at 1000nM using *Clostridium butyricum* as inoculum. The maximum hydrogen production yield was 0.97 mol H₂/mol of glucose.

Copper nanoparticles are antibacterial, have high surface area, and have catalytic, magnetic and optical properties when compared with precision metals (for instance, silver, gold and palladium). Mohanraj et al. (2016) reported the effect of 2.5 mg/l copper nanoparticles using *C. acetobutylicum* as an inoculum and glucose as a substrate. The maximum hydrogen production yield was 1.74 mol H₂/mol glucose. The use of copper nanoparticles showed a negative effect on hydrogen production. The reason probably the deactivation of hydrogenase in both facultative. Another role of copper NPs is encapsulation in porous matrix which can improve the hydrogen production with the regulation of its antimicrobial activity. In addition, Cu NPs was applied in hydrogen fermentation. The highest H₂ yield was 1.01 mol H₂/mol glucose at 1000nM of concentration (Beckers et al., 2013).

Moreover, palladium nanoparticle was applied for biohydrogen production using *E. cloacae* 81110 as an inoculum. The hydrogen yield was 1.48 mol H₂/mol glucose. However, Mohanraj, Anbalagan, Kodhaiyolii, and Pugalenthii (2014) used mixed culture as an inoculum showed higher hydrogen production yield of 2.48 mol H₂/mol glucose under similar condition. Pd has negative effect on lag phase and

hydrogen yield. In addition, the supplement of palladium nanoparticles up to 20 mg/L showed no effect on bioactivity of both *E. cloacae* 811101 and mixed culture. Thus, the Pd²⁺ ions can inhibit effect on hydrogen production when compared with palladium nanoparticles due to reduction in the glucose conversion efficiency. The use of palladium nanoparticle has higher hydrogen production than use of Pd²⁺ ions due to higher hydrogenase activity.

Table 2.1 Metals nanoparticles used in batch biohydrogen production

Metal NPs	Optimum dose	Substrate	Microbial inoculum	Operating conditions		Hydrogen yield mol H ₂ /mol substrate	Ref
				pH	Temp		
Ag NPs	20nM	Glucose	Anaerobic sludge	8	35	2.48 ^b	(Zhao et al., 2013)
	1000nM	Glucose	<i>Clostridium butyricum</i> CWBI1900	7.6	30	0.97 ^b	(Beckers et al., 2013)
Cu NPs	2.5mg/l	Glucose	Acetobutylicm	7	37	1.74 ^b	(Mohanraj et al., 2016)
	1000nM	Glucose	<i>Clostridium butyricum</i> CWBI1900	7.6	30	1.01	(Beckers et al., 2013)
Pd NPs	5 mg/l	Glucose	<i>E.cloacae</i>	7	7	1.48 ^b	(Mohanraj et al., 2014)
			Anaerobic			2.48 ^b	
Au NPs	10nM	Sucrose	Anaerobic sludge	7.2	37	4.48 ^a	(Zhang & Shen, 2007)

^amol H₂/mol sucrose; ^bmol H₂/mol glucose

Table 2.2 Application of metal ions in dark fermentation

Metals ions	Postulated function in fermentation	Ref
Au	- Small-size particles to adsorb electrons (electron sink)	(Zhang & Shen, 2007)
Zn ⁺ , Zn ²⁺	- Active site of several enzyme - Can work as catalyst for some reaction	(Wimonsong et al., 2014)
Ni ²⁺	- Metals ion in the central complex of [Ni-Fe] hydrogenases - Micronutrient	(Le & Nitisoravut, 2015)
Mn ⁺	- Mimics the functions of Mg ²⁺ in its base - Activates the Ni-Fe hydrogenase	(David L. Nelson, 2008)
Fe ²⁺ , Fe ³⁺	- Mediates and Micronutrient between NADH-ferredoxin and hydrogenase - Component in active site of hydrogenase - When the temperature is low, microorganisms require more amount of ferrous ion to activate the hydrogenases enzyme.	(Wang & Wan, 2009; Zhang & Shen, 2006)
Mg ²⁺	- Essential element for ribosomes - Help to activate membrane component - One of the constituents of cell walls and membrane - Activate ten enzymes such as phosphofructokinase, hexokinase and phosphor-glycerate kinase during process of glycolysis	(David L. Nelson, 2008; Sinha & Pandey, 2011)
Cu ²⁺	- Replace metals of active center of enzymes - Can bind to sulfhydryl groups	(Han, Jia, Wei, & Shen, 2014)
Ca ²⁺	- Enhance their mechanical strength	(Lee, Lo, Lo, Lin, & Chang, 2004; Yuan, Yang, Zhi, & Shen, 2010)

2.3.2 Nickel and Nickel oxide

The traces of metals ions are necessary for growth of the most microorganism. Nickel can improve hydrogen production yield by activity of hydrogenases enzyme. Nickel is also one of the fundamental components of [NiFe] hydrogenases. Its role is important in fermentative hydrogen production. Furthermore, [Ni-Fe] hydrogenases are normally among fermentative bacteria. However, the [Fe-Fe] hydrogenases are limited to only some species of bacteria. Ni^{2+} ions have been known to be cofactors in active site of Ni-Fe hydrogenase. The use of 0.6 mg/l Ni^{2+} could enhance hydrogen production using sucrose as a substrate. The maximum hydrogen production reached 2.5 mol H_2 /mol sucrose (Gou et al., 2015). Hydrogen production yield was achieved up to 2.54 mol H_2 /mol glucose with the optimum concentration of nickel nanoparticles at 5.67 mg/L using anaerobic microflora as inoculum and glucose as a substrate (Mullai et al., 2013). In addition, hydrogen production yield for nickel nanoparticles with concentration of 60 mg/L by mixed culture from wastewater as substrate was 24.73 mg/g COD (Elreedy et al., 2017). Nickel oxide (NiO) would be able to improve the hydrogen production yield with the optimum concentration of 200 mg/L using anaerobic sludge as an inoculum and glucose as a substrate. The maximum hydrogen production yield was 1.30 mol H_2 /mol glucose (Engliman et al., 2017). Further, nickel oxide was investigated for biohydrogen production using anaerobic sludge as an inoculum and complex distiller wastewater as a substrate. The maximum hydrogen production yield was 7.85 mmol /g COD (Gadhe, Sonawane, & Varma, 2015b). At very high concentration of Nickel, [Ni-Fe] hydrogenases activity would be inhibited. This is because Nickel is toxic to bacteria which caused drop in hydrogen production. In dark fermentation, a higher NiO nanoparticles concentration than optimum also inhibited hydrogen-producing bacteria. This was due to a disruption of active structure of metabolic enzyme, and cell membrane carried out by disruption of dithiolate bridge in the active site of enzyme (Taherdanak, Zilouei, & Karimi, 2016). Nickel could be either nutrient for hydrogen-producing bacteria or component of enzyme in biohydrogen production. **Table 2.3** shows the influence of Ni and NiO nanoparticles in biohydrogen production.

Table 2.3 The use of Ni and NiO nanoparticles in batch biohydrogen production

Materials	Optimum dose (mg/L)	Substrate	Microbial inoculum	Operating conditions		Hydrogen yield mol H ₂ /mol substrate	Ref
				pH	Temp		
Ni NPs	5.67	Glucose	Anaerobic sludge	5.61	30-35	2.54 ^b	(Mullai et al., 2013)
	2.5	Glucose	Anaerobic sludge	7	55	250 ^b	(Taherdanak et al., 2016)
	60	Wastewater	Anaerobic sludge	5.0	55	24.73 ^c	(Elreedy et al., 2017)
NiO	5	distiller Wastewater	Anaerobic sludge	5.5	37	7.85 ^d	(Gadhe et al., 2015b)
	1.5	Palm oil milk effluent	Bacillus anthrasis PUNAJAN 1		37	560 ^c	(P. Mishra et al., 2018)
	200	Glucose and starch	Anaerobic sludge	5.5	60	1.30 ^b	(Engliman et al., 2017)
	10	Dairy wastewater	Anaerobic sludge	5.5	37	15.7 ^d	(Gadhe et al., 2015a)
Ni ²⁺	0.6	Sucrose	Cow dung	6	35	2.05 ^a	(Gou et al., 2015)

^amol H₂/mol sucrose; ^bmol H₂/mol glucose; ^cmg/g COD; ^dmmol/g COD

2.3.3 Iron and iron oxide

During fermentation, the microorganism or hydrogen-producing bacteria requires micronutrients such as magnesium, sodium, iron and zinc for metabolism. These are all very important trace metals affecting hydrogen production. In biohydrogen production, iron is an essential nutrient element to form hydrogenases (Yang & Shen, 2006). Metal oxide such as iron is one of micronutrients, which can significantly perform the activity of hydrogenase enzyme that improves hydrogen production (Engliman et al., 2017; Zhang & Shen, 2006). Researchers have demonstrated the effect of iron nanoparticles (Fe) (Taherdanak et al., 2016) and hematite nanoparticles (Fe_2O_3) (Engliman et al., 2017) in biological hydrogen production. The effect of iron (Fe) nanoparticles using anaerobic sludge as the inoculum and water hyacinth as the substrate at the optimum concentration 5 mg/L. The maximum hydrogen production yield was reached to 391 mg/g VS. while, the concentration of Fe NPs at 25 mg/L gave hydrogen yield 338 mg/g VS. The possible role due to ferredoxin electron transfer after the Fe NPs supplementation, which is promote the hydrogenase activity (Taherdanak et al., 2016). The effect of hematite nanoparticle at 200 mg/L concentration applied in fermentation. The initial pH 8.48 using sucrose as feed and anaerobic mixed bacteria as the inoculum found that maximum hydrogen production yield was achieved at 3.21 mol H_2 /mol sucrose. Hwang et al. (2019) found that the concentration of 2.5 g Fe^0 nanoparticle was applied for improving H_2 production using 10g COD/L substrate. The highest hydrogen production yield was 1.62 mol H_2 / mol glucose added. Nath et al. (2015) reported that with the use of 100 mg/L Fe nanoparticle by using *E. cloacae* DH-89, the highest H_2 production yield reached to 1.9 mol H_2 /mol glucose. The function of Fe NPs is cell growth of fermentative bacteria to enhance the metabolic process for hydrogen production.

In addition, the optimum concentration at 200 mg/L of hematite nanoparticle was investigated at initial pH 6.0 under similar conditions; the highest hydrogen production was achieved 3.57 mol H_2 /mol sucrose. Hematite nanoparticles could improve the hydrogen production, modify the bacteria growth as well as their metabolites distribution (Han et al., 2011). Engliman et al. (2017) found that iron (II)

oxide nanoparticles of 50 mg/L in fermentative hydrogen production under thermophilic condition. In dark fermentation, hematite nanoparticles were applied as catalyst at concentration 200 mg/L using anaerobic sludge as an inoculum and complex distiller wastewater as a substrate. The maximum hydrogen production yield achieved to 8.83 mmol/g COD (Gadhe et al., 2015b). Interestingly, Fe₂O₃ NPs was applied for enhancing hydrogen production using dairy wastewater as a substrate. The highest hydrogen yield was achieved up to 16.75 mmol/g COD at 50 mg/L concentration (Gadhe et al., 2015a). Fe₂O₃ NPs was also applied in continuous mode for improving hydrogen yield. The highest yield reached 300 mol H₂/mol sucrose using sewage sludge as an inoculum (Salem, Mietzel, Brunstermann, & Widmann, 2017). Similarity, the effect of Fe₂O₃ NPs was investigated by using *E.aerogenes* ATCC13408 as inoculum. The maximum hydrogen yield was achieved up to 192.4 mol H₂/ mol glucose (Lin et al., 2016). In addition, the use of 200 mg/L Fe₂O₃ NPs using *E. cloacae* 811101 found that the maximum hydrogen yield was 5.44 H₂/mol sucrose (Sunderasan, Kodhaiyolii, M, & Pugalenth, 2014). The significant improvement in hydrogen production was due to contribution of Fe²⁺ in the ferredoxin and hydrogenase enzyme (Dolly, Pandey, Pandey, & Gopal, 2015). The mechanism of hematite nanoparticles is that the mixed microorganism cell was immobilized on FeCO₃ sediment by sorption, which can enhance hydrogen production by microorganisms to meet substrate. The optimum concentration of iron raised hydrogen production in the beginning, but more than optimum concentration was very toxic to the microorganism. Besides that, hematite nanoparticle in nano-size provide high surface area promising the activity of microorganism during fermentative hydrogen production. The nano-size also performs a major function in providing the active site. Iron nanoparticles can help microorganism to transfer electrons to the acceptor that causes kinetic enhancement and improvement the microorganism activity (Engliman et al., 2017).

Besides Fe NPs and Fe₂O₃ NPs, magnetite nanoparticle (Fe₃O₄ NPs) is also one of metals oxide that is used for improving hydrogen production. Many researchers attempted to use Fe₃O₄ NPs with different substrate and inoculum. The use of 100 mg/L Fe₃O₄ NPs using wastewater as the substrate found that the highest hydrogen yield was 112.4 mg/g COD (Mostafa et al., 2016). Another study showed that the use of Fe₃O₄

NPs could improve hydrogen production by using glucose as a substrate under mesophilic condition. The maximum hydrogen production yield achieved at 1.53 mol H₂/ mol glucose (Zhao et al., 2011). Furthermore, Fe₃O₄ NPs was also applied for enhancing hydrogen production by using sugarcane bagasse as a substrate. The highest hydrogen production yield was 122 mol H₂/ mol glucose at optimum of 200 mg/L of Fe₃O₄ NPs. The Fe₃O₄ revealed higher concentration of hydrogen producing bacteria and hydrogenase enzyme (Reddy et al., 2017). Similarly, the influence of Fe₃O₄ NPs on biohydrogen production from distillery wastewater as the substrate found that the highest hydrogen production yield was achieved 257 mg/g COD at 50mg/L (Malik, Pugalenti, Vaidya, Ghosh, & Mudliar, 2014).

FeSO₄NPs was also used for enhancing hydrogen production by using sewage sludge as inoculum. The maximum hydrogen production yield increased from 158 to 217 mol H₂/ mol glucose at 200 mg/L (Zhang, Fan, & Zang, 2017). Another study found the effect of FeSO₄NPs on anaerobic hydrogen production using glucose as a substrate. The highest H₂ production yield reached to 296.2 mol H₂/ g starch at 55.3 mg/L concentration (Yang & Shen, 2006). FeSO₄NPs was applied for fermentative hydrogen production by using anaerobic sludge as an inoculum. The best concentration at 300 mg/L showed the highest hydrogen yield of 320 mol H₂/ mol glucose (Wang & Wan, 2008). In addition, the concentration at 73.7 mg/L of FeSO₄NPs could improve hydrogen production from cracked cereals as an inoculum. The maximum hydrogen production rate was 371mL. In a similar study, FeSO₄NPs was applied for promoting hydrogen yield from cracked cereals as inoculum. The highest hydrogen production yield was 2.73 mol H₂/mol sucrose at 589.5 mg/L (Zhang et al., 2005). Furthermore, two researcher studied the effect of FeSO₄NPs investigated on dark fermentation by using two types of pure culture such as *E. cloacae* and *C.butyricum* EB6 as the inoculum. At 25 mg/L and 300 mg/L FeSO₄NPs concentration provided maximum hydrogen production was 1.7 mol H₂/mol glucose (Mohanraj et al., 2014) and 2.24 mol H₂/ mol glucose (Chong et al., 2009), respectively. The iron and iron oxide NPs on the biohydrogen production is presented in **Table 2.4**

Table 2.4 The use of Fe, Fe₂O₃, Fe₃O₄ and FeSO₄ nanoparticles in batch biohydrogen production

Materials	Optimum dose (mg/L)	Substrate	Microbial inoculum	Operation conditions		Hydrogen yield mol H ₂ /mol substrate	Ref
				pH	Temp		
Fe NPs	5	Glucose	Anaerobic sludge	7	35	391 ^b	(Taherdanak et al., 2016)
	2.5	Glucose	Anaerobic sludge	-	35	1.62 ^b	(Hwang et al., 2019)
	25	Glucose	Anaerobic sludge	7	35	338 ^f	(Taherdanak et al., 2016)
	100	Glucose	<i>E. cloacae</i> DH-89	7	37	1.9 ^b	(Nath et al., 2015)
Fe ₂ O ₃ NPs	200	sucrose	Cracked cereals	8.48	35	3.21 ^a	(Han et al., 2011)
	200	sucrose	Cracked cereals	6	35	3.57 ^a	
	200	Distillery wastewater	Anaerobic sludge	5.5	37	8.83 ^e	(Gadhe et al., 2015b)
	50	Dairy wastewater		5.5	37	16.75 ^e	(Gadhe et al., 2015a)
	50	Glucose and starch	Anaerobic sludge	5.5	60	1.92 ^b	(Engliman et al., 2017)
	200	sucrose	<i>E. cloacae</i> 811101	7	37	5.44 ^a	(Sunderasan et al., 2014)
	200	Glucose	<i>E.aerogenes</i> ATCC13408	6	37	192.4 ^b	(Lin et al., 2016)
	Fe ₃ O ₄ NPs	100	wastewater	Sewage sludge	6	35	112.4 ^c

-	Glucose	Anaerobic sludge	7	35	1.53 ^b	(Zhao et al., 2011)
200	sugarcane	Anaerobic sludge	5	30	1.22 ^b	(Reddy et al., 2017)
50	Distillery wastewater	Anaerobic sludge	6	37	257 ^c	(Malik et al., 2014)
FeSO ₄ NPs 200	Glucose	Sewage sludge	7	37	217.4 ^b	(J. Zhang et al., 2017)
55.3	Starch	Anaerobic sludge	7	35	296.2 ^d	(Yang & Shen, 2006)
300	Glucose	Anaerobic sludge	7	35	302.3 ^b	(Wang & Wan, 2008)
73.7	sucrose	Cracked cereals	8	35	371.7 ^g	
25	Glucose	<i>E. cloacae</i>	8	37	1.7 ^b	(Mohanraj et al., 2014)
589.5	sucrose	Cracked cereals	7.4-7.6	35	2.73 ^a	(Zhang et al., 2005)
300	Glucose	<i>C.butyricum</i> EB6	5.5	37	2.24 ^b	(Chong et al., 2009)

^amol H₂/mol sucrose; ^bmol H₂/mol glucose; ^cmg/g COD; ^d mol H₂/ g starch; ^emmol/g COD; ^fmg/g

2.3.4 Hydrotalcites

Hydrotalcites and hydrotalcite-like compounds (HTLCs) or layered double hydroxides (LDHs), which are also known as anionic clays, which have been used in many fields are used as absorption, catalysis, biomedicine, separation, high ion-exchange capacity, acidic-basic buffering, capacity and environmental applications (Garcés Polo, Villarroel Rocha, Sapag, Korili, & Gil, 2018; Mishra, Dash, & Pandey, 2018; Zhou, Jiang, & Wei, 2018). The structure of HTs has various anions and cations such as Zn, Mg, Na and Fe which are necessary micro-elements for microbial activities (**Figure 2.4**). There are also few studies that used hydrotalcites to improve hydrogen production via dark fermentation. Different hydrotalcite materials were investigated. The effect of Fe-Zn-Mg-Al Hydrotalcite that ranged between 0 mg/L to 833 mg/L were studied and found that the optimum concentration was 167 mg/L using anaerobic sludge as an inoculum and sucrose as a substrate. The maximum hydrogen production was achieved up to 2.30 mol H₂/mol sucrose (Wimonsong et al., 2013). Furthermore, hydrotalcites named Ni-Mg-Al hydrotalcite was used in batch experiment using sucrose as substrate and anaerobic sludge as inoculum. The optimum concentration of 250 mg/L and the maximum hydrogen production yield achieved was 3.37 mol H₂/mol sucrose (Le & Nitisoravut, 2015). In another study (Wimonsong et al., 2014), Au/Zn-Mg-Al hydrotalcite was applied with the optimum concentration of 167 mg/L using anaerobic sludge as an inoculum and sucrose as a substrate. The maximum hydrogen production yield achieved was 2.74 mol H₂/mol sucrose. The higher concentration of hydrotalcite than the optimum concentration presented highly basic property that impeded the hydrogen production. Another reason is the interaction between hydrotalcite and hydrogen-producing bacteria. Hydrotalcites are layered double hydroxides with electrostatic charge sheet. The biohydrogen production was enhanced due to the presence of basic centers in hydrotalcites and bacteria being immobile in the interlaminar structure of HTs, which enables electron transfer and has better chance to contact with substrate (Le & Nitisoravut, 2015; Wimonsong et al., 2014).

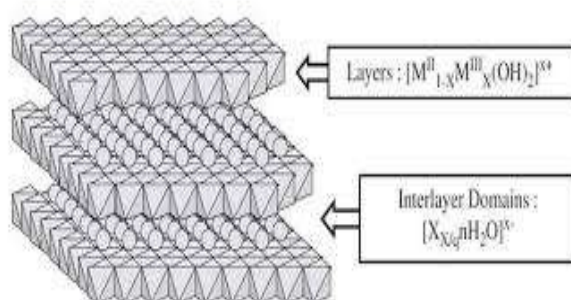


Figure 2.4 Structure of Hydrotalcite (Rahman, 2013)

2.3.5 Activated carbon

Activated carbon are mainly used for removing metals from wastewater; unwanted compounds from gases, vapors and liquid in the chemical industry; and remove pollutants in soil. This may associate with highly porous structure, large surface area and high adsorption capacity of activated carbon (Jamali, Jahim, Isahak, & Abdul, 2017; Kammerer, Kammerer, & Carle, 2014; Sabir, Zia ur Rehman, Hakeem, & Ullah, 2014). Activated carbon was also used in biohydrogen production to enhance hydrogen production (Wimonsong & Nitorisavut, 2014; C. Zhang et al., 2017). In dark fermentation, activated carbon was added into a system with optimum concentration of 200 g/L using cocultures as the inoculum. The highest hydrogen production yield was achieved at 1.203 mol H₂/mol (C. Zhang et al., 2017). Wimonsong and Nitorisavut (2014) found that the optimum loading of 33.0 mg/L activated carbon provided a good effect in enhancing hydrogen production yield to 2.60 mol H₂/mol sucrose and 73% as compared to control. The role of activated carbon provided high surface area where the microorganism could grow easily and freely as well as help to the sustain cell viability and enhance density (Jamali et al., 2017; C. Zhang et al., 2017). The function of activated carbon on biohydrogen production could provide a suitable matrix for cell and adherence and colonization, which enhances the hydrogen production yield. In addition, higher concentration of activated carbon could not transfer nutrients while lower concentration could not provide abundant matrix for higher cell density (C. Zhang et al., 2017). Activated carbon showed high activity to fermentative hydrogen production because activated carbon could adsorb the volatile fatty acids during process of hydrogen fermentation. In addition, increase in the length of non-polar hydrocarbon

chain can decrease the polar characteristic of fatty acid, thus improving the affinity between activated carbon and the acids (Wimonsong & Nitorisavut, 2014).

2.3.6 Nanocomposite of catalyst

The composite materials were found to have effect on the biohydrogen production process. For example, gold is very active catalyst, when gold combined with other support materials. It exhibits different performance during fermentation. The main factors that determines the performance of gold catalysts are the composition of support materials and the oxidation state of gold catalyst. In dark fermentation, Wimonsong et al. (2014) report that four different types of hydrotalcite supported Au catalysts were applied in the system. The best catalyst was Au/Zn Mg-Al hydrotalcite with optimum concentration of 167 mg/L using anaerobic sludge as an inoculum and sucrose as a substrate. The maximum hydrogen production yield was achieved up to 2.74 mol H₂/mol sucrose (Wimonsong et al., 2014). Zn was very highly active site especially when combined with Au nanoparticle. Enhancement could be due to combination effect of metabolic dispersion of Au on Au/Zn-Mg-Al hydrotalcites. Zinc is an important trace element for most microorganisms as it can act as bridge between enzymes and substrate. Zinc is also found to be the active sites of several enzymes such hydrogenase. Au catalyst is an electron sinks at active site, which a highly affinity for electrons transfer and allowed further reduction of protons to hydrogen. Elreedy et al. (2017) found that when using Nickel-graphene nanocomposite as catalyst with the optimum concentration of 60 mg/L using mixed culture as the inoculum and wastewater as the substrate, the maximum hydrogen production yield reached to 41.28 mg/g COD. The effect of nickel-graphene nanoparticle on biohydrogen production showed that nickel nanoparticles and the microorganism being immobilized on graphene, which provides a uniform dispersion of nickel nanoparticles (Elreedy et al., 2017).

The use of 600 mg/L biochar combined with 400 mg/L Fe⁰ nanoparticle showed the highest hydrogen production yield achieved was 50.6 mL/g dry grass (*Lolium perenne* L), which was 89.8% higher than control (Yang & Wang, 2019). The role of this nanoparticle could improve hydrogen production by reducing lag time and enhance the microorganism in the system especially *Clostridium* species. Mishra et al. (2019)

reported that the effect of Ni/Co oxide nanoparticle was investigated using palm oil mill effluent (POEM) as a substrate. The best performance was observed at ratio of 3:1 (Ni/Co). The maximum hydrogen production rate and COD removal was 45mL/h and 94%, respectively (Mishra et al., 2019). Fe₂O₃ NPs is also co-addition with other catalyst. For example, Gadhe et al. (2015b) used Fe₂O₃ to ferment distillery wastewater combined with NiO NPs and found that the highest hydrogen production yield from distillery wastewater was 17.2 mmol/g COD. Fe₂O₃ + NiO NPs was also used for enhancing hydrogen production from dairy wastewater. The maximum hydrogen production yield achieved 3.75 mmol/g COD (Gadhe et al., 2015a). **Table 2.5** shows the nanocomposite of catalyst use for biohydrogen production.

Table 2.5 The use of combination catalyst in batch biohydrogen production

Catalyst	Optimum dose (mg/L)	Substrate	Microbial inoculum	Operating conditions		Hydrogen yield (mol H ₂ /mol substrate)	Ref
				pH	Temp		
Au/Zn-Mg-Al	167	Sucrose	Anaerobic sludge	5.5	37	2.74 ^a	(Wimonsong et al., 2014)
Ni-Gr NPs	60	wastewater	Anaerobic sludge	5	55	41.82 ^b	(Elreedy et al., 2017)
Biochar+Fe ⁰	600+400	Grass (<i>Lolium perenne</i> L)	Anaerobic sludge	7	37	56.6 ^c	(Yang & Wang, 2019)
Ni + Co oxide	2.5+7.5	Palm oil	<i>Bacillus anthracis</i> PUNAJAN 1	6.5	35	1.9 ^b	(Mishra et al., 2019)
Fe ₂ O ₃ +NiO NPs	200 + 5	Distillery wastewater	Anaerobic sludge	5.5	37	17.2 ^d	(Gadhe et al., 2015b)
	50+10	Dairy waste water	Anaerobic sludge	6	35	3.57 ^d	(Gadhe et al., 2015a)

^a mol H₂/mol sucrose; ^b mg/g COD; ^c mg/g dry grass; ^d mmol/g COD

Table 2.6 The possible roles of catalysts in biohydrogen production

Catalyst	Activities	Ref
Hydrotalcites	Buffering and cell immobilization	(Le & Nitorisavut, 2015; Wimonsong et al., 2013; Wimonsong et al., 2014)
Au nanoparticle	Electron sink	(Zhang & Shen, 2007)
Activated carbon	Adsorbent	(Wimonsong & Nitorisavut, 2014)
Cu and Ag nanoparticles	Antimicrobial activities	(Mohanraj et al., 2016; Zhao et al., 2013)
Fe ₂ O ₃ nanoparticle	Cell immobilization on FeCO ₃ sediment by sorption	(Wang & Wan, 2009; Zhang & Shen, 2006)
Ni nanoparticle	Micronutrient and enzyme	(Gou et al., 2015; Le & Nitorisavut, 2015)
Zn	Active site	(Wimonsong et al., 2014)

CHAPTER 3

MATERIALS AND METHODS

3.1 Materials

3.1.1 Inoculum

The inoculum was collected from an up-flow anaerobic sludge blanket (UASB) reactor from a brewery company in Thailand. The anaerobic sludge was pre-treated at 105°C for 30 minutes to inhibit the activity of methanogens prior to use as an inoculum.

3.1.2 Substrate

Sucrose (20g/L) was used as a carbon source for bacteria. The nutrient solution was comprised of NH_4HCO_3 (160 mg/L), KH_2PO_4 (80 mg/L), $\text{FeCl}_2 \cdot 4\text{H}_2\text{O}$ (70.5 mg/L), $\text{MgSO}_4 \cdot 7\text{H}_2\text{O}$ (4 mg/L), NaCl (0.4 mg/L), $\text{MnSO}_4 \cdot 7\text{H}_2\text{O}$ (0.6 mg/L), $\text{Na}_2\text{MoO}_4 \cdot 2\text{H}_2\text{O}$ (0.4 mg/L) and $\text{CaCl}_2 \cdot 2\text{H}_2\text{O}$ (0.4mg/L).

3.1.3 Commercial activated carbon

Commercial activated carbon (CAC) was obtained from the Carbokarn Co., Ltd. It was made from coconut shell and consists of granules. The activated carbon was sieved to approximately 1 mm particles size. Commercial activated carbon was modified by the impregnation method using H_3PO_4 . The ratio of commercial activated carbon to concentrated H_3PO_4 was 1:1(w/w). The acid solution was prepared with 14 mL of H_3PO_4 (85% W/V) diluted to 150-mL. Commercial activated carbon (20g) was soaked in the H_3PO_4 solution and shaken at 90 rpm for 12 h. The mCAC were then heated at temperatures of 400°C, 500°C, 600°C, 700°C, 800°C and 900°C under N_2 atmosphere for 1 h. After the heating process, it was washed with distilled water until pH 7 and dried at 105°C for 24 h.

3.1.4 Hydrotalcites

HT (Zn-Ni-Mg-HT) with the molar of $\text{M}^{2+}/\text{M}^{3+}$ 3:1 ($\text{M}^{2+} = \text{Zn}, \text{Ni}$). Modified HT with Zn^{2+} and Ni^{2+} was synthesized by co-precipitation method. The ratio of hydrotalcite was showed in the **Table 3.1**.

Table 3.1 The ratio of HT

Hydrotalcie	M ²⁺ : Mg ²⁺ : Al ³⁺	
	Atomic ratio	Formula
Zn-Ni-Mg-Al-HT	0.25:0.25:2.5:1	[Zn _{0.25} Ni _{0.25} Mg _{2.5} Al(OH) ₈](CO ₃) _{0.5} ·2.5H ₂ O

Table 3.2 Hydrotalcites preparation and loading methods

Solution	MW (g/mol)	Molar	g of chemical in 6 mL of water
Zn-Mg-Al HT			
Mg (NO ₃) ₂ ·6H ₂ O	256.4070	0.75	1.17
Zn (NO ₃) ₂ ·6H ₂ O	297.1700	0.075	0.13
Al (NO ₃) ₃ ·9H ₂ O	357.1345	0.15	0.34
Ni-Mg-Al HT			
Mg (NO ₃) ₂ ·6H ₂ O	256.4070	0.75	1.17
Ni (NO ₃) ₃ ·6H ₂ O	290.7949	0.075	0.13
Al (NO ₃) ₃ ·9H ₂ O	357.1345	0.15	0.34

3.1.5 Activated carbon supported HT

Activated carbon was used as a support for HT to explore the possible enhancement of fermentative hydrogen production. Activated carbon supported HT was prepared by the incipient impregnation method. The Zn-HT solution was prepared using 0.13 g of Zn(NO₃)₂·6H₂O, 1.17 g of Mg(NO₃)₂·6H₂O and 0.34 g of Al(NO₃)₃·9H₂O in 6-mL of water. Likewise, Ni-HT solution was prepared using 0.13 g of Ni(NO₃)₃·6H₂O, 1.17 g of Mg(NO₃)₂·6H₂O, and 0.34 g of Al(NO₃)₃·9H₂O in 6-mL of water. The 6-mL Zn-HT solution was added dropwise to 6 g of activated carbon under continuous mixing. Then, the samples were dried in an oven at 60°C for 1 h. After that, the mixture was dried at 105°C for 3 h. Similarly, these processes were also applied to Ni-HT. Then, a 6-mL mixed solution of NaOH (2.25 M) and Na₂CO₃ (0.45 M) was

prepared and co-precipitated by adding dropwise onto the activated carbon. Aging was performed in an autoclave at 60°C for 24 h. The samples were then dried at 60°C for 4 h, washed with distilled water until pH 7 was obtained, and dried at 105°C for 24 h.

3.1.6 Volatile fatty acid solution

The mixed of VFA solution was prepared at concentration of 1000ppm by diluted laboratory grade 99.5% acetic acid, 99% butyric acid, 85% lactic acid and 99.5% propionic acid with distilled water.

3.2 Methodology

3.2.1 Experimental procedures

3.2.1.1 Fermentative hydrogen production

Batch experiments were conducted in 120-mL serum bottles. The optimum concentration of catalyst was determined by adding the CAC, mCAC, activated carbon supported HT at a concentration of 8.33g/L to the fermentation mixture, comprised of 5-ml nutrient solution, 10-mL solution pre-treated sludge, and 45-mL of the substrate. The control samples were without activated carbon supported HT. The initial pH was adjusted to 5.5 by using NaOH (1N) or HCl (1N). The bottles were capped with butyl rubber stoppers and sealed with aluminum crimps. To create anaerobic conditions, the bottles were sparged with nitrogen for 3 minutes. To prevent the activities of photosynthetic bacteria, the serum bottles were wrapped with aluminum foil. Finally, the serum bottles were cultivated in an incubated shaker under mesophilic conditions at 37°C and shaken at 90 rpm. The amounts of produced gases were measured by syringes at room temperature. The compositions of gases were determined by a gas chromatograph. After 240 h of fermentation, mixed liquor samples were drawn to determine the volatile fatty acids (VFAs), metal leaching and pH.

3.2.2 Catalytic activity of activated carbon supported HT

3.2.2.1 Volatile fatty acid adsorption

The serum bottles with working volume of 60mL contained 0.5g of catalysts and 60mL of VFAs solution. Then, the serum bottles were shaken at 90 rpm under mesophilic conditions at 37°C. The mix liquor was collected for VFAs analysis periodically at 15min, 30min, 1h, 3h, 5h, 7h, 9h, 22h, 24h, 48h and 72h.

3.2.2.2 Catalysts recyclability

After fermentation and there was no gas produced, 50-mL of supernatant was withdrawn. It was then added with 45-mL of sucrose and 5-mL of nutrient in each bottle. The pH was adjusted to 5.5. The bottles were capped with butyl rubber stoppers and seal with aluminum crimps and purged with nitrogen gas for 3 minutes. The serum bottles were covered with aluminum foil to prevent sunlight. Finally, the samples were shake at 90 rpm, 37°C. The experiments were repeated for 3 cycles.

3.2.3 Analytical methods

3.2.3.1 Commercial activated carbon supported HT characterization

The characteristics of commercial activated carbon supported HT were analyzed by nitrogen adsorption isotherms (surface area analyzer, BET), and the morphologies of the activated carbon supported HT were examined by a field emission scanning electron microscope (FESEM) at the Center of Scientific Equipment for Advanced Research, Thammasat University, Thailand. Fourier transform infrared spectroscopy (FTIR) was used to determine the functional groups. FTIR spectra were recorded on a 6700 spectrophotometer at ambient temperature using the potassium bromide (KBr) disk method. All samples were prepared from a disk containing 0.001 g of sample mixed with 0.1 g of potassium bromide (KBr). The spectra were recorded at 4 cm⁻¹ resolution for a total of 32 scans with wavenumbers ranging from 400 to 4000 cm⁻¹. The structure of HT was analyzed by X-ray diffraction (XRD) at the National Nanotechnology Center, Thailand.

3.2.3.2 Determination of gas compositions

The gas compositions were analyzed by a gas chromatograph (Pierkin Elmer, model AutoSystem XL, USA) fitted with PorapakQ column 50/80 mesh column. The operating of injector, column and detector were 100°C, 45°C, and 100°C, respectively. Helium was used as at the carrier gas at a flow rate of 25 mL/min. The 50 µL of biogas production volume was collected by using syringe.

After the biogas was injected, the volume of biogas was measured by using 50 mL syringe.

3.2.3.3 Determination of metals

Inductively couple plasma atomic emission spectrometry (ICP-OES) was used to determine metals concentration. The samples were taken and filtered before analyses.

3.2.3.4 Determination of VFAs

The concentration of volatile fatty acids particularly acetic acids, butyric acids, propionic acid and lactic acid were determined by a high-performance liquid chromatograph (HPLC) (Agilent 1200 infinity series) equipped with Vertisept™ OA column, 8 µm, 7.8 × 300 mm at 35°C. Sulfuric acid 0.01 N at flow rate of 0.8 ml/min was used as a mobile phase. Prior to analyses, the supernatants of the sample were filtered through a 0.2 µm millipore membrane.

3.2.3.5 Kinetic modeling

The modified Gompertz model was used for fermentative hydrogen production, to describe the progress of a batch fermentative hydrogen production process and to establish the relationships among the substrate degradation rate, the hydrogen-producing growth rate, and the product formation rate. The equation can be expressed as:

$$H = H_{\text{maz}} \cdot \exp \left\{ -\exp \left[\frac{R_m \times e}{H_{\text{max}}} (\lambda - t) + 1 \right] \right\} \quad (3.1)$$

Where H and H_{max} are the cumulative hydrogen production (mL) and the maximum cumulative hydrogen production (mL). R_m is the maximum hydrogen production rate (mL/h); λ , t and e are Lag-phase time (h), Cultivation time (h) and Euler's constant (2.718), respectively.

3.2.3.6 Langmuir adsorption isotherm

Langmuir isotherm is widely used for modeling adsorption data to describe the relationship between the amount of fatty acid adsorbed and the corresponding equilibrium concentration. The Langmuir model considers the formation of a monolayer during the sorption onto the homogeneous surface plane. The equation can be expressed as:

$$\frac{1}{q_e} = \frac{1}{Q_0} + \frac{1}{Q_0 b C_e} \quad (3.2)$$

Where

C_e = The equilibrium concentration of adsorbate (mg/L).

q_e = The amount of adsorbed per gram of the adsorbent at equilibrium (mg/g).

Q_0 = The capacity of adsorption (mg/g).

b = Langmuir isotherm constant (L/mg).

The values of q_{\max} and b were computed from the slope and intercept of the Langmuir plot of $\frac{1}{q_e}$ versus $\frac{1}{C_e}$. The essential features of the Langmuir isotherm maybe expressed in terms of equilibrium parameters.

3.2.3.7 Freundlich adsorption isotherm

Freundlich model is used for monolayer accumulation onto heterogeneous surfaces or multilayer adsorption onto a surface of adsorbent. The equation can be expressed as:

$$\text{Log} q_e = \text{Log} k_F + \frac{1}{n} \text{Log} C_e \quad (3.3)$$

C_e = The equilibrium concentration of adsorbate (mg/L).

q_e = The amount of adsorbed per gram of the adsorbent at equilibrium (mg/g).

K_F = The capacity of adsorption (mg/g).

n = Freundlich equilibrium coefficient.

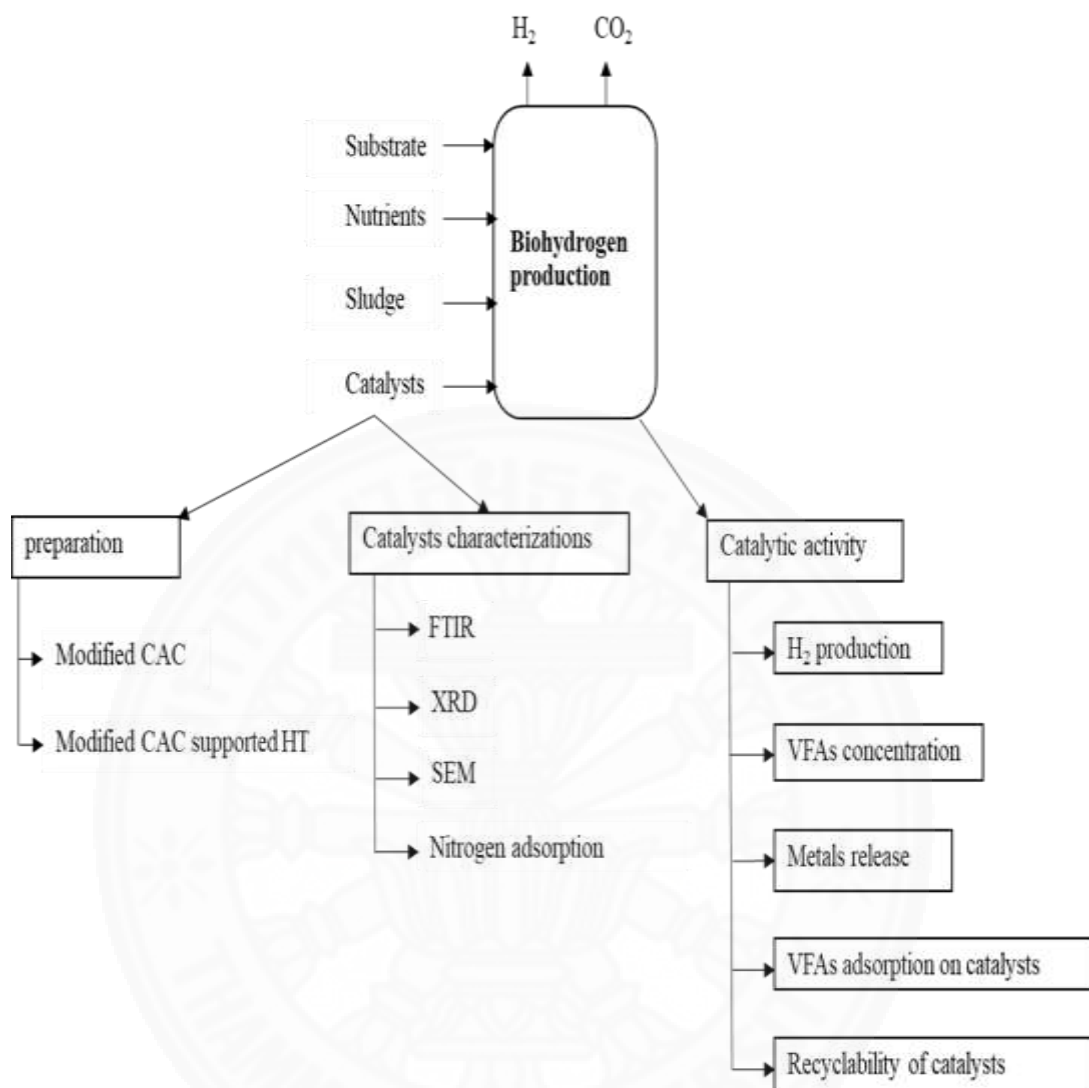


Figure 3.1 Overall of experimentation analyses

CHAPTER 4

RESULTS AND DISCUSSION

4.1 Modified activated carbon characterizations

4.1.1 Functional groups

FTIR was used to characterize the structure and functional groups of materials. **Figure 4.1** shows FTIR spectra region 400-4000 cm^{-1} of CAC and modified CAC (400°C, 500°C, 600°C, 700°C, 800°C and 900°C). The spectra show alike peaks with and without modification. The broad band and strong absorption line at 3570-3200 cm^{-1} represents hydroxyl group (O-H stretching), while 2370 cm^{-1} is attributed to CO_2 (CO_2 stretching). The band at 1500-1650 cm^{-1} is assigned to C=C aromatic ring stretching. The band at 1200 cm^{-1} represents C-C and C-O vibration in alcohols, ethers and phenols. The peak from 700 to 800 cm^{-1} is assigned to the presence of C-H out of plane bending in benzene derivatives.

However, after H_3PO_4 activation, some phosphate compounds were left on the activated carbon surface. The bands at 900-1300 cm^{-1} are assigned to phosphorous species. The band around 1275 cm^{-1} is assigned to the stretching mode of hydrogen-bonded P=O, C-O stretching vibration in the P-O-C aromatic linkage, and P=OOH. The band around 1100 cm^{-1} is attributed to be the P=O bond. The peak around 1000 cm^{-1} is assigned to ionized linkage the $\text{P}^+ - \text{O}^-$ in acid phosphate esters (Chen, Zhang, He, Lu, & Xv, 2019; Sun, Yang, Zhang, Wang, & Yao, 2012; Yakout & Sharaf El-Deen, 2016). mCAC900 did not change the functional group due to the volatilization of different of p-containing compound and elemental phosphorous (P_4). The modification also caused the chemical changes with adding of phosphate functional groups, which could affect hydrogen production. H_3PO_4 is high oxygen-containing functional groups, which was creator the pore of the activated carbon. **Table 4.1** provides the functional groups that presence in the structure of mCAC.

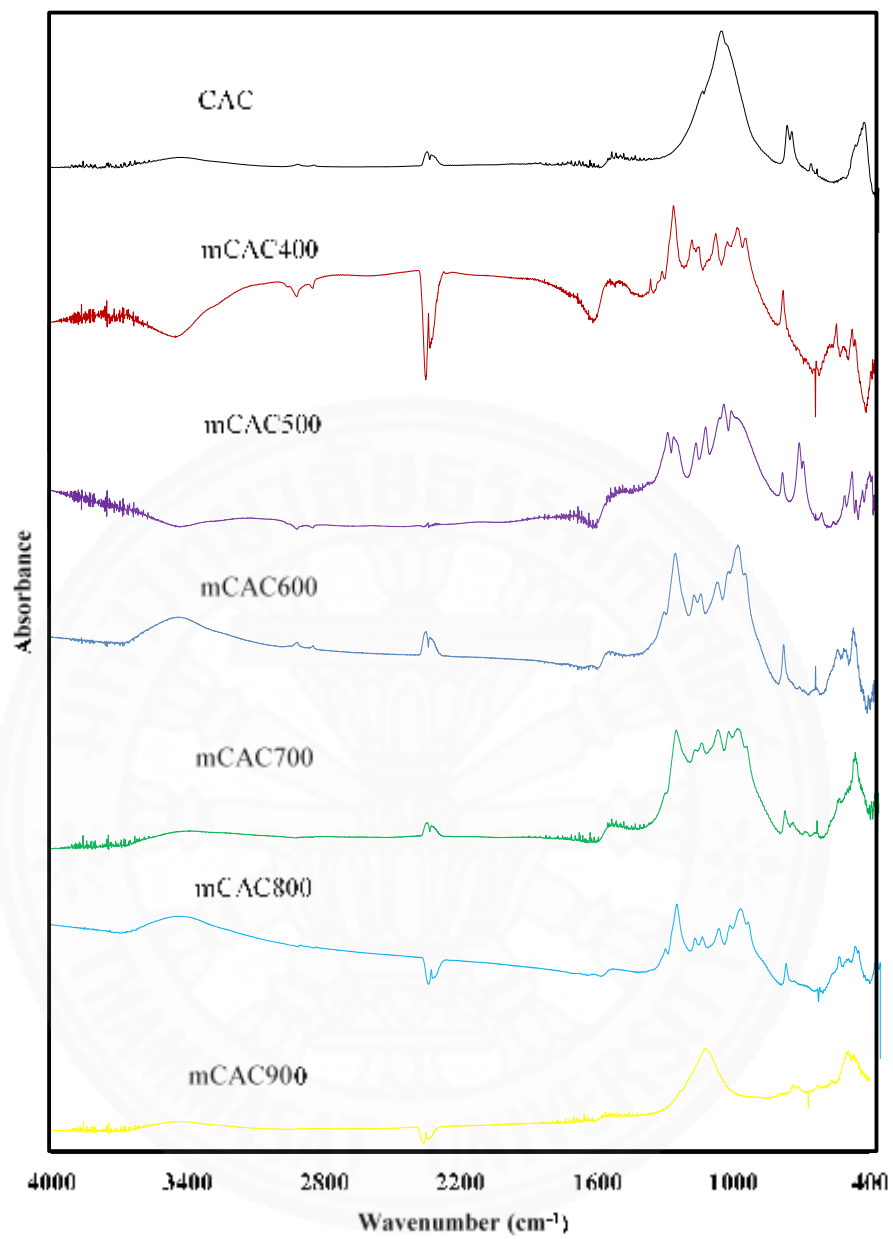


Figure 4.1 FTIR spectra for CAC and modified CAC

Table 4.1 The possible functional groups present on CAC and mCAC

Band position (cm ⁻¹)							Possible assignments
CAC	mCAC400	mCAC500	mCAC600	mCAC700	mCAC800	mCAC900	
3443.3	3446.1	3449.4	3453.5	3420.6	3439.1	3435.0	Hydroxyl group (O-H stretching),
2378.8	-	-	2370.6	2362.4	2366.5	2364.4	CO ₂ (CO ₂ stretching)
1571.2	-	-	1585.6	1577.4	1591.7	1567.1	C=C aromatic ring stretching
-	1285.0	1290.2	1275.3	1283.5	1283.5	-	Hydrogen-bonded P=O,
-	1190.8	1181.81	1199.30	1203.4	1205.4	-	P-O-C aromatic, P=OOH
-	1070.9	1011.9	1098.6	1100.6	1100.6	-	P=O bond
-	1033.1	975.1	1010	1024	1012	-	Ionized linkage P ⁺ -O ⁻ in acid phosphate esters
1084.2	-	-	-	-	-	1115.0	C-C and C-O vibration in alcohols, ethers and phenols
802.6	816.8	813.4	806.8	808.8	806.9	738.9	C-H out of plane bending in benzene derivatives

Table 4.2 shows the functional groups of mCAC supported Zn-Ni-HT. The functional groups of all materials were not destroyed by the impregnation method. The spectra show almost nearly peaks as before the impregnation method. The peak around 1556 cm^{-1} is assigned to H_2O (Thi Hong Le & Nitorisavut, 2015; Wimonsong et al., 2013; Wimonsong et al., 2014). The band around 1384 cm^{-1} is assigned to carbonate the (CO_3^{2-}) group. The peak around $400\text{-}800\text{ cm}^{-1}$ is assigned to the metal oxide group (**Figure 4.2**).

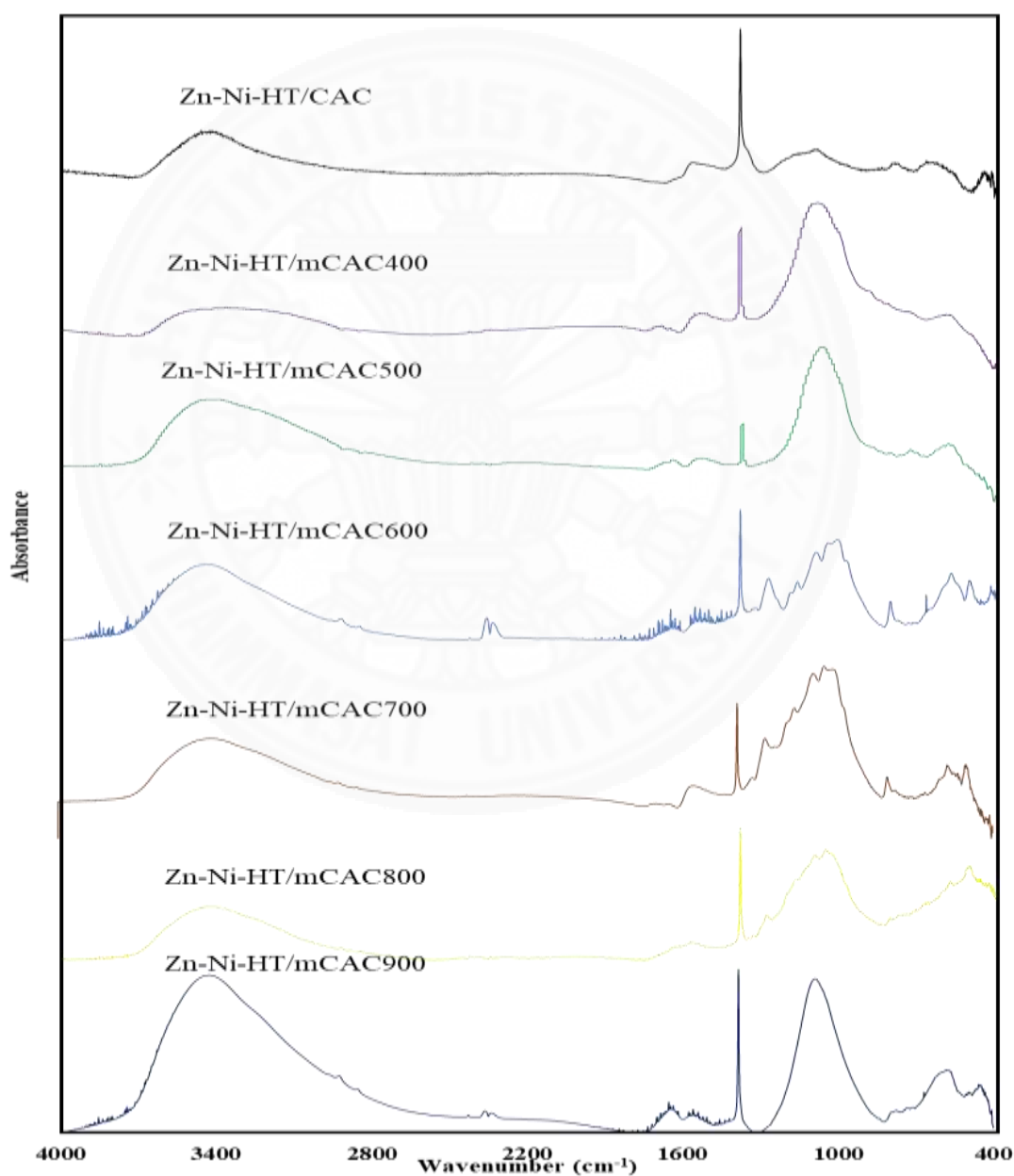


Figure 4.2 FTIR spectra of modified CAC supported HT

Table 4.2 The functional groups present in modified CAC supported HT

Band position (cm ⁻¹)							Possible assignments
Zn-Ni-HT/CAC	Zn-Ni-HT/mCAC400	Zn-Ni-HT/mCAC500	Zn-Ni-HT/mCAC600	Zn-Ni-HT/mCAC700	Zn-Ni-HT/mCAC800	Zn-Ni-HT/mCAC900	
3461.68	3445.37	3445.1	3480.9	3399.98	3396.68	3427.46	hydroxyl group (O-H stretching),
1566.05	1550	1523	1506.3	1557.88	1591.79	1558.70	C=C aromatic ring stretching
1384.11	1384.42	1387.78	1384.14	1384.13	3184.14	1384.13	Carbonate (CO ₃) group
-	-	-	1275.21	1275.97	1283.55	-	hydrogen-bonded P=O, P-O-C aromatic, P=OOH
-	-	-	1163.53	1203.40	1205.46	-	
-	-	-	1091.39	1100.60	1100.66	-	P=O bond
-	-	-	1007.67	1024	1012	-	ionized linkage P ⁺ -O ⁻ in acid phosphate esters
1084.22	1101.99	1085.79	-	-	-	1085.55	C-C and C-O vibration in alcohols, ethers and phenols
569	573.9	594.1	400-800	400-800	400-800	400-800	Metal oxide

4.1.2 Surface area and pore volume

Commercial activated carbon may vary in properties and qualities, depending upon the carbon precursors and activation processes. The specific surface area is typically from 500 to 1,500 m²/g (Lopes, Carvalho, Brasil, Mendes, & Lima, 2015). Re-activation using H₃PO₄ was implemented to refresh the properties of CAC and remove impurities such as acids, alcohols, and other chemical compounds contained in the pores. Thus, the pores became open, leading to an increase in pore sizes. Moreover, the re-activation could improve the properties of the surface by increasing the adsorption capacity (Arneli et al., 2017). As reported by many researchers, this process could increase the specific surface area by up to 15% (**Table 4.3**).

As this study incorporated not only H₃PO₄ activation but also heat treatment, the modifications caused a decrease in specific surface area by up to 98%. This almost destroyed the porous structure of CAC. A decrease in the specific surface area as a result of heat treatment was also observed by Martinez Castillejo et al. (2014). However, the consequences were more severe in this study. This indicated the negative impact of heat treatment on the specific surface area of CAC, as it physically destroyed the porous structure, resulting in a pore volume reduction from 0.26 to 0.05 cm³/g. Anisuzzaman et al. (2015) also reported a loss of weight, shrinkage of the carbon structure, and a porosity reduction for temperature above 500°C.

When the CAC was impregnated with Zn-Ni-HT, the specific surface area was slightly decreased. This was possibly due to the nanosized HT which blocked the pores of CAC, causing a reduction in the specific surface area (Foungchuen, Pairin, & Phalakornkule, 2016; Wimonsong et al., 2014). When mCAC600 was impregnated with Zn-Ni-HT, the specific surface area was nearly the same as Zn-Ni-HT/CAC. This indicated that the specific surface area was mainly contributed by HT as the porous structure of CAC and mCAC was blocked and destroyed.

Table 4.3 Surface area and pore distribution of mCAC and modified CAC supported HT

Samples	(S_{BET}) area (m²/g)	Average Pore size (nm)	V total (cm³/g)	V micro (cm³/g)	V meso (cm³/g) [by difference]	Ref.
CAC	645	1.60	0.26	0.25	0.010	This study
mCAC400 (H ₃ PO ₄ , 400°C)	54	1.82	0.03	0.02	0.002	
mCAC500 (H ₃ PO ₄ , 500°C)	109	1.77	0.05	0.04	0.005	
mCAC600 (H ₃ PO ₄ , 600°C)	15	2.31	0.01	0.01	0.002	
mCAC700 (H ₃ PO ₄ , 700°C)	98	1.71	0.04	0.04	0.003	
Zn-Ni-HT/CAC	437	1.67	0.30	0.17	0.130	
Zn-Ni-HT/mCAC600 (H ₃ PO ₄ , 600°C)	431	1.66	0.18	0.17	0.010	
CAC	659	-	-	-	-	(Eustáquio et al., 2015)
mCAC (H ₃ PO ₄)	711	-	-	-	-	
CAC Granular	856	-	0.38	0.34	0.04	(Carvajal Bernal et al., 2015)
mCAC Granular (H ₃ PO ₄)	857	-	0.39	0.32	0.07	
CAC Pellet	1040	-	0.52	0.37	0.15	
mCAC Pellet (H ₃ PO ₄)	1142	-	0.58	0.44	0.14	
CAC Cloth	1235	-	0.62	0.50	-	(Martinez Castillejo et al., 2014)
mCAC Cloth (H ₃ PO ₄ , 350°C)	995	-	0.60	0.58	-	
mCAC Cloth (H ₃ PO ₄ , 550°C)	885	-	0.40	0.42	-	

4.1.3 Structure of hydrotalcite

The XRD profiles of the CAC and mCAC supported HT are shown in **Figure 4.3**. The diffraction peak at 2θ at 23° can be attributed to the structure of activated carbon (Liu et al., 2010). The peak at 2θ of 43° and 62° correspond to NiO (200) and NiO (220) (Rakshit et al., 2013; Srivastava & Srivastava, 2010). The peak at 2θ of 31° , 34.5° and 36.3° , which have been identified as Zinc oxide (ZnO) could be indexed to (100), (002) and (101), respectively (Yedurkar, Maurya, & Mahanwar, 2016). The XRD patterns confirmed the existence of Zn and Ni ions, which were the components of hydrotalcite used in this study.

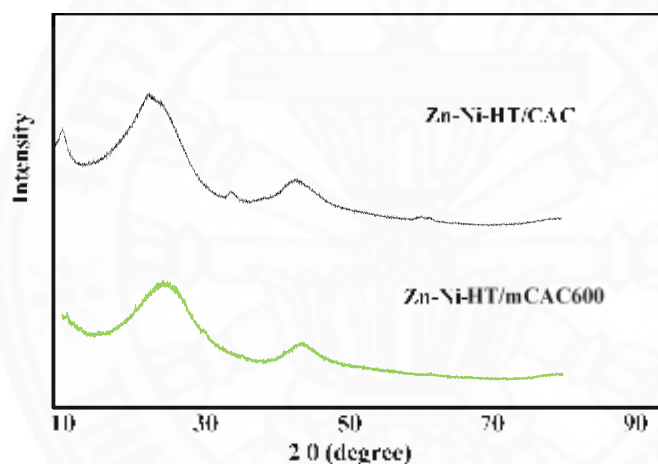


Figure 4.3 XRD pattern of Zn-Ni-HT/CAC and Zn-Ni-HT/mCAC600

4.1.4 Morphology and porosity

FESEM was applied to observe the morphology and pore size of activated carbon (**Figure 4.4**). Generally, FESEM observations of mCAC in terms of porosity structure and size are easier and traceable. The surface of the mCAC is not smooth and full of cavities. On the surface of the mCAC is full of small particles. This may probably be due to the H_3PO_4 and the temperature caused destroyed the pore and surface area. The modifications of CAC by H_3PO_4 and heat treatments caused physical changes through the loss of the porous structure.

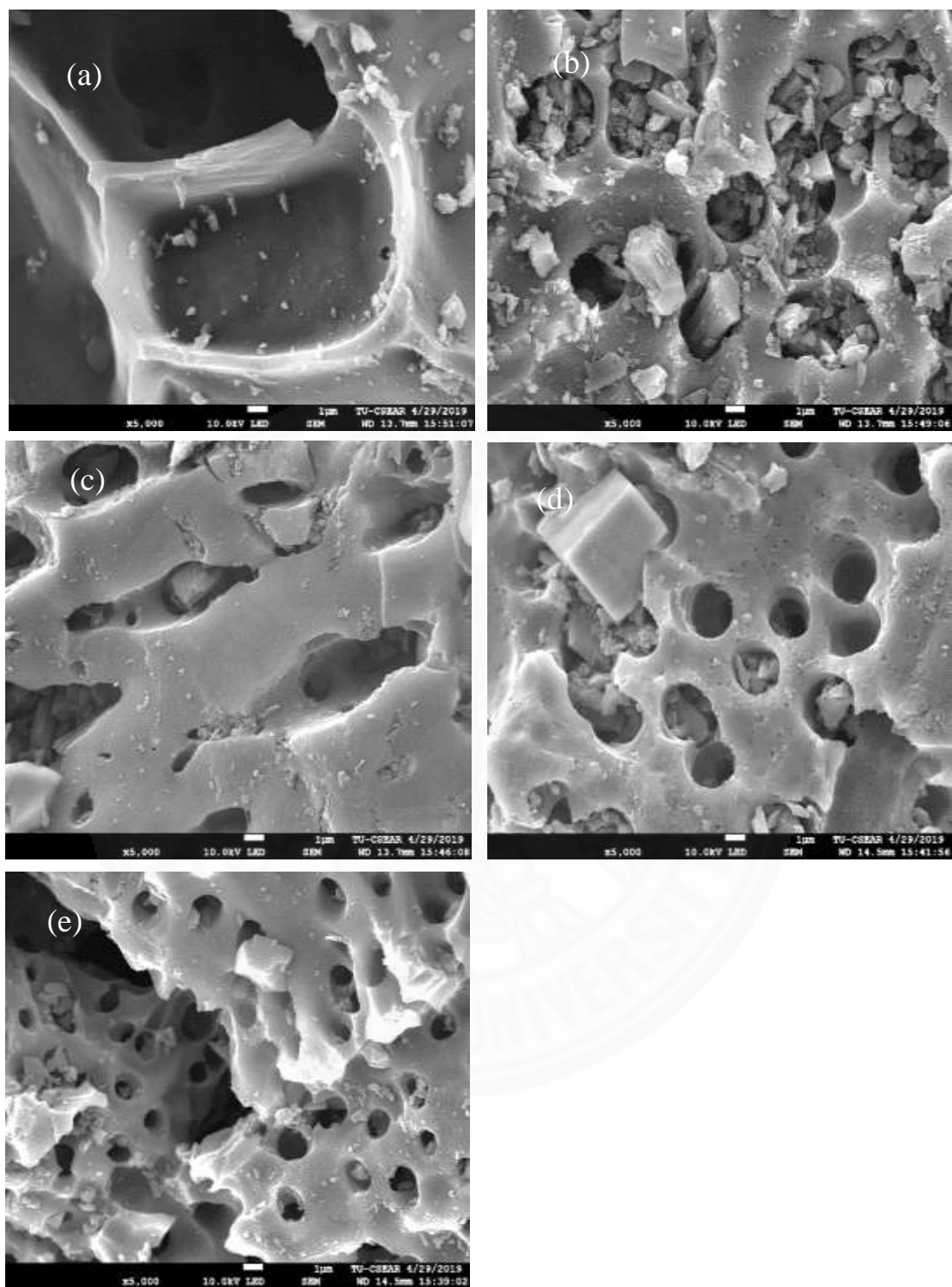


Figure 4.4 FESEM image of mCAC: (a) CAC, (b) mCAC400, (c) mCAC500, (d) mCAC600 and (e) mCAC700

Figure 4.5 shows the morphology and porosity structure of Zn-Ni-HT/CAC and Zn-Ni-HT/mCAC600. Examinations of Zn-Ni-HT/CAC and Zn-Ni-HT/mCAC600 showed that very small platelets and some large aggregates composed particles of hydroxalcalcite was formed within cavities on the surface of the activated carbon.

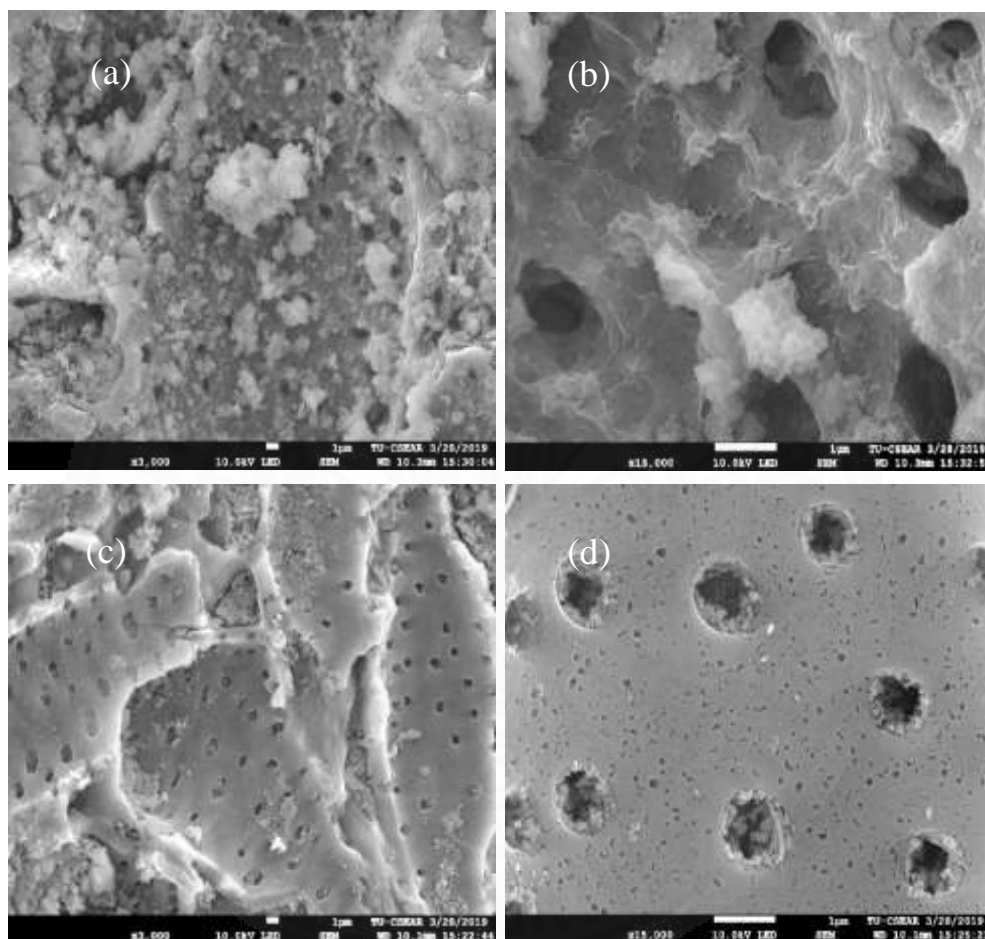


Figure 4.5 FESEM images of Zn-Ni-HT/CAC: (a) $\times 3000$, (b) $\times 15,000$ and Zn-Ni-HT/mCAC600: (c) $\times 3000$, (d) $\times 15,000$

4.2 Effect of modified commercial activated carbon on biohydrogen production

Commercial activated carbon was modified using H_3PO_4 as a chemical activation agent and heated at different temperature at $400^\circ C$, $500^\circ C$, $600^\circ C$, $700^\circ C$, $800^\circ C$ and $900^\circ C$. **Figure 4.6** shows the daily volumetric hydrogen production. The initial activity of mCAC600 was more active than other materials added during 72 h. After that, the hydrogen production decreased along with the pH. The temperature above $600^\circ C$ showed very poor hydrogen production rate, especially $800^\circ C$ and $900^\circ C$

(**Figure 4.6**). However, the temperature below 600°C (mCAC400 and mCAC500) showed better performance as compared to mCAC700, mCAC800 and mCAC900). The temperatures continuous to increase the temperature practically 700 to 900°C was mainly caused the weight loss by volatilization of phosphorous compounds. Similar with the low temperature (400-500°C). This possible reason the modification of CAC by H₃PO₄ at temperature above 600 did not show a good effect on biohydrogen production.

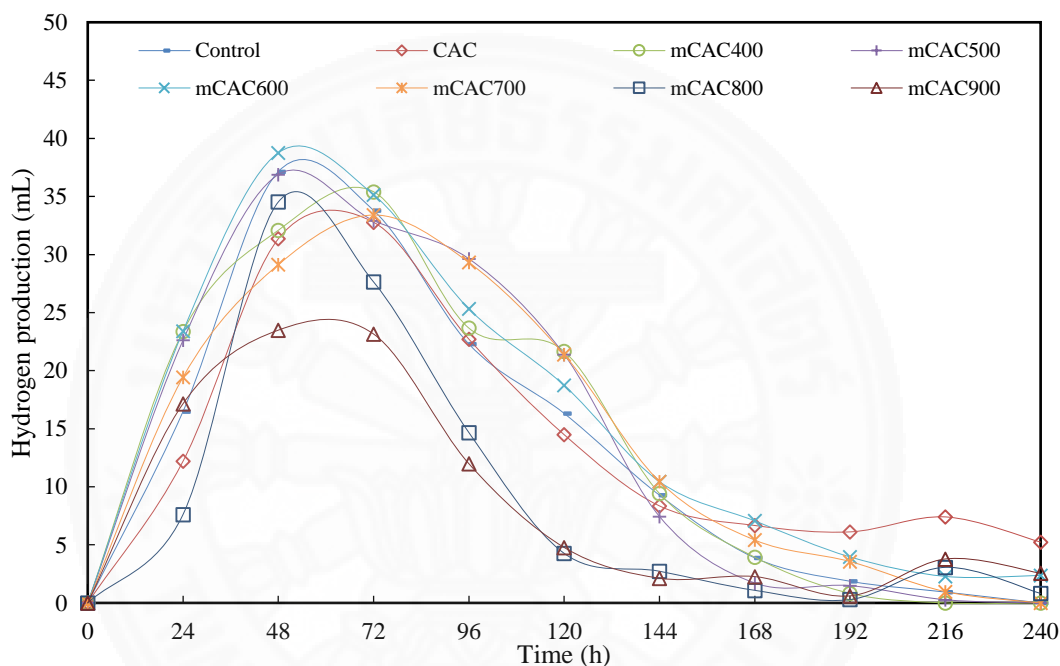


Figure 4.6 Hydrogen production of modified CAC in dark fermentation

The addition of supporting materials resulted in a higher hydrogen production yield and rate, as compared to control (no added supporting material). **Figure 4.7** shows the highest cumulative hydrogen production was observed for mCAC600 about 168 ml which was 17% higher than the control (**Figure 4.8**). The lowest cumulative hydrogen production was observed at 97 and 92 ml of mCAC800 and mCAC900, respectively. The addition of CAC and mCAC increased the hydrogen production yield.

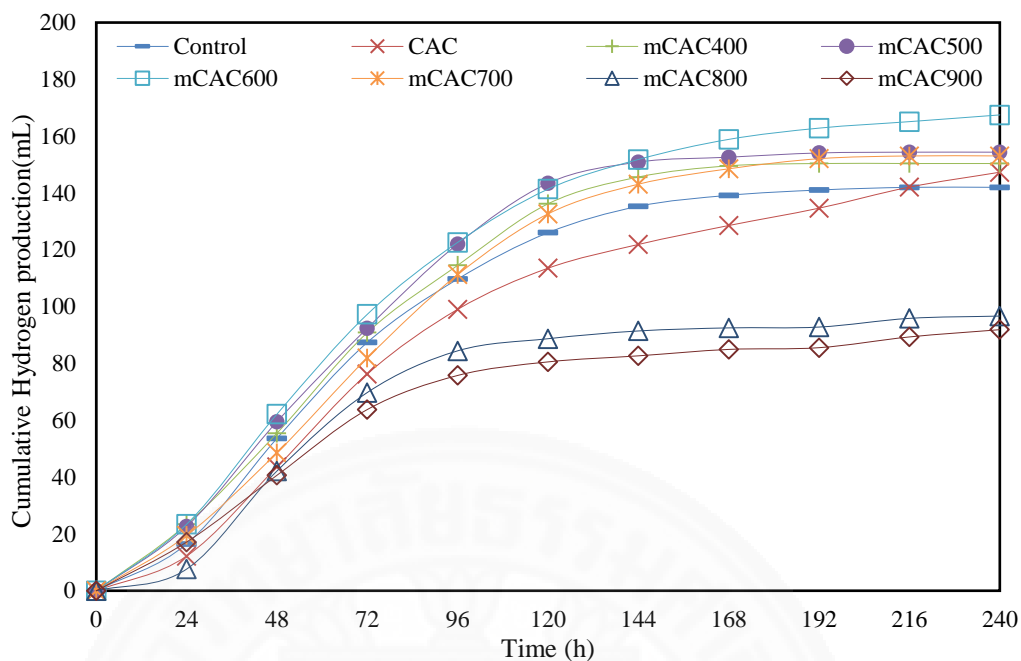


Figure 4.7 Cumulative hydrogen production yield of the modified CAC

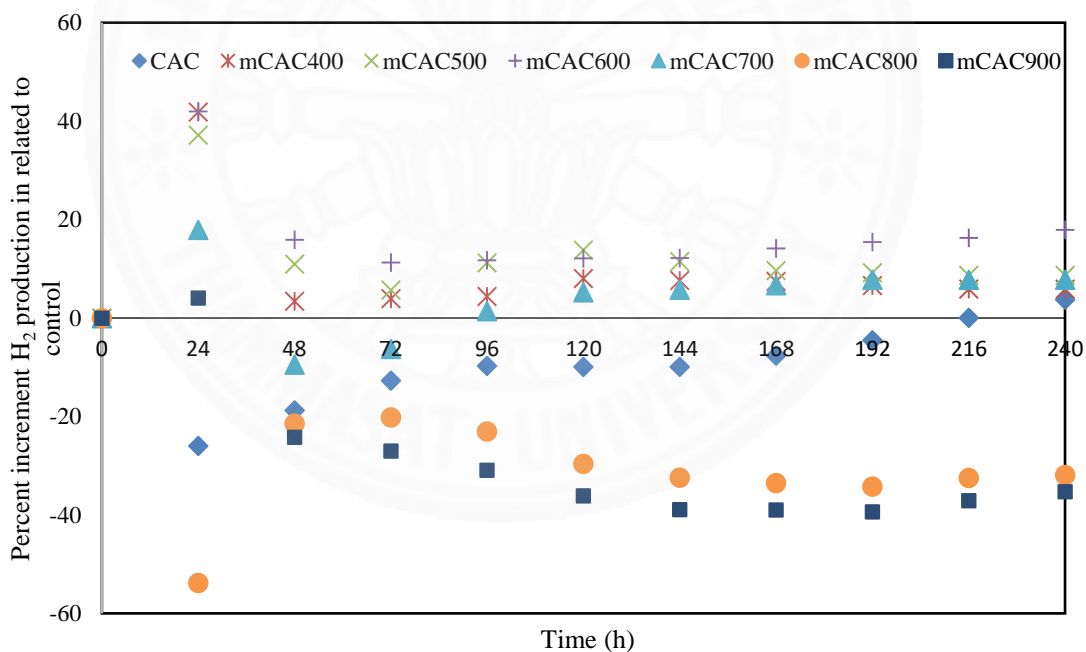


Figure 4.8 Percent increments of H₂ production of modified CAC as related to control

The t-test was calculated as indicated in **Table 4.4** to provide a clearer understanding of the effects of modified CAC on biohydrogen production. For each term, a greater significance is expected at a smaller p-value. The modified CAC for H₃PO₄ and heat treatments showed statistically significant differences in the hydrogen

production yield, compared to the control ($p < 0.01$). This that the acid and temperature activation affect the hydrogen production yield. There was no statistically significant difference between CAC and the control ($p > 0.01$). Among the mCAC, mCAC600 showed a statistically significant difference ($p < 0.01$) in hydrogen yield compared to other treatment conditions. The highest hydrogen production yield was 2.62 mol H_2 /mol sucrose. In addition, the modified CAC (by H_3PO_4) changed the characteristics of the activated carbon such as the surface area, pore size, volume, and functional groups. This affected the adsorption ability as it depended on these characteristics. H_3PO_4 with a high amount of oxygen changed the functional groups of the activated carbon, creating large pores on the surface of the activated-carbon surface (Yakout & Sharaf El-Deen, 2016). Despite the loss of surface area and pore. mCAC600 showed better performance on hydrogen production due to the pore size. The pore size of mCAC600 is the biggest as compared to all treatments (2.31 nm), which could improve microbial colonization. Therefore, enhancing the hydrogen production.

Table 4.4 Samples descriptive statistics using the t-test for H_2 yield, compared to the control

Sample	Mean	SD	SE	DF	t-test (p value)
Control	2.262	0.021	0.011	-	-
CAC	2.216	0.132	0.066	3	0.4703
mCAC400	2.408	0.007	0.003	3	0.0003
mCAC500	2.468	0.014	0.007	3	0.0000
mCAC600	2.623	0.059	0.029	3	0.0003
mCAC700	2.432	0.035	0.017	3	0.0001
mCAC800	1.540	0.007	0.003	3	0.0000
mCAC900	1.460	0.020	0.010	3	0.0000

Note: Significant level at $p < 0.01$

In this study, the kinetic parameter such as lag time, the hydrogen production rate and the maximum hydrogen production were fitted onto the Gompertz model (**Table 4.5**). All experiments were fitted, with $R^2 > 0.99$. The mCAC600 gave the highest hydrogen production rate. The lag time of mCAC600 was the shortest time as compared to mCAC400, mCAC500, mCAC700, mCAC800 and mCAC900.

Table 4.5 Parameters estimation by Gompertz model and Hydrogen production yield for CAC and mCAC

Sample	Gompertz model				H ₂ yield (mol H ₂ /mol sucrose)	Ref.
	H _{max} (mL of H ₂)	R _m (ml H ₂ /h)	λ (h)	R ²		
Control	142.71	1.56	14.97	0.99	2.28	
CAC	142.37	1.26	14.63	0.99	2.36	
mCAC400	153.15	1.58	12.79	0.99	2.41	This study
mCAC500	158.67	1.67	13.50	0.99	2.47	
mCAC600	166.68	1.60	10.76	0.99	2.68	
mCAC700	156.40	1.50	15.80	0.99	2.45	
Treated AC	147.13	2.00	18.53	0.99	2.60	(Wimonsong & Nitisoravut, 2014)

4.3 Effect of modified commercial activated carbon supported HT on biohydrogen production

The modified CAC was used as supported HT (Zn-Ni-HT) namely Zn-Ni-HT/mCAC400, Zn-Ni-HT/mCAC500, Zn-Ni-HT/mCAC600 and Zn-Ni-HT/mCAC700. The experiments were conducted for 240h or until there was no biogas produced. The daily volumetric hydrogen production shown in **Figure 4.9**. Zn-Ni-HT/mCAC600 could effectively enhance the hydrogen production rate from 24h to 96h. After 96h, hydrogen production started decreasing because substrate consumption and pH also started decrease. However, the hydrogen production still occurred after 120h. This maybe sucrose breaking down into glucose and fructose. Moreover, the hydrogen production rate of Zn-Ni-HT/CAC was higher than all supported materials but not higher than Zn-Ni-HT/mCAC600. **Figure 4.10** shows the cumulative hydrogen production of Zn-Ni-HT loaded on CAC and mCAC (400-700°C). The highest cumulative hydrogen production obtained for Zn-Ni-HT/mCAC600 at 184 ml whereas Zn-Ni-HT/mCAC generated 150 ml H₂. The cumulative hydrogen production of Zn-Ni-HT/mCAC400, Zn-Ni-HT/mCAC500 and Zn-Ni-HT/mCAC700 were not much different. Zn-Ni-HT/mCAC600 increased the hydrogen production rate approximately 30% as compared to the control and about 12% higher than mCAC600 (**Figure 4.11**).

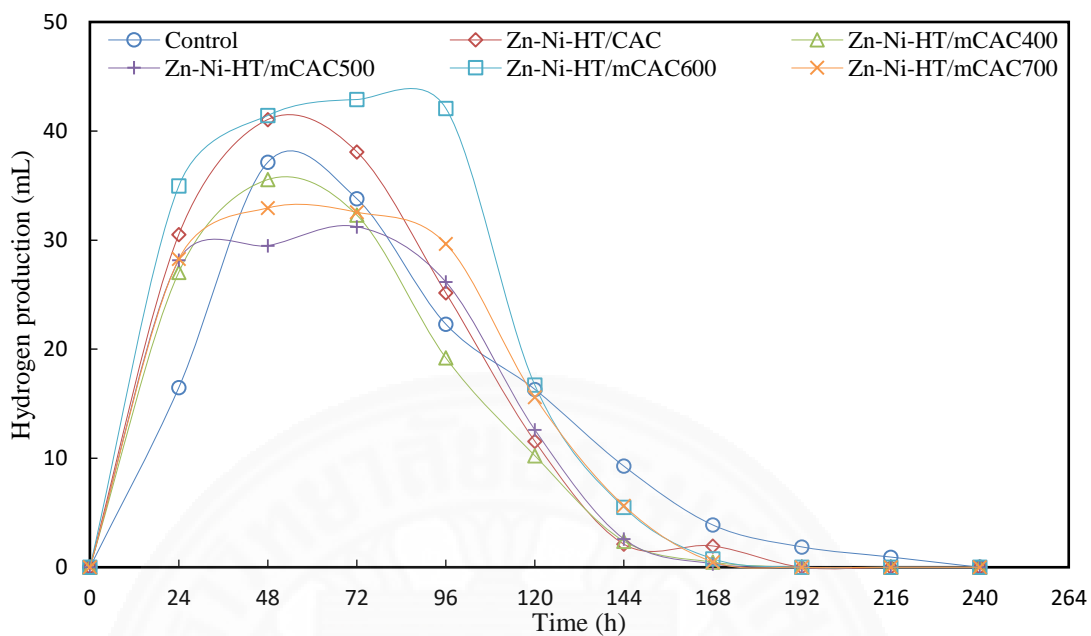


Figure 4.9 Hydrogen production of modified CAC supported HT during fermentation

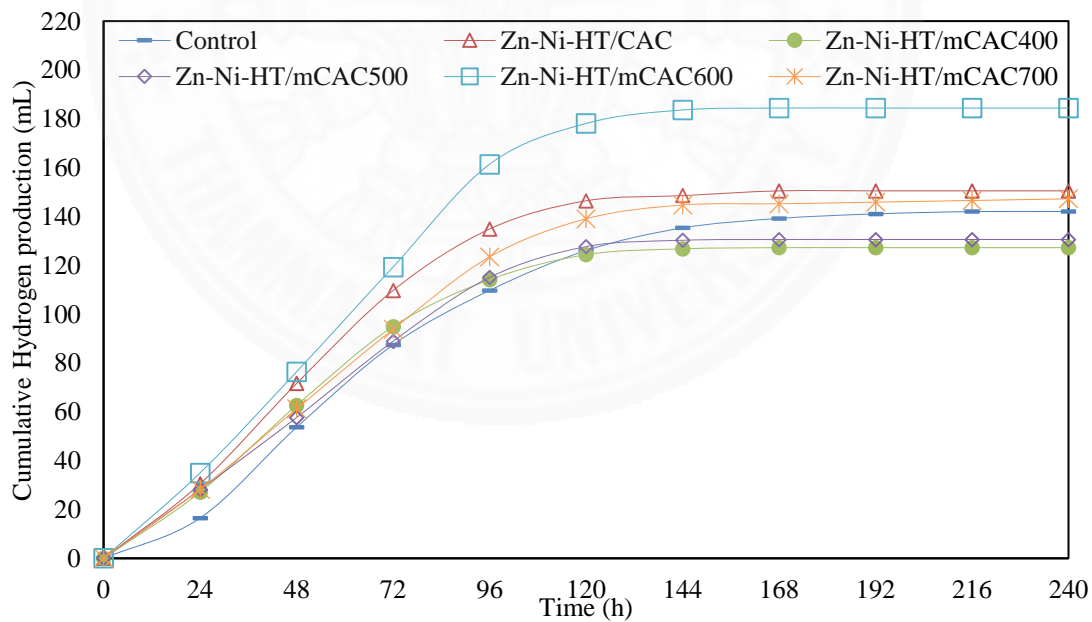


Figure 4.10 Cumulative hydrogen production of modified CAC supported HT

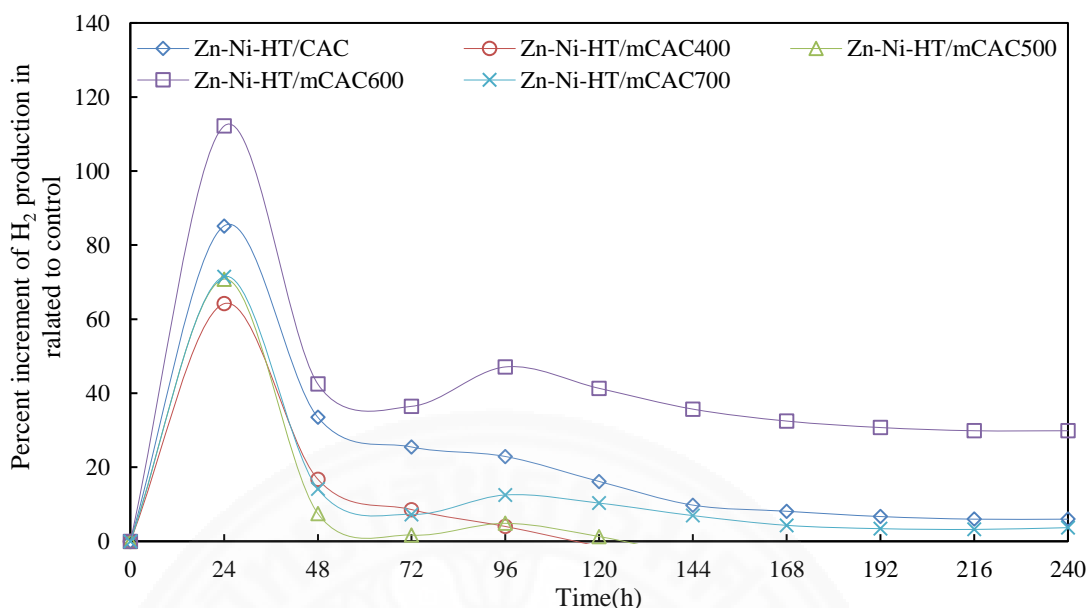


Figure 4.11 Percent increments of H₂ production of modified CAC supported HT as related to control

Table 4.6 shows a statistically significant difference ($p < 0.01$) of Zn-Ni-HT/mCAC600 compared to mCAC600 and Zn-Ni-HT/CAC. A positive effect may be due to the properties of HT that benefit fermentative conditions. First, the alkaline nature of HT can neutralize hydrogen ion during fermentation. Second, the structure of HT contains various anions and cations such as CO_3^{2-} , Cl^- , NO_3^- , Zn^{2+} , Mg^{2+} , Na^{2+} and Fe^{2+} which are necessary micro-nutrients for microbial activities. Third, Zn was found to be an active site of several enzymes such as hydrogenase (Wimonsong et al., 2014). It is also an important trace element for most microorganisms as it can act as a bridge between enzymes and substrates. Last, Zn and Ni can help efficient transfer of electrons to hydrogenase, which increases hydrogen production (Wimonsong et al., 2013). As mentioned above (section 4.2), the catalytic activity of the mCAC (400°C, 500°C, 700°C, 800°C and 900°C) except mCAC600 did not show good performance on hydrogen production. When the mCAC combined with Zn-Ni-HT but did not show affect on hydrogen production. The phenomenon could be explained by the fact that the mCAC were not suitable use as supported materials for Zn-Ni-HT in the system. The possible reason is that mCAC600 has the biggest in pore size (2.31 nm). When Zn-Ni-HT loaded on mCAC600, it could help HT spread in the pore. Therefore, Zn-Ni-HT/mCAC600 showed a good performance.

In this study, CAC is low in efficiency despite its ability to adsorb VFAs (Wimonsong & Nitorisavut, 2014). However, the modification of CAC by using H_3PO_4 could improve hydrogen production. An inclusion of mCAC600 as a supporting material for Zn-Ni-HT in dark fermentation gave a better performance as it provided hybrid functions in association with the alkaline properties of HT and availability of micronutrients.

Table 4.6 Samples descriptive statistics using t-test for H_2 yield of Zn-Ni-HT/mCAC600 compared to mCAC600 and Zn-Ni-HT/CAC

Sample	Mean	SD	SE	DF	t-test (p value)
Control	2.262	0.021	0.011	-	-
Zn-Ni-HT/mCAC600 VS mCAC600	2.958	0.001	0.001	3	0.0013
Zn-Ni-HT/mCAC600 VS Zn-Ni-HT/CAC	2.958	0.001	0.001	3	0.0000

Note: Significant level at $p < 0.01$

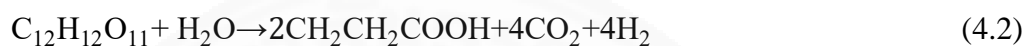
The kinetic parameter such as lag phrase time, the hydrogen production rate and the maximum hydrogen production were obtained by fitting data to the Gompertz model (**Table 4.7**). All experiments were fitted, with $R^2 > 0.99$. The mCAC600 gave the highest hydrogen production rate. The Zn-Ni-HT/mCAC600 shows the highest hydrogen production rate and yield. The addition of composite could significantly reduce the lag phase of fermentative hydrogen production as compared to the control.

Table 4.7 Parameters estimation by the Gompertz model and Hydrogen production yield of mCAC supported HT

Sample	Gompertz model			R ²	H ₂ yield (mol H ₂ /mol sucrose)	Ref.
	H _{max} (mL of H ₂)	R _m (ml H ₂ /h)	λ (h)			
Control	142.71	1.56	14.97	0.99	2.28	
Zn-Ni-HT/CAC	159.72	1.94	10.60	0.99	2.41	
Zn-Ni-HT/mCAC400	129.91	1.67	9.66	0.99	2.10	This study
Zn-Ni-HT/mCAC500	136.12	1.53	9.25	0.99	2.22	
Zn-Ni-HT/mCAC600	187.74	2.22	12.43	0.99	2.95	
Zn-Ni-HT/mCAC700	148.79	1.67	10.79	0.99	2.27	
Ni-Mg-Al HT	215.00	1.40	2.59	0.98	3.37	(Le & Nitorisavut, 2015)
Mg-Al HT	174.30	1.10	6.15	0.97	2.73	
Zn-Mg-Al	142.70	1.00	4.00	0.99	2.28	(Wimonsong et al., 2013)

4.4 Metabolize distribution

The residual volatile fatty acids (VFAs) are an important indicator for hydrogen production performance. Acetic, butyric, lactic and propionic acids were determined after fermentation. Theoretically, 8 moles and 4 moles of hydrogen per mol of sucrose are produced when acetic and butyric are by-products of reactions (Khanal et al., 2004), respectively (Equations 4.1 and 4.2).



In this study, both acetic and butyric acids were observed, indicating multiple path-ways for hydrogen production. There were no lactic and propionic acids found. As can be seen in the **Figure 4.12**, high concentrations of butyric acid were found in all treatments and the control. The concentration of butyric acid at the end of fermentation was highest at 6,816 mg/L for the control while the lowest was 2,210 mg/L for mCAC600. It is well known that the practical hydrogen production yield is about 2 moles or slightly higher. In this study, the highest concentration of acetic acid was observed at 2,704 mg/L for Zn-Ni-HT/mCAC600, which also provided the highest hydrogen production yield. The maximum hydrogen production yield with composite material was higher than the control but still lower than that in theory. Moreover, pH is a factor that affects hydrogen production. A lower pH inhibits the hydrogenase activity and production of VFAs in the system.

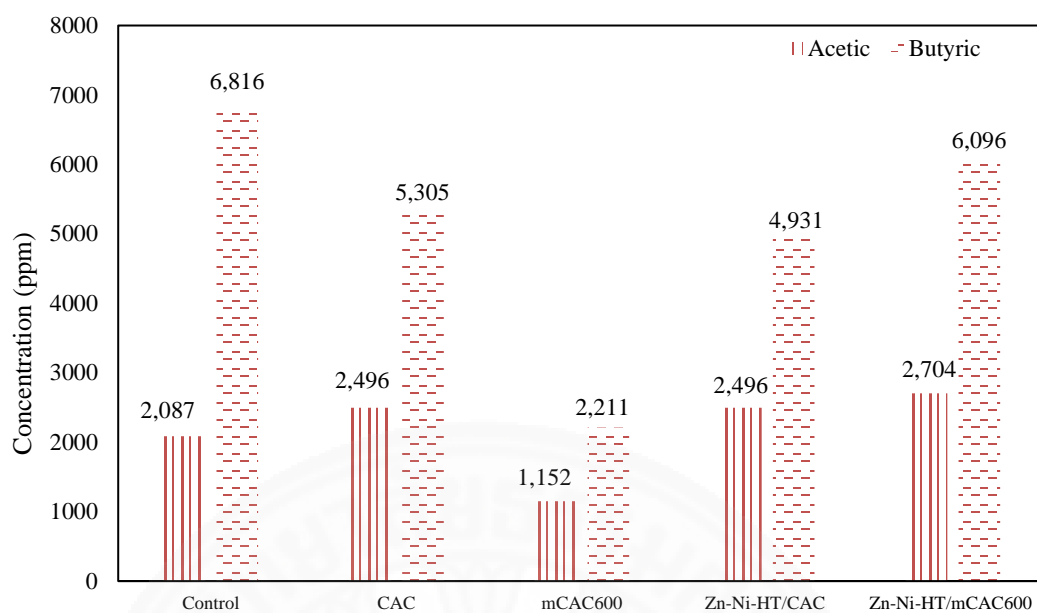


Figure 4.12 Metabolites concentration

A higher ending pH was observed for the Zn-Ni-HT/CAC and Zn-Ni-HT/mCAC600 at 4.11 and 3.89, respectively (**Figure 4.13**). The pH of samples containing HT was generally higher than the samples without HT. When HT was loaded on the activated carbon, it could slow down and prevent or slow a drop of pH and help adsorb unfavourable VFAs during fermentation.

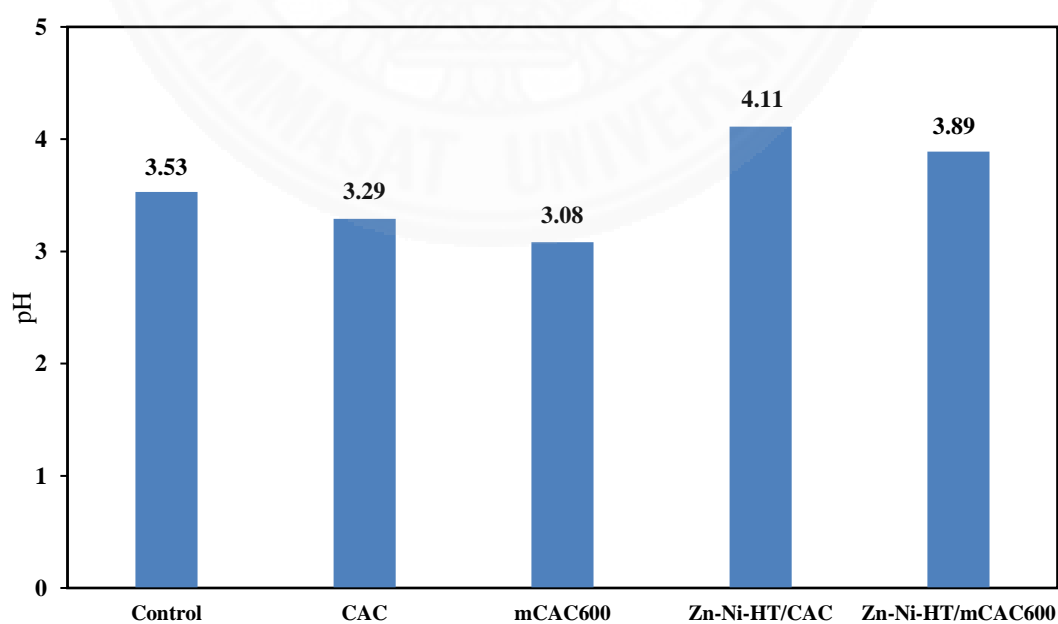


Figure 4.13 Final pH of different samples

4.5 Metals leaching of supporting materials

As HT is constructed from multiple metal elements, there is a possibility of metal leaching causing effects on fermentative hydrogen production. **Figure 4.14** shows the metals, particularly Ni^{2+} , Mg^{2+} , and Al^{3+} , which were leached out from the supporting materials under acidic conditions. It should be noted that Zn^{2+} was not detected in the fermentation broth. As Zn-HT was loaded prior to Ni-HT on the activated carbon during impregnation, it adheres firmly onto the surface causing poor or no release of Zn^{2+} . A gradually slow release of Ni^{2+} was detected at a low concentration of Zn-Ni-HT/mCAC600 and Zn-Ni-HT/CAC. High concentrations of Mg^{2+} were observed, ranging from 104.30 to 292.60 mg/L for Zn-Ni-HT/CAC and 82.42 to 152.30 for Zn-Ni-HT/mCAC600. A low concentration of Al^{3+} was observed, at 3.66 to 59.48 mg/L for Zn-Ni-HT/CAC and 3.51 to 7.55 mg/L for Zn-Ni-HT/mCAC600. Both Mg^{2+} and Al^{3+} were affected by heat activation, causing fixation and stabilization. This was not clearly observed for Ni^{2+} .

Depending upon the type of metals and their concentrations, both positive and negative effects can be found on biohydrogen fermentation. Mg^{2+} ion is the active site component for many enzymes which are functioned as electron transfer (Srikanth & Mohan, 2012). Feng, Li, Mei, and Zhang (2013) reported that the addition of 0.3g/L Mg^{2+} ion concentration generated a hydrogen production rate of 256 ml H_2 /l, while excessive or lack of Mg^{2+} ion caused a decrease in the hydrogen production rate. A higher rate and yield of H_2 production were found for Zn-Ni-HT/mCAC600 at 152.3 mg Mg^{2+} /L and Zn-Ni-HT/CAC at 292.60 mg Mg^{2+} /L. This means that this level of Mg^{2+} concentration did not outweigh other positive factors of biohydrogen production such as heat activation and Ni^{2+} concentration. This was confirmed by a higher amount of Ni^{2+} for Zn-Ni-HT/mCAC600 as compared to Zn-Ni-HT/CAC. It is noteworthy to mention that Ni^{2+} is a fundamental component of Ni-Fe hydrogenase, which can improve the hydrogen production yield.

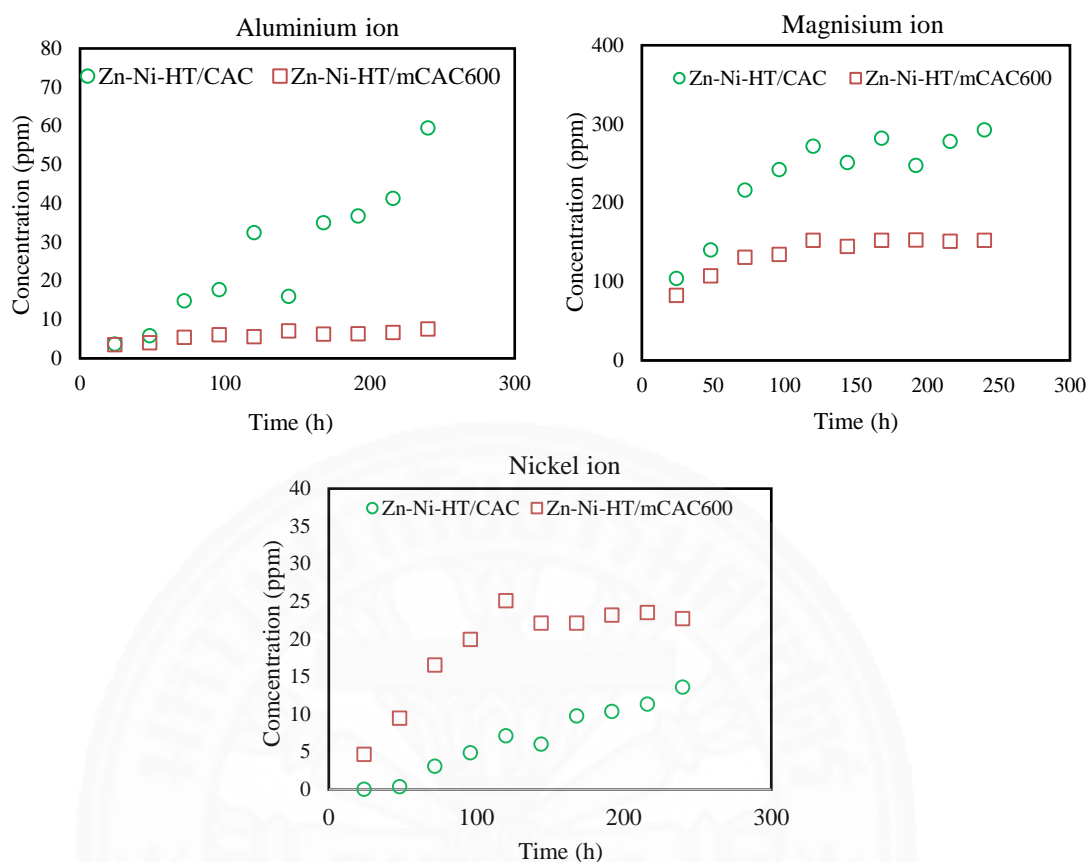


Figure 4.14 Metals leaching during fermentative hydrogen production

4.6 Volatile fatty acids adsorption

In this study, two adsorption isotherm models were applied to confirm the amount of adsorbate adsorbed (VFAs) on the surface of adsorbent (activated carbon). Langmuir adsorption isotherm was determined the relationship of the equilibrium between adsorbate and adsorbent system, which is a monolayer adsorption onto surface. From the calculated data in **Table 4.8** the high capacity of adsorption (Q_0) from Langmuir isotherm model caused to adsorb more butyric and propionic acids for mCAC600 and Zn-Ni-HT/mCAC600. Zn-Ni-HT/mCAC600 could selectively adsorb butyric and propionic acids with high adsorption capacity of 0.395 and 0.202 mg/g, respectively. Similarly, the adsorption capacity of butyric and propanoic acid were high with 0.198 and 0.330 mg/g for mCAC600. The percent adsorption of VFAs for Zn-Ni-HT/mCAC600 showed significant difference in higher adsorbed VFAs particularly butyric acid, which was 63.78%. While the percent adsorption of VFAs for mCAC600 was found for butyric acid only 25.93%. Zn-Ni-HT/mCAC600 is 40% higher than

mCAC600. This means Zn-Ni-HT/mCAC600 has the highest affinity on butyric acid as compared to acetic acid, lactic acid and propionic acid.

Table 4.8 Langmuir parameters and percent adsorption of VFAs on materials

VFAs	Parameters	Materials	
		mCAC600	Zn-Ni-HT/mCAC600
Acetic	R^2	0.95	0.97
	Q_0	0.018	0.009
	%adsorption	25.93	63.78
Butyric	R^2	0.92	0.95
	Q_0	0.198	0.2025
	%adsorption	6.04	58.28
Lactic	R^2	0.95	0.96
	Q_0	0.033	0.1200
	%adsorption	12.54	55.35
Propanoic	R^2	0.97	0.96
	Q_0	0.330	0.395

The adsorption isotherm matched with Langmuir model as seen in **Figure 4.15** and **Figure 4.16**. The lowest R^2 was found for butyric acid (0.92) with mCAC600. While higher R^2 was observed for Zn-Ni-HT/mCAC600 as 0.97, 0.95, 0.96 and 0.96 for acetic, butyric, lactic and propionic acids, respectively.

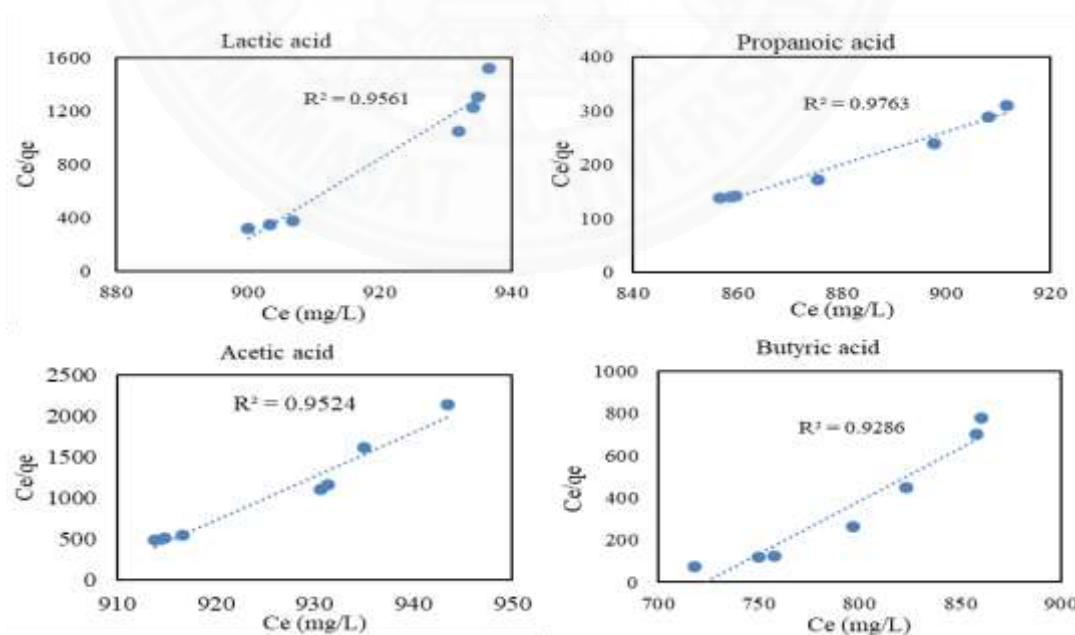


Figure 4.15 Langmuir adsorption of VFAs on mCAC600

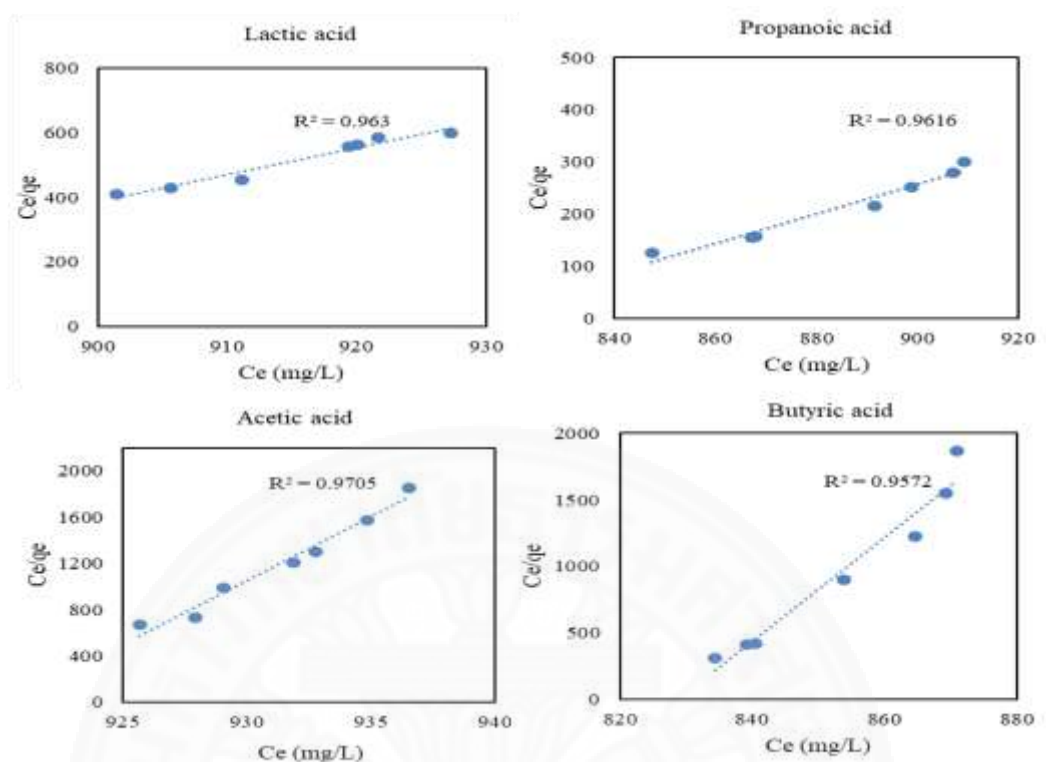


Figure 4.16 Langmuir adsorption of VFAs onto Zn-Ni-HT/mCAC600

Freundlich isotherm is used for monolayer accumulation onto heterogeneous surfaces (multilayer surface). The Freundlich parameters for the adsorption of VFAs are given in **Table 4.9**. The result shows that the adsorption capacity (K_f) mCAC600 and Zn-Ni-HT/mCAC600 had very large values. It indicates that Freundlich adsorption isotherm is not suitable for this experiment (Desta, 2013). The n value indicates the degree of nonlinearity between solution concentration and adsorption as follows: if $n = 1$, then adsorption is linear; if $n > 1$, then adsorption is a physical process; if $n < 1$, then adsorption is a chemical process. The n value within the range of 1-10 represent in good adsorption (Khayyun & Mseer, 2019). The n values obtained from Freundlich equation were found at n less than 1 for mCAC600 and Zn-Ni-HT/mCAC600. It means very poor adsorption of fatty acids onto the material in terms of a chemical adsorption process.

Table 4.9 Freundlich adsorption isotherm for VFAs adsorption onto materials

Material	VFAs	Equation	Estimate isotherm parameter		
			K_f	n	R^2
mCAC600	Acetic	$Y=-41,015x+142.45$	10×10^{142}	-1.2×10^{-3}	0.98
	Butyric	$Y=-12,687x+37.36$	2.29×10^{37}	-6.3×10^{-3}	0.92
	Lactic	$Y=-32,134x+95.32$	4.78×10^{96}	-3.1×10^{-3}	0.95
	Propionic	$Y=-11.624x+34.88$	7.58×10^{35}	-8.8×10^{-3}	0.99
Zn-Ni-HT/mCAC600	Acetic	$Y=-81.152x+204.76$	1×10^{204}	-1.2×10^{-3}	0.92
	Butyric	$Y=-15.663x+46.00$	10×10^{45}	-6.3×10^{-3}	0.80
	Lactic	$Y=-36.771x+109.14$	1×10^{109}	-2.7×10^{-3}	0.97
	Propionic	$Y=-12.104x+36.302$	2.00×10^{35}	-8.3×10^{-3}	0.98

However, Freundlich adsorption correlation coefficients (R^2), as represented in the **Figure 4.17** and **Figure 4.18** indicate that the isotherm suits well for mCAC600 metabolites. The lowest value (0.92) is corresponding to butyric acid. The R^2 of Zn-Ni-HT/mCAC600 had 0.92 and 0.80 for acetic and butyric acids, respectively. High R^2 in Freundlich isotherm does not imply to fit in good agreement the isotherm model, due to the bias from the forced linearization. It means the VFAs is covered only by a monolayer on the surface of the materials. There are no stacking adsorbed molecules. It is clear that the volatile fatty acids were adsorbed on the pore of the supported materials. The Langmuir isotherm model is a better predictor than Freundlich model.

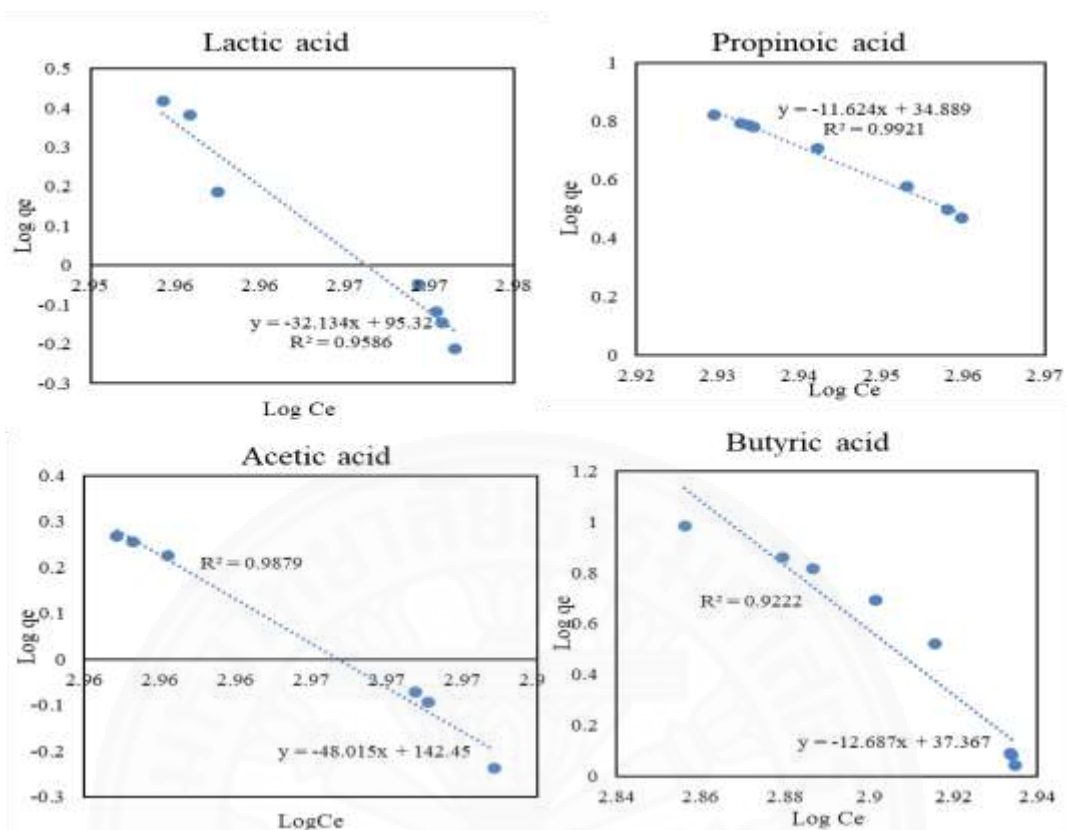


Figure 4.17 Freundlich adsorption of VFAs on mCAC600

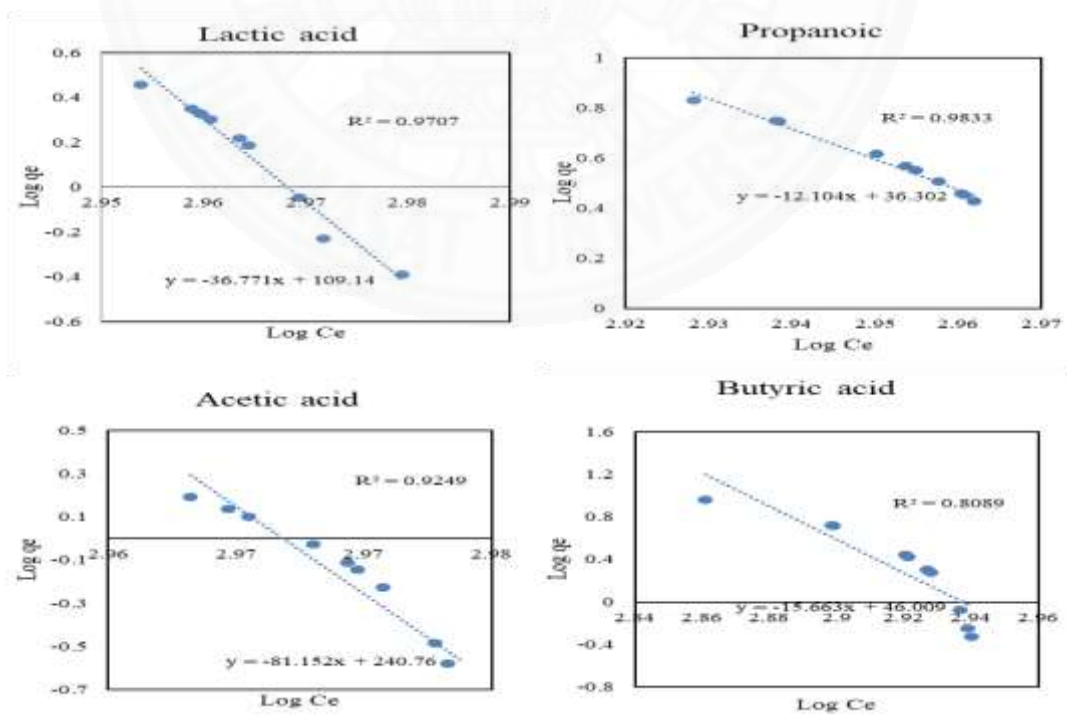


Figure 4.18 Freundlich adsorption of VFAs on Zn-Ni-HT/mCAC600

4.7 Recyclability of Zn-Ni-HT/mCAC600

In this study, the ability to recycle mCAC 600 and Zn-Ni-HT/mCAC600 were investigated in three cycles using fresh medium with repeated use of the optimum dose at 8.33 g/L. The results showed that the treatments could be only one cycle. As seen in the **Figure 4.19** shows the hydrogen production yield of mCAC600 was decreased from 2.68 to 0.42 mol H₂/mol sucrose, which was decreased 80% from first cycle. Zn-Ni-HT/mCAC600 was decreased from 2.95 to 0.32 mol H₂/mol sucrose, which was decreased 80% from first cycle. After three recycles, the hydrogen production was no longer produced due to the pH was very low (data not shown). According to the theory, the lower in pH causes inhibit the hydrogen yield. Another reason is that the metals leaching from the supported material particularly Mg²⁺ and Al³⁺ ion could not recycle, which was decreased in hydrogen production yield.

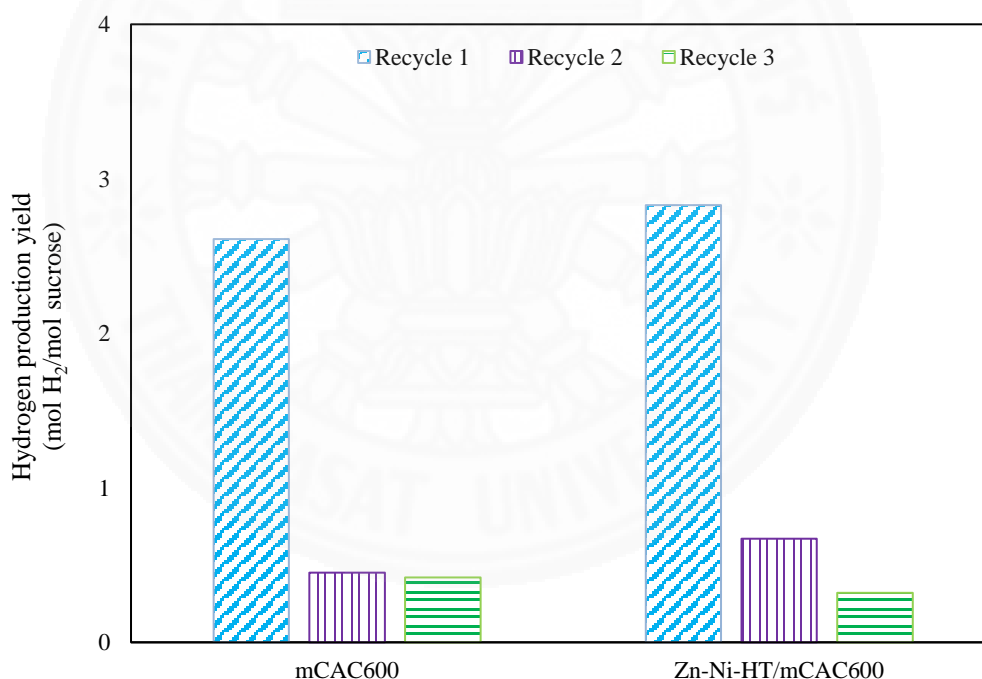


Figure 4.19 Hydrogen production yield of mCAC600 and Zn-Ni-HT/mCAC600 for repeat use three cycles for biohydrogen production

CHAPTER 5

CONCLUSIONS AND RECOMMENDATION

Biohydrogen production was enhanced by adding modified commercial activated carbon using H_3PO_4 and heat treatments. The highest hydrogen production yield was observed at $600^\circ C$ (mCAC600) with hydrogen yield of 2.68 mol H_2 /mol sucrose which was 17% increment compared to the control. The modification of CAC by H_3PO_4 at high ($700-900^\circ C$) or low temperature ($400-500^\circ C$) did not show a good effect on biohydrogen production. In addition, the increment of hydrogen production was associated with the properties of activated carbon such as surface area, pore structure, and adsorption ability especially pore size. The modified CAC by H_3PO_4 reduced the surface area and pore volume. However, the mCAC600 has the biggest pore size (2.31 nm) as compared to all treatments, which could improve microbial colonization and thereby enhanced the hydrogen production.

Further enhancement could be obtained through the application of Zn-Ni-HT onto mCAC (400 to $700^\circ C$) to produce composite materials. The maximum hydrogen production yield was observed for Zn-Ni-HT/mCAC600 with 2.95 mol H_2 /mol of sucrose, which was nearly 12% and 30% higher than mCAC600 and the control, respectively. The possible reason is that mCAC600 has the biggest pore size. When Zn-Ni-HT loaded on mCAC600, it could help HT spreading in the pore. Therefore, Zn-Ni-HT/mCAC600 showed a good performance as compared to all materials. Moreover, both acetic and butyric acids were observed as by-products. The highest concentration of acetic acid was observed at 2,704 mg/L for Zn-Ni-HT/mCAC600, which also provided the highest hydrogen production yield. The pH of samples containing HT were generally higher than the samples without HT. When HT was loaded on the activated carbon, it could slow down and prevent a drop of pH and help to adsorb unfavourable VFAs during fermentation. A higher ending pH was observed for the Zn-Ni-HT/CAC and Zn-Ni-HT/mCAC600 at 4.11 and 3.89, respectively. Moreover, Zn-Ni-HT/mCAC600 released metal ions less than Zn-Ni-HT/CAC particularly Mg and Al ions. Zn^{2+} was not detected in the fermentation for all materials because it adheres firmly onto the surface.

Zn-Ni-HT/mCAC600 had the highest percent adsorption of VFAs particularly for butyric acid, which was 63.78%. While the percent adsorption of VFAs for mCAC600 was found for butyric acid only 25.93%. Zn-Ni-HT/mCAC600 is 40% higher than mCAC600. which was 40% higher than mCAC600. Langmuir and Freundlich isotherm models showed that the volatile fatty acids were covered only by a monolayer on the surface of the materials. There is no stacking of adsorbed molecules. Therefore, volatile fatty acids were adsorbed on the pore of the supported materials. The Langmuir isotherm model is a better predictor than Freundlich model.

In addition, the recyclability study Zn-Ni-HT/mCAC600 indicated that it can only be used once for improving hydrogen production. For the repeated use of the materials the hydrogen production yield decreased 80% from the first cycle. From the results, Zn-Ni-HT/mCAC600 could not be reused due to high release of some metal ions. It is, therefore, concluded that the enhancement was due to the multiple functions of Zn-Ni-HT/mCAC600. These functions include microbial-colonization habitat, buffer capacity, adsorption abilities for unfavorable VFAs, and a slow release of beneficial metals such as Ni²⁺.

Recommendation

1. Modified commercial activated carbon can be further develop as supported material for other catalysts besides HT to see the performance in biohydrogen production.
2. The performance of modified commercial activated carbon supported hydrotalcite has been investigated in batch, Continuous mode should be studied.
3. The application of actual wastewater needs to be investigated.

REFERENCES

- Ahmed, M. B., Hasan Johir, M. A., Zhou, J. L., Ngo, H. H., Nghiem, L. D., Richardson, C., . . . Bryant, M. R. (2019). Activated carbon preparation from biomass feedstock: Clean production and carbon dioxide adsorption. *Journal of Cleaner Production*, 225, 405-413. doi:<https://doi.org/10.1016/j.jclepro.2019.03.342>
- Akbayrak, S., Özçifçi, Z., & Tabak, A. (2019). Noble metal nanoparticles supported on activated carbon: Highly recyclable catalysts in hydrogen generation from the hydrolysis of ammonia borane. *Journal of Colloid and Interface Science*, 546, 324-332. doi:<https://doi.org/10.1016/j.jcis.2019.03.070>
- Anisuzzaman, S. M., Joseph, C. G., Taufiq-Yap, Y. H., Krishnaiah, D., & Tay, V. V. (2015). Modification of commercial activated carbon for the removal of 2,4-dichlorophenol from simulated wastewater. *Journal of King Saud University - Science*, 27(4), 318-330. doi:<https://doi.org/10.1016/j.jksus.2015.01.002>
- Arneli, Safitri, Z. F., Pangestika, A. W., Fauziah, F., Wahyuningrum, V. N., & Astuti, Y. (2017). The influence of activating agents on the performance of rice husk-based carbon for sodium lauryl sulfate and chrome (Cr) metal adsorptions. *IOP Conference Series: Materials Science and Engineering*, 172, 012007. doi:<https://doi.org/10.1088/1757-899X/172/1/012007>
- Bai, Z., Chen, H., Li, B., & Li, W. (2007). Methane decomposition over Ni loaded activated carbon for hydrogen production and the formation of filamentous carbon. *International Journal of Hydrogen Energy*, 32(1), 32-37. doi:<https://doi.org/10.1016/j.ijhydene.2006.06.030>
- Baldi, F., Iannelli, R., Pecorini, I., Poletti, A., Pomi, R., & Rossi, A. (2019). Influence of the pH control strategy and reactor volume on batch fermentative hydrogen production from the organic fraction of municipal solid waste. *Waste management & research : the journal of the International Solid Wastes and Public Cleansing Association, ISWA*, 37(5), 478-485. doi:<https://doi.org/10.1177/0734242x19826371>
- Batista, F. (2014). Hydrogen production by dark fermentation. *CHEMICAL ENGINEERING TRANSACTIONS*, 38, 481-486. doi:<https://doi.org/10.3303/CET1438081>
- Beckers, L., Hilgsmann, S., Lambert, S. D., Heinrichs, B., & Thonart, P. (2013). Improving effect of metal and oxide nanoparticles encapsulated in porous silica on fermentative biohydrogen production by *Clostridium butyricum*. *Bioresource Technology*, 133, 109-117. doi:<https://doi.org/10.1016/j.biortech.2012.12.168>
- Bundhoo, M. A. Z., & Mohee, R. (2016). Inhibition of dark fermentative bio-hydrogen production: A review. *International Journal of Hydrogen Energy*, 41(16), 6713-6733. doi:<https://doi.org/10.1016/j.ijhydene.2016.03.057>
- Carvajal Bernal, A. M., Gómez, F., Giraldo, L., & Moreno Pirajá, J. C. (2015). Chemical modification of activated carbons and its effect on the adsorption of phenolic compounds. *Ingeniería y competitividad*, 17, 109-119. doi:http://www.scielo.org.co/scielo.php?script=sci_arttext&pid=S0123-30332015000100010&lng=en&nrm=iso

- Chen, W., Zhang, S., He, F., Lu, W., & Xv, H. (2019). Porosity and surface chemistry development and thermal degradation of textile waste jute during recycling as activated carbon. *Journal of Material Cycles and Waste Management*, 21(2), 315-325. doi:<https://doi.org/10.1007/s10163-018-0792-8>
- Chong, M.-L., Abdul Rahman, N. A., Yee, P. L., Aziz, S. A., Rahim, R. A., Shirai, Y., & Hassan, M. A. (2009). Effects of pH, glucose and iron sulfate concentration on the yield of biohydrogen by *Clostridium butyricum* EB6. *International Journal of Hydrogen Energy*, 34(21), 8859-8865. doi:<https://doi.org/10.1016/j.ijhydene.2009.08.061>
- Costantino, U., Nocchetti, M., Gorrasi, G., & Tammaro, L. (2011). Hydrotalcites in nanobiocomposites. In J.-M. Lagarón (Ed.), *Multifunctional and Nanoreinforced Polymers for Food Packaging* (pp. 43-85). Cambridge, UK: Woodhead Publishing.
- David L. Nelson, M. C. (2008). Lehninger Principles of Biochemistry. In.
- Desta, M. B. (2013). Batch sorption experiments: Langmuir and Freundlich isotherm studies for the adsorption of textile metal ions onto Teff straw (*Eragrostis tef*) agricultural waste. *Journal of Thermodynamics*, 2013, 375830. doi:<https://doi.org/10.1155/2013/375830>
- Dolly, S., Pandey, A., Pandey, B. K., & Gopal, R. (2015). Process parameter optimization and enhancement of photo-biohydrogen production by mixed culture of *Rhodobacter sphaeroides* NMBL-02 and *Escherichia coli* NMBL-04 using Fe-nanoparticle. *International Journal of Hydrogen Energy*, 40(46), 16010-16020. doi:<https://doi.org/10.1016/j.ijhydene.2015.09.089>
- Elbeshbishy, E., Dhar, B. R., Nakhla, G., & Lee, H. S. (2017). A critical review on inhibition of dark biohydrogen fermentation. *Renewable and Sustainable Energy Reviews*, 79, 656-668. doi:<https://doi.org/10.1016/j.rser.2017.05.075>
- Elreedy, A., Ibrahim, E., Hassan, N., El Dissouky, A., Fujii, M., Yoshimura, C., & Tawfik, A. (2017). Nickel-graphene nanocomposite as a novel supplement for enhancement of biohydrogen production from industrial wastewater containing mono-ethylene glycol. *Energy Conversion and Management*, 140, 133-144. doi:<https://doi.org/10.1016/j.enconman.2017.02.080>
- Engliman, N., Abdul, P., Wu, S. Y., & Jamaliah, M. (2017). Influence of iron (II) oxide nanoparticle on biohydrogen production in thermophilic mixed fermentation. *International Journal of Hydrogen Energy*, 42(45), 27482-27493. doi:<https://doi.org/10.1016/j.ijhydene.2017.05.224>
- Eustáquio, H., Lopes, C., Rocha, R., Cardoso, B., & Pergher, S. (2015). Modification of activated carbon for the adsorption of humic acid. *Adsorption Science & Technology*, 33, 117-126. doi:<https://doi.org/10.1260/2F0263-6174.33.2.117>
- Feng, Y., Li, G. H., Mei, H. Y., & Zhang, L. S. (2013). The effect of magnesium ions on the hydrogen-producing bacteria in the water during the ecological restoration process. *Advanced Materials Research*, 610-613, 264-267. doi:<https://doi.org/10.4028/www.scientific.net/AMR.610-613.264>
- Foungchuen, J., Pairin, N., & Phalakornkule, C. (2016). Impregnation of chitosan onto activated carbon for adsorption selectivity towards CO₂: Biohydrogen purification. *KMUTNB International Journal of Applied Science and Technology*, 9(3), 197-209. doi:<https://doi.org/10.14416/j.ijast.2016.03.003>

- Gadhe, A., Sonawane, S. S., & Varma, M. N. (2015a). Enhancement effect of hematite and nickel nanoparticles on biohydrogen production from dairy wastewater. *International Journal of Hydrogen Energy*, 40(13), 4502-4511. doi:<https://doi.org/10.1016/j.ijhydene.2015.02.046>
- Gadhe, A., Sonawane, S. S., & Varma, M. N. (2015b). Influence of nickel and hematite nanoparticle powder on the production of biohydrogen from complex distillery wastewater in batch fermentation. *International Journal of Hydrogen Energy*, 40(34), 10734-10743. doi:<https://doi.org/10.1016/j.ijhydene.2015.05.198>
- Garcés Polo, S. I., Villarroel Rocha, J., Sapag, K., Korili, S. A., & Gil, A. (2018). Adsorption of CO₂ on mixed oxides derived from hydrotalcites at several temperatures and high pressures. *Chemical Engineering Journal*, 332, 24-32. doi:<https://doi.org/10.1016/j.cej.2017.09.056>
- Ghimire, A., Frunzo, L., Pirozzi, F., Trably, E., Escudie, R., Lens, P. N. L., & Esposito, G. (2015). A review on dark fermentative biohydrogen production from organic biomass: Process parameters and use of by-products. *Applied Energy*, 144, 73-95. doi:<https://doi.org/10.1016/j.apenergy.2015.01.045>
- Girgis, B. S., Attia, A. A., & Fathy, N. A. (2007). Modification in adsorption characteristics of activated carbon produced by H₃PO₄ under flowing gases. *Colloids and Surfaces A: Physicochemical and Engineering Aspects*, 299(1), 79-87. doi:<https://doi.org/10.1016/j.colsurfa.2006.11.024>
- Gou, C., Guo, J., Lian, J., Guo, Y., Jiang, Z., Yue, L., & Yang, J. (2015). Characteristics and kinetics of biohydrogen production with Ni²⁺ using hydrogen-producing bacteria. *International Journal of Hydrogen Energy*, 40(1), 161-167. doi:<https://doi.org/10.1016/j.ijhydene.2014.10.100>
- Guo, X. M., Trably, E., Latrille, E., Carrère, H., & Steyer, J. P. (2010). Hydrogen production from agricultural waste by dark fermentation: A review. *International Journal of Hydrogen Energy*, 35(19), 10660-10673. doi:<https://doi.org/10.1016/j.ijhydene.2010.03.008>
- Han, H., Cui, M., Wei, L., Yang, H., & Shen, J. (2011). Enhancement effect of hematite nanoparticles on fermentative hydrogen production. *Bioresource Technology*, 102(17), 7903-7909. doi:<https://doi.org/10.1016/j.biortech.2011.05.089>
- Han, H., Jia, Q., Wei, L., & Shen, J. (2014). Influence of Cu²⁺ concentration on the biohydrogen production of continuous stirred tank reactor. *International Journal of Hydrogen Energy*, 39(25), 13437-13442. doi:<https://doi.org/10.1016/j.ijhydene.2014.04.022>
- Hwang, Y., Sivagurunathan, P., Lee, M. K., Yun, Y. M., Song, Y. C., & Kim, D. H. (2019). Enhanced hydrogen fermentation by zero valent iron addition. *International Journal of Hydrogen Energy*, 44(6), 3387-3394. doi:<https://doi.org/10.1016/j.ijhydene.2018.06.015>
- Jamali, N. S., Jahim, J. M., Isahak, W. N. R. W., & Abdul, P. M. (2017). Particle size variations of activated carbon on biofilm formation in thermophilic biohydrogen production from palm oil mill effluent. *Energy Conversion and Management*, 141, 354-366. doi:<https://doi.org/10.1016/j.enconman.2016.09.067>
- Jamali, N. S., Md Jahim, J., & Wan Isahak, W. N. R. (2016). Biofilm formation on granular activated carbon in xylose and glucose mixture for thermophilic

- biohydrogen production. *International Journal of Hydrogen Energy*, 41(46), 21617-21627. doi:<https://doi.org/10.1016/j.ijhydene.2016.05.092>
- Joshi, G., Pandey, J. K., Rana, S., & Rawat, D. S. (2017). Challenges and opportunities for the application of biofuel. *Renewable and Sustainable Energy Reviews*, 79, 850-866. doi:<https://doi.org/10.1016/j.rser.2017.05.185>
- Kammerer, D., Kammerer, J., & Carle, R. (2014). Resin adsorption and ion exchange to recover and fractionate polyphenols. *Polyphenols in Plants: Isolation, Purification and Extract Preparation*, 219-230. doi:<https://doi.org/10.1016/B978-0-12-397934-6.00011-5>
- Kapdan, I. K., & Kargi, F. (2006). Bio-hydrogen production from waste materials. *Enzyme and Microbial Technology*, 38(5), 569-582. doi:<https://doi.org/10.1016/j.enzmictec.2005.09.015>
- Karnib, M., Kabbani, A., Holail, H., & Olama, Z. (2014). Heavy metals removal using activated carbon, Silica and Silica activated carbon composite. *Energy Procedia*, 50, 113-120. doi:<https://doi.org/10.1016/j.egypro.2014.06.014>
- Khanal, S. K., Chen, W. H., Li, L., & Sung, S. (2004). Biological hydrogen production: effects of pH and intermediate products. *International Journal of Hydrogen Energy*, 29(11), 1123-1131. doi:<https://doi.org/10.1016/j.ijhydene.2003.11.002>
- Khayyun, T. S., & Mseer, A. H. (2019). Comparison of the experimental results with the Langmuir and Freundlich models for copper removal on limestone adsorbent. *Applied Water Science*, 9(8), 170. doi:10.1007/s13201-019-1061-2
- Kim, J. K., Nhat, L., Chun, Y. N., & Kim, S. W. (2008). Hydrogen production conditions from food waste by dark fermentation with *Clostridium beijerinckii* KCTC 1785. *Biotechnology and Bioprocess Engineering*, 13(4), 499-504. doi:<https://doi.org/10.1007/s12257-008-0142-0>
- Kim, M. H., Jeong, I. T., Park, S. B., & Kim, J. W. (2019). Analysis of environmental impact of activated carbon production from wood waste. *Environmental Engineering Research*, 24(1), 117-126. doi:<https://doi.org/10.4491/eer.2018.104>
- Kumar, G., Mathimani, T., Rene, E. R., & Pugazhendhi, A. (2019). Application of nanotechnology in dark fermentation for enhanced biohydrogen production using inorganic nanoparticles. *International Journal of Hydrogen Energy*, 44(26), 13106-13113. doi:<https://doi.org/10.1016/j.ijhydene.2019.03.131>
- Le, D. T. H., & Nitorisavut, R. (2015). Modified hydrotalcites for enhancement of biohydrogen production. *International Journal of Hydrogen Energy*, 40(36), 12169-12176. doi:<https://doi.org/10.1016/j.ijhydene.2015.06.142>
- Lee, H. S., Vermaas, W., & Rittmann, B. (2010). Biological hydrogen production: Prospects and challenges. *Trends in biotechnology*, 28, 262-271. doi:<https://doi.org/10.1016/j.tibtech.2010.01.007>
- Lee, K. S., Lo, Y. S., Lo, Y. C., Lin, P. J., & Chang, J. S. (2004). Operation strategies for biohydrogen production with a high-rate anaerobic granular sludge bed bioreactor. *Enzyme and Microbial Technology*, 35(6), 605-612. doi:<https://doi.org/10.1016/j.enzmictec.2004.08.013>
- Lin, R., Cheng, J., Ding, L., Song, W., Liu, M., Zhou, J., & Cen, K. (2016). Enhanced dark hydrogen fermentation by addition of ferric oxide nanoparticles using *Enterobacter aerogenes*. *Bioresource Technology*, 207, 213-219. doi:<https://doi.org/10.1016/j.biortech.2016.02.009>

- Liu, X. Y., Huang, M., Ma, H. L., Zhang, Z., Gao, J. M., Zhu, Y. L., . . . Guo, X. (2010). Preparation of a carbon-based solid acid catalyst by sulfonating activated carbon in a chemical reduction process. *Molecules (Basel, Switzerland)*, *15*, 7188-7196. doi:<https://doi.org/10.3390/molecules15107188>
- Lopes, A., Carvalho, S., Brasil, D., Mendes, R., & Lima, M. (2015). Surface modification of commercial activated carbon (CAG) for the adsorption of benzene and toluene. *American Journal of Analytical Chemistry*, *06*, 528-538. doi:<https://doi.org/10.4236/ajac.2015.66051>
- Malik, S. N., Pugalenti, V., Vaidya, A. N., Ghosh, P. C., & Mudliar, S. N. (2014). Kinetics of nano-catalysed dark Fermentative hydrogen production from distillery wastewater. *Energy Procedia*, *54*, 417-430. doi:<https://doi.org/10.1016/j.egypro.2014.07.284>
- Martinez Castillejo, F., Pariente, M., Brempon, C., Molina, R., Melero, J., Bremner, D., & Mantzavinos, D. (2014). Chemical surface modified-activated carbon cloth for catalytic wet peroxide oxidation of phenol. *Journal of Chemical Technology and Biotechnology*, *89*, 1182-1188. doi:<https://doi.org/10.1002/jctb.4368>
- Mishra, A., Medhi, K., Maheshwari, N., Srivastava, S., & Thakur, I. S. (2018). Biofuel production and phycoremediation by *Chlorella* sp. ISTLA1 isolated from landfill site. *Bioresource Technology*, *253*, 121-129. doi:<https://doi.org/10.1016/j.biortech.2017.12.012>
- Mishra, G., Dash, B., & Pandey, S. (2018). Layered double hydroxides: A brief review from fundamentals to application as evolving biomaterials. *Applied Clay Science*, *153*, 172-186. doi:<https://doi.org/10.1016/j.clay.2017.12.021>
- Mishra, P., Singh, L., Amirul Islam, M., Nasrullah, M., Mimi Sakinah, A. M., & Wahid, Z. A. (2019). NiO and CoO nanoparticles mediated biological hydrogen production: Effect of Ni/Co oxide NPs-ratio. *Bioresource Technology Reports*, *5*, 364-368. doi:<https://doi.org/10.1016/j.biteb.2018.02.004>
- Mishra, P., Thakur, S., Mahapatra, D. M., Wahid, Z. A., Liu, H., & Singh, L. (2018). Impacts of nano-metal oxides on hydrogen production in anaerobic digestion of palm oil mill effluent – A novel approach. *International Journal of Hydrogen Energy*, *43*(5), 2666-2676. doi:<https://doi.org/10.1016/j.ijhydene.2017.12.108>
- Mohanraj, S., Anbalagan, K., Kodhaiyolii, S., & Pugalenti, V. (2014). Comparative evaluation of fermentative hydrogen production using *Enterobacter cloacae* and mixed culture: Effect of Pd (II) ion and phyto-genic palladium nanoparticles. *Journal of Biotechnology*, *192*, 87-95. doi:<https://doi.org/10.1016/j.jbiotec.2014.10.012>
- Mohanraj, S., Anbalagan, K., Rajaguru, P., & Pugalenti, V. (2016). Effects of phyto-genic copper nanoparticles on fermentative hydrogen production by *Enterobacter cloacae* and *Clostridium acetobutylicum*. *International Journal of Hydrogen Energy*, *41*(25), 10639-10645. doi:<https://doi.org/10.1016/j.ijhydene.2016.04.197>
- Mostafa, A., El-Dissouky, A., Fawzy, A., Farghaly, A., Peu, P., Dabert, P., . . . Tawfik, A. (2016). Magnetite/graphene oxide nano-composite for enhancement of hydrogen production from gelatinaceous wastewater. *Bioresource Technology*, *216*, 520-528. doi:<https://doi.org/10.1016/j.biortech.2016.05.072>

- Mudhoo, A., Forster Carneiro, T., & Sánchez, A. (2011). Biohydrogen production and bioprocess enhancement: A review. *Critical Reviews in Biotechnology*, 31(3), 250-263. doi:<https://doi.org/10.3109/07388551.2010.525497>
- Mullai, P., Yogeswari, M. K., & Sridevi, K. (2013). Optimisation and enhancement of biohydrogen production using nickel nanoparticles – A novel approach. *Bioresource Technology*, 141, 212-219. doi:<https://doi.org/10.1016/j.biortech.2013.03.082>
- Nath, D., Manhar, A., Gupta, K., Saikia, D., Das, S., & Mandal, M. (2015). Phytosynthesized iron nanoparticles: Effects on fermentative hydrogen production by *Enterobacter cloacae* DH-89. *Bulletin of Materials Science*, 38. doi:<https://doi-org/10.1007/s12034-015-0974-0>
- Patel, S. K. S., Lee, J. K., & Kalia, V. C. (2017). Nanoparticles in biological hydrogen production: An overview. *Indian journal of microbiology*, 58(1), 8-18. doi:<https://doi.org/10.1007/s12088-017-0678-9>
- Pugazhendhi, A., Shobana, S., Nguyen, D. D., Banu, J. R., Sivagurunathan, P., Chang, S. W., . . . Kumar, G. (2019). Application of nanotechnology (nanoparticles) in dark fermentative hydrogen production. *International Journal of Hydrogen Energy*, 44(3), 1431-1440. doi:<https://doi.org/10.1016/j.ijhydene.2018.11.114>
- Rahman, A. (2013). Structure characterization and application of Ni hydrotalcite as environmentally friendly catalysts for reductive amination of benzaldehyde. *International Journal of Engineering Sciences & Emerging Technologies*, 4(2), 78-82. doi:<http://citeseerx.ist.psu.edu/viewdoc/download?doi=10.1.1.429.393&rep=rep1&type=pdf>
- Rakshit, S., Ghosh, S., Chall, S., Mati, S., Moulik, S., & Bhattacharya, S. (2013). Controlled synthesis of spin glass nickel oxide nanoparticles and evaluation of their potential antimicrobial activity: A cost effective and eco friendly approach. *RSC Advances*, 3, 19348-19356. doi:<https://doi.org/10.1039/C3RA42628A>
- Reddy, K., Nasr, M., Kumari, S., Kumar, S., Gupta, S. K., Enitan, A. M., & Bux, F. (2017). Biohydrogen production from sugarcane bagasse hydrolysate: effects of pH, S/X, Fe²⁺, and magnetite nanoparticles. *Environmental Science and Pollution Research*, 24(9), 8790-8804. doi:<https://doi.org/10.1007/s11356-017-8560-1>
- Sabir, M., Zia ur Rehman, M., Hakeem, K., & Ullah, S. (2014). Phytoremediation of metal contaminated soils using organic amendments: Prospectus and challenges. In
- Salem, A. H., Mietzel, T., Brunstermann, R., & Widmann, R. (2017). Effect of cell immobilization, hematite nanoparticles and formation of hydrogen-producing granules on biohydrogen production from sucrose wastewater. *International Journal of Hydrogen Energy*, 42(40), 25225-25233. doi:<https://doi.org/10.1016/j.ijhydene.2017.08.060>
- Seelert, T., Ghosh, D., & Yargeau, V. (2015). Improving biohydrogen production using *Clostridium beijerinckii* immobilized with magnetite nanoparticles. *Applied Microbiology and Biotechnology*, 99(9), 4107-4116. doi:<https://doi.org/10.1007/s00253-015-6484-6>

- Sekoai, P. T., & Daramola, M. O. (2015). Biohydrogen production as a potential energy fuel in South Africa. *Biofuel Research Journal*, 2(2), 223-226. doi:<https://doi.org/10.18331/BRJ2015.2.2.3>
- Sikander, U., Sufian, S., & Salam, M. A. (2017). A review of hydrotalcite based catalysts for hydrogen production systems. *International Journal of Hydrogen Energy*, 42(31), 19851-19868. doi:<https://doi.org/10.1016/j.ijhydene.2017.06.089>
- Sinha, P., & Pandey, A. (2011). An evaluative report and challenges for fermentative biohydrogen production. *International Journal of Hydrogen Energy*, 36(13), 7460-7478. doi:<https://doi.org/10.1016/j.ijhydene.2011.03.077>
- Srikanth, S., & Mohan, S. V. (2012). Regulatory function of divalent cations in controlling the acidogenic biohydrogen production process. *RSC Advances*, 2(16), 6576-6589. doi:<https://doi.org/10.1039/C2RA20383A>
- Srivastava, D. N., & Srivastava, P. (2010). Realizing NiO nanocrystals from a simple chemical method. *Bulletin of Materials Science*, 33, 653-656. doi:<https://doi.org/10.1007/s12034-011-0142-0>
- Srivastava, N., Srivastava, M., D. Malhotra, B., Gupta, V. K., Ramteke, P., Silva, R., . . . Mishra, P. (2019). Nanoengineered cellulosic biohydrogen production via dark fermentation: A novel approach. *Biotechnology Advances*, 37, 107384. doi:<https://doi.org/10.1016/j.biotechadv.2019.04.006>
- Sun, Y., Yang, G., Zhang, J., Wang, Y., & Yao, M. (2012). Activated carbon preparation from lignin by H₃PO₄ activation and its application to gas separation. *Chemical Engineering & Technology*, 35(2), 309-316. doi:<https://doi.org/10.1002/ceat.201100309>
- Sunderasan, M., Kodhaiyolii, S., M, R., & Pugalenth, V. (2014). Phytosynthesized iron oxide nanoparticles and ferrous iron on fermentative hydrogen production using *Enterobacter cloacae*: Evaluation and comparison of the effects. *International Journal of Hydrogen Energy*, 39, 11920-11929. doi:<https://doi.org/10.1016/j.ijhydene.2014.06.027>
- Taherdanak, M., Zilouei, H., & Karimi, K. (2016). The effects of Fe₀ and Ni₀ nanoparticles versus Fe²⁺ and Ni²⁺ ions on dark hydrogen fermentation. *International Journal of Hydrogen Energy*, 41(1), 167-173. doi:<https://doi.org/10.1016/j.ijhydene.2015.11.110>
- Thi Hong Le, D., & Nitorisavut, R. (2015). Ni-Mg-Al hydrotalcite for Improvement of dark fermentative hydrogen production. *Energy Procedia*, 79, 301-306. doi:<https://doi.org/10.1016/j.egypro.2015.11.491>
- Villalan, A., Mannacharaju, M., Ramasamy, B., Karthikeyan, S., Mary, R., & Sekaran, G. (2017). Functioned silver nanoparticle loaded activated carbon for the recovery of bioactive molecule from bacterial fermenter for its bactericidal activity. *Applied Surface Science*, 427. doi:<https://doi.org/10.1016/j.apsusc.2017.08.128>
- Wang, J., & Wan, W. (2008). Effect of Fe²⁺ concentration on fermentative hydrogen production by mixed cultures. *International Journal of Hydrogen Energy*, 33(4), 1215-1220. doi:<https://doi.org/10.1016/j.ijhydene.2007.12.044>
- Wang, J., & Wan, W. (2009). Factors influencing fermentative hydrogen production: A review. *International Journal of Hydrogen Energy*, 34(2), 799-811. doi:<https://doi.org/10.1016/j.ijhydene.2008.11.015>

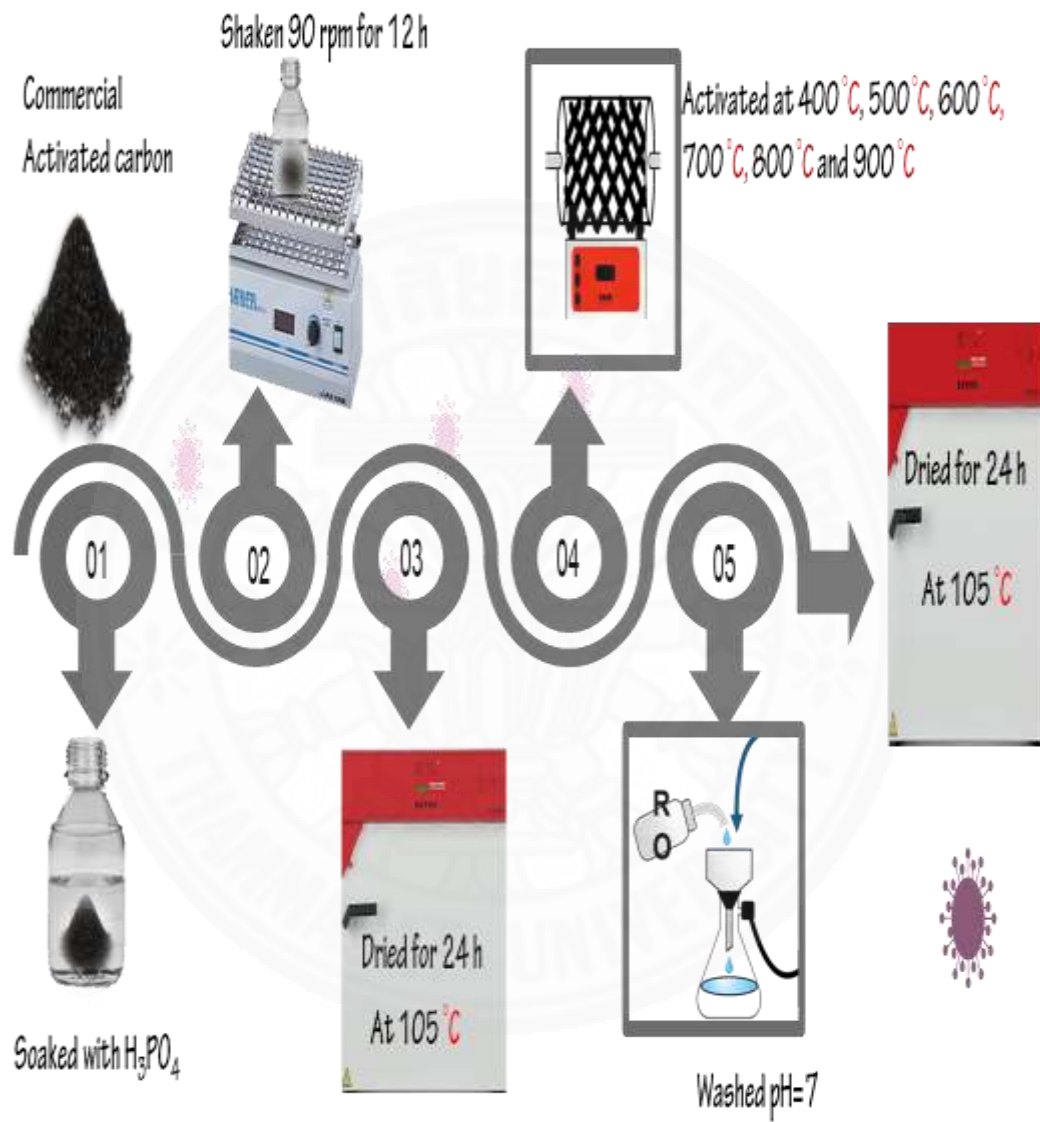
- Wimonsong, P., Llorca, J., & Nitorisavut, R. (2013). Catalytic activity and characterization of Fe–Zn–Mg–Al hydrotalcites in biohydrogen production. *International Journal of Hydrogen Energy*, 38(25), 10284-10292. doi:<https://doi.org/10.1016/j.ijhydene.2013.06.066>
- Wimonsong, P., & Nitorisavut, R. (2014). Biohydrogen enhancement using highly porous activated carbon. *Energy & Fuels*, 28(7), 4554-4559. doi:<https://doi.org/10.1021/ef500530v>
- Wimonsong, P., Nitorisavut, R., & Llorca, J. (2014). Application of Fe–Zn–Mg–Al–O hydrotalcites supported Au as active nano-catalyst for fermentative hydrogen production. *Chemical Engineering Journal*, 253, 148-154. doi:<https://doi.org/10.1016/j.cej.2014.05.047>
- Yakout, S. M., & Sharaf El-Deen, G. (2016). Characterization of activated carbon prepared by phosphoric acid activation of olive stones. *Arabian Journal of Chemistry*, 9, S1155-S1162. doi:<https://doi.org/10.1016/j.arabjc.2011.12.002>
- Yang, G., & Wang, J. (2019). Synergistic enhancement of biohydrogen production from grass fermentation using biochar combined with zero-valent iron nanoparticles. *Fuel*, 251, 420-427. doi:<https://doi.org/10.1016/j.fuel.2019.04.059>
- Yang, H., & Shen, J. (2006). Effect of ferrous iron concentration on anaerobic biohydrogen production from soluble starch. *International Journal of Hydrogen Energy*, 31(15), 2137-2146. doi:<https://doi.org/10.1016/j.ijhydene.2006.02.009>
- Yedurkar, S., Maurya, C., & Mahanwar, P. (2016). Biosynthesis of zinc oxide nanoparticles using ixora coccinea leaf extract: A Green Approach. *Open Journal of Synthesis Theory and Applications*, 05, 1-14. doi:<https://doi.org/10.4236/ojsta.2013.22006>
- Yi, N., Wu, Y., Fan, L., & Hu, S. (2019). Remediating Cd-contaminated soils using natural and chitosan-introduced zeolite, bentonite, and activated carbon. *Polish Journal of Environmental Studies*, 28(3), 1461-1468. doi:<https://doi.org/10.15244/pjoes/89577>
- Yokoyama, H., Waki, M., Ogino, A., Ohmori, H., & Tanaka, Y. (2007). Hydrogen fermentation properties of undiluted cow dung. *Journal of Bioscience and Bioengineering*, 104(1), 82-85. doi:<https://doi.org/10.1263/jbb.104.82>
- Yuan, Z., Yang, H., Zhi, X., & Shen, J. (2010). Increased performance of continuous stirred tank reactor with calcium supplementation. *International Journal of Hydrogen Energy*, 35(7), 2622-2626. doi:<https://doi.org/10.1016/j.ijhydene.2009.04.018>
- Zhang, C., Kang, X., Liang, N., & Abdullah, A. (2017). Improvement of biohydrogen production from dark fermentation by cocultures and activated carbon immobilization. *Energy & Fuels*, 31(11), 12217-12222. doi:<https://doi.org/10.1021/acs.energyfuels.7b02035>
- Zhang, J., Fan, C., & Zang, L. (2017). Improvement of hydrogen production from glucose by ferrous iron and biochar. *Bioresource Technology*, 245, 98-105. doi:<https://doi.org/10.1016/j.biortech.2017.08.198>
- Zhang, L., Zhang, L., & Li, D. (2015). Enhanced dark fermentative hydrogen production by zero-valent iron activated carbon micro-electrolysis. *International Journal of Hydrogen Energy*, 40(36), 12201-12208. doi:<https://doi.org/10.1016/j.ijhydene.2015.07.106>

- Zhang, Y., Liu, G., & Shen, J. (2005). Hydrogen production in batch culture of mixed bacteria with sucrose under different iron concentrations. *International Journal of Hydrogen Energy*, 30(8), 855-860. doi:<https://doi.org/10.1016/j.ijhydene.2004.05.009>
- Zhang, Y., & Shen, J. (2006). Effect of temperature and iron concentration on the growth and hydrogen production of mixed bacteria. *International Journal of Hydrogen Energy*, 31(4), 441-446. doi:<https://doi.org/10.1016/j.ijhydene.2005.05.006>
- Zhang, Y., & Shen, J. (2007). Enhancement effect of gold nanoparticles on biohydrogen production from artificial wastewater. *International Journal of Hydrogen Energy*, 32(1), 17-23. doi:<https://doi.org/10.1016/j.ijhydene.2006.06.004>
- Zhao, W., Zhang, Y., Du, B., Wei, D., Wei, Q., & Zhao, Y. (2013). Enhancement effect of silver nanoparticles on fermentative biohydrogen production using mixed bacteria. *Bioresource Technology*, 142, 240-245. doi:<https://doi.org/10.1016/j.biortech.2013.05.042>
- Zhao, W., Zhao, J., Chen, G., Feng, R., Yang, J., Zhao, Y., . . . Zhang, Y. (2011). Anaerobic biohydrogen production by the mixed culture with mesoporous Fe₃O₄ nanoparticles activation. *Advanced Materials Research*, 306-307, 1528-1531. doi:10.4028/www.scientific.net/AMR.306-307.1528
- Zhou, H., Jiang, Z., & Wei, S. (2018). A new hydrotalcite-like absorbent FeMnMg-LDH and its adsorption capacity for Pb²⁺ ions in water. *Applied Clay Science*, 153, 29-37. doi:<https://doi.org/10.1016/j.clay.2017.11.033>

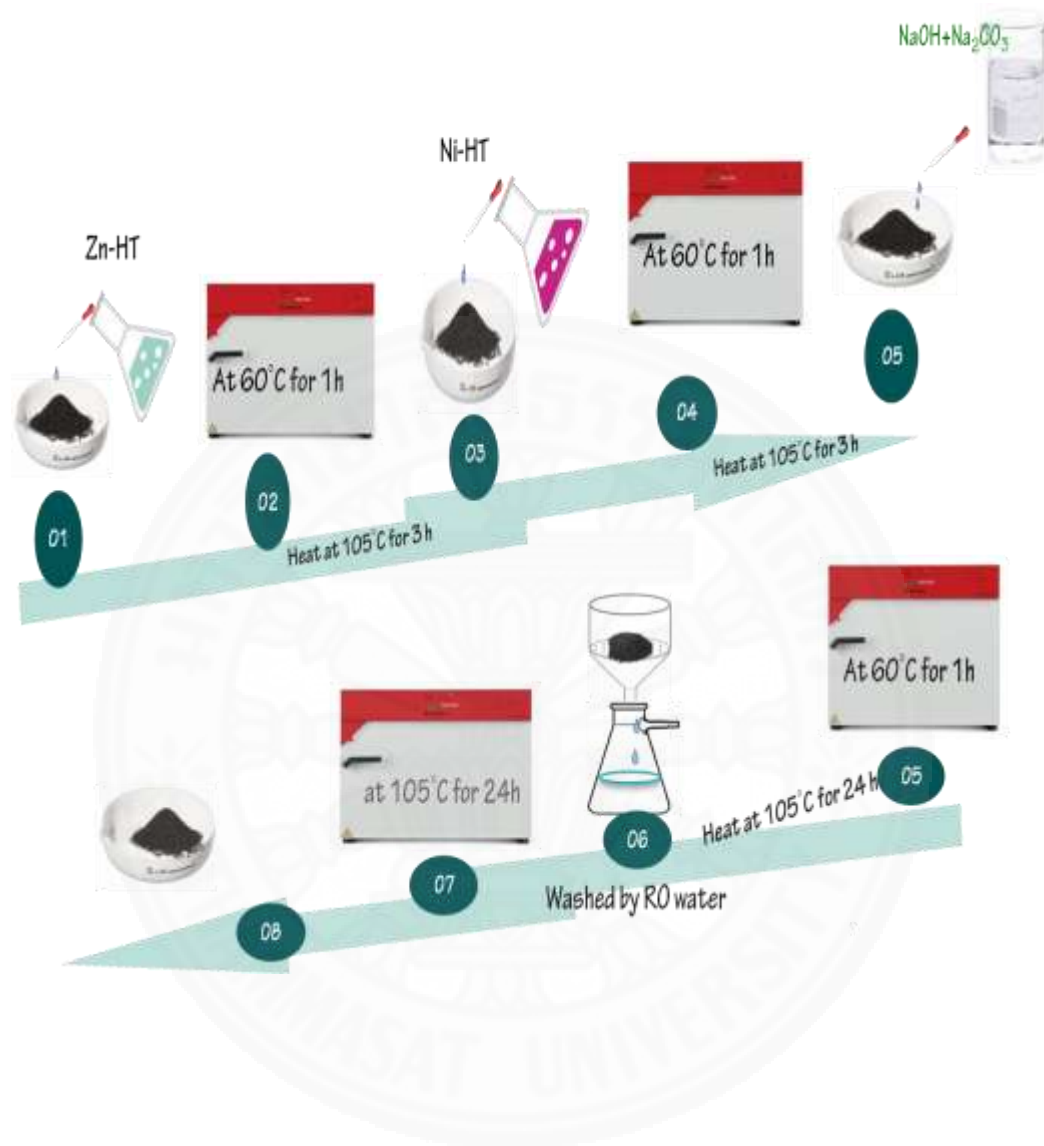


APPENDIX A

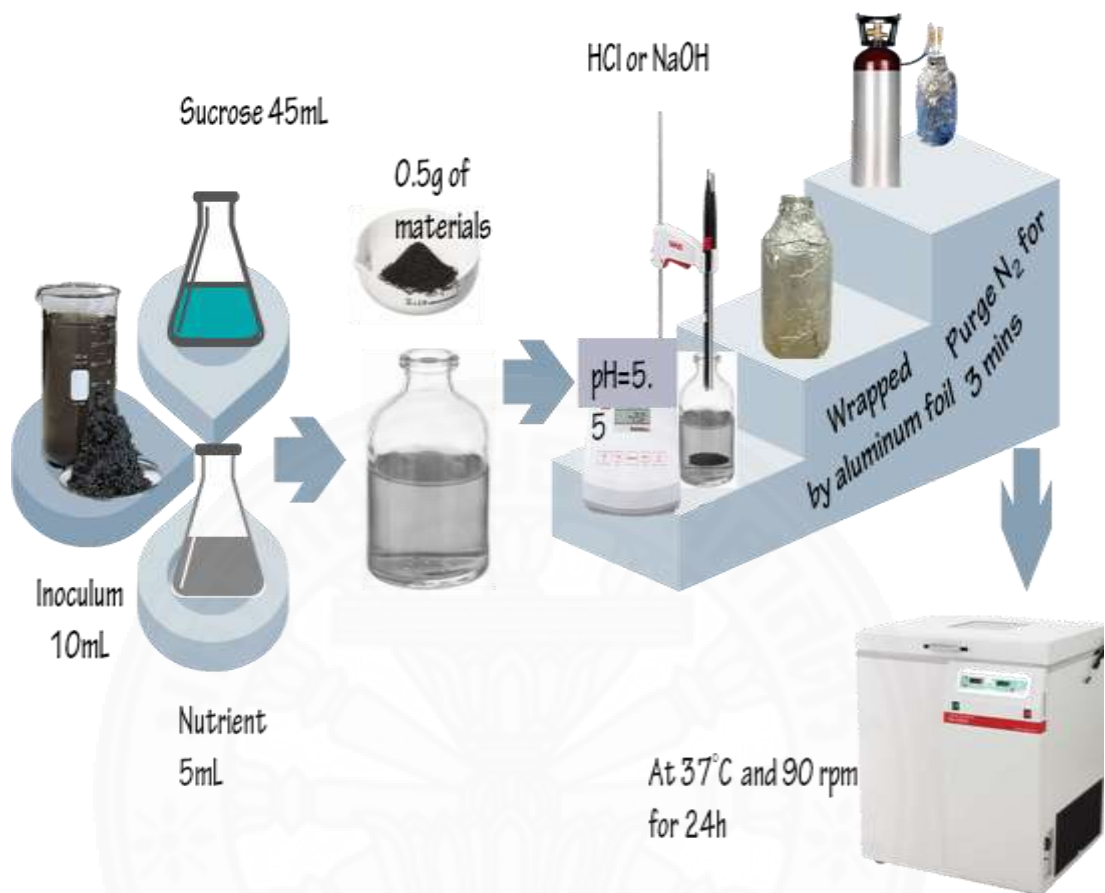
Preparation of modified commercial activated carbon



Preparation of commercial activated carbon supported hydrotalcite



Experiment procedure



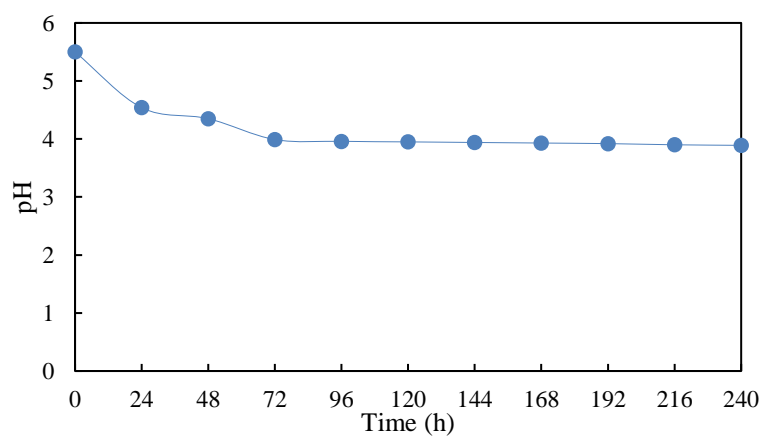
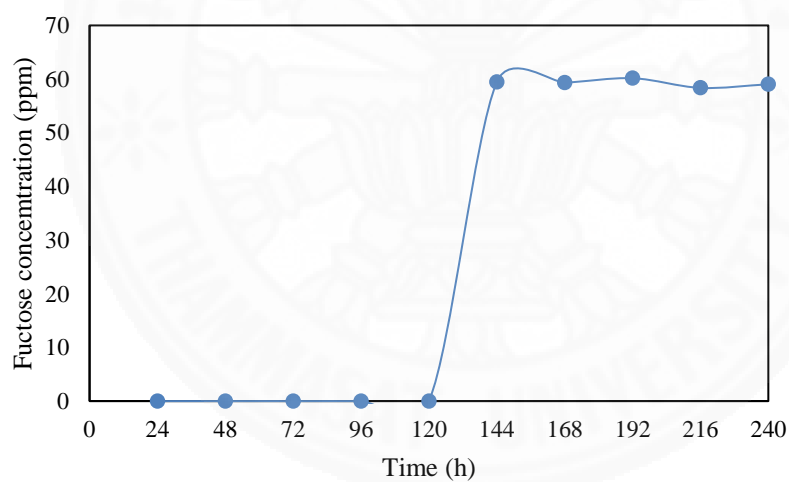
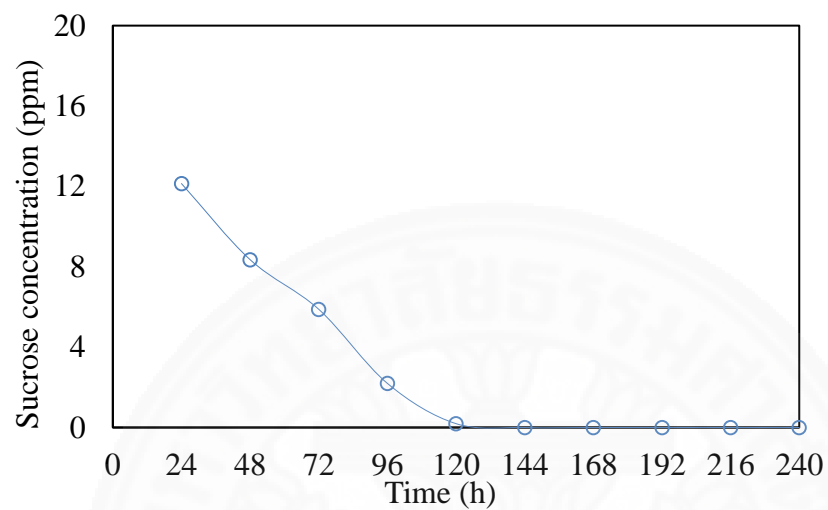
APPENDIX B

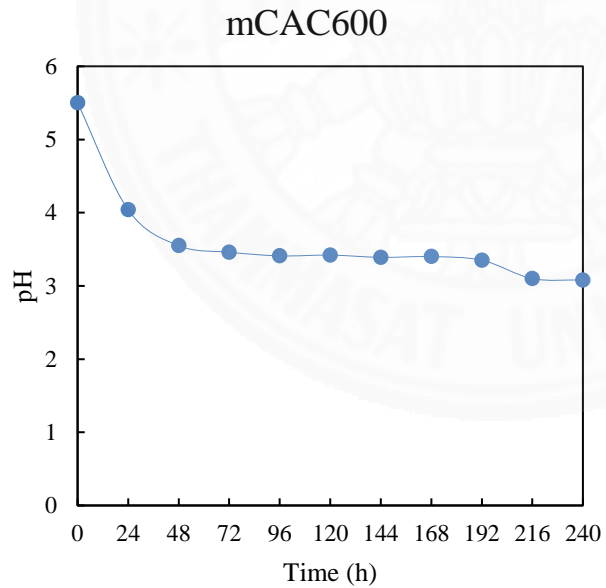
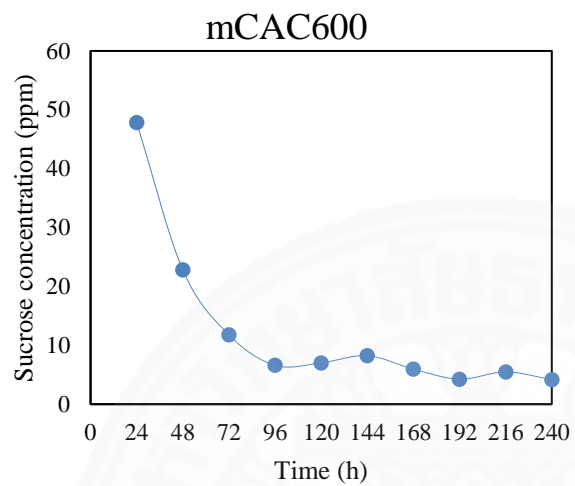
Samples descriptive statistics using t-Test for H₂ yield of supported materials in comparison to control

Sample	Mean	SD	SE	DF	T test (p value)
Zn-Ni-HT/mCAC600	2.95	0.00	0.00	-	-
Zn-Ni-HT/mCAC	2.41	0.001	0.000	3	0.0000
Zn-Ni-HT/mCAC400	2.03	0.00	0.00	3	0.0000
Zn-Ni-HT/mCAC500	2.17	0.00	0.00	3	0.0000
Zn-Ni-HT/mCAC700	2.34	0.00	0.00	3	0.0000

Note: Significant level at $p < 0.01$

APPENDIX C

Substrate concentration and pH of Zn-Ni-HT/mCAC600 during fermentative hydrogen production

APPENDIX D**Sucrose concentration and pH of mCAC600 during fermentative hydrogen production**

BIOGRAPHY

Name Ms. Southisa Sybounya
Date of Birth May 15, 1995
Education 2017: Bachelor of Science (Environmental chemistry)
National university of Laos
2020: Master of Science (Engineering and
Technology)
Sirindhorn International Institute of Technology
Thammasat University

Publications

- Sybounya, S., Nitorisavut, R., & Wimonsong, P. (2019, 21-23 Sept. 2019). Addition of activated carbon as supported Material for hydrotalcite to promote fermentative hydrogen production. Paper presented at the 2019 4th International Conference on Power and Renewable Energy (ICPRE) (pp.157-161), Chengdu,China
- Sybounya, S., & Nitorisavut, R. (2021). Hybrid composite of modified commercial activated carbon and Zn-Ni hydrotalcite for fermentative hydrogen production. *Journal of Environmental Chemical Engineering*, 9(1), 104801